RAMAN SPECTROSCOPIC STUDIES OF *ras*-p21 PROTEINS: MECHANISM OF GTP HYDROLYSIS IN PROTEINS

by

Dongguang Xiao

A dissertation submitted to the Graduate Faculty in Physics in partial fulfillment of the requirements for the degree of Doctor of Philosophy, The City University of New York

1995

This manuscript has been read and accepted for the Graduate Faculty in Physics in the satisfaction of the dissertation requirement for the degree of Doctor of Philosophy.

Sept. 13, 1995
Date

Chair of Examining Committee

Sept 15, 1995
Date

Executive Officer

Supervisory Committee

The City University of New York

ABSTRACT

Raman Spectroscopic Studies of *ras*-p21 Proteins: Mechanism of GTP Hydrolysis in Proteins

by

Dongguang Xiao

Advisor: Professor Robert H. Callender

We have studied the interactions of *ras*-p21 proteins, including wild type p21, mutant p21(G12V), mutant p21(G12D) and mutant p21(G12P), with guanine nucleotides, and the mechanism of GTP hydrolysis in proteins, by using nonresonance difference Raman spectroscopy.

A 30 cm^{-1} downshift observed in the P=O symmetric stretching motion of the terminal PO_3^{2-} group of GTP upon binding to proteins indicates the strong hydrogen bonding interactions between the γ-phosphate group of GTP and the proteins. The in-phase symmetric stretching band of the α-PO^{2-} and β-PO^{2-} group of GTP had no significant changes upon binding to proteins. This result suggests that the hydrogen

bonding environment around the α-PO^{2-} and β-PO^{2-} group of GTP in proteins is similar with that in solution.

The downshift of the P=O symmetric stretching band indicates the decrease of the P=O bond order of the terminal PO_3^{2-} group of GTP, therefore the increase of the O_β-P_γ bond order in proteins. This result suggests that the mechanism of GTP hydrolysis is an associative reaction in p21 proteins.

We have also found strong interactions between p21 proteins and guanine nucleotides at the guanine ring moiety. Both the 2-amino and 6-carbonyl groups strongly hydrogen bonded with proteins.

A series of phosphate model compounds were studied by Raman spectroscopy. Our studies of mono-phosphate compounds show that the -O-P- bond order of these phosphate compounds is linearly related with the pK_a of their corresponding R-O-H compounds.

We have done normal mode analysis of phosphate model compounds with empirical method. We have obtained the correlation between Raman frequencies and force constants. We have also found that the Raman frequencies of phosphate compounds are very sensitive to the coupling between different vibrational modes.

I dedicate this thesis to my family

ACKNOWLEDGMENT

I would like to express my sincere gratitude to Professor Robert H. Callender for his guidance, patience and inspiration during the course of this thesis work. His ideas have been central and essential parts of all the research work.

I would like to thank Dr. Hua Deng for his valuable suggestion, discussion and help. His extensive experiences and clear discernment are always good guidance for my research. I would also like to thank Drs. Danny Manor, Gezhi Weng for leading me into the active research work including teaching me all the experimental skills.

I feel grateful to Drs. Marilyn Gunner, Sharon Cosloy and Valeria Balogh-Nair for their valuable advice and help. I would like to thank Drs. Martin Webb and Chungxiang Chen for synthesizing the compounds used in my experiments.

I would like to thank Dr. Sondra Vitols for reading and correcting the thesis. I would also like to thank Drs. Rudolf Gilmanshin, Larry Senak, Jerron Van-Beek, Yongqing Chen, Liewen Huang, Messrs. Zhongmo Ju, Hui Zhong, Jianghua Wang, Zunhai Dong and Mrs. Naomi Hellmann for their generous help.

Finally, I would like thank my wife, Ying Wan, for her patience and support during the course of this work. I would also like to thank my parents and all my family members for their encouragement and help in all these years.

TABLE OF CONTENTS

ABBREVIATIONS

p21	gene product of the human c-H-ras proto-oncogene
p21(G12D)	point mutation of p21 at residue Gly12 by Asp
p21(G12P)	point mutation of p21 at residue Gly12 by Pro
p21(G12V)	point mutation of p21 at residue Gly12 by Val
ADP	adenosine 5' diphosphate
ATP	adenosine 5' triphosphate
IDP	inosine 5' diphosphate
GDP	guanosine 5' diphosphate
8D-GDP	guanosine 5' diphosphate with deuterium labeled at the 8 position of guanine ring
6-^{18}O-GDP	guanosine 5' diphosphate with ^{18}O labeled on the 6-oxygen atom of guanine ring
β-$^{18}O_3$GDP	guanosine 5' diphosphate with ^{18}O labeled on three oxygen atoms of β-phosphate
GTP	guanosine 5' triphosphate
β-$^{18}O_3$GTP	guanosine 5' triphosphate with ^{18}O labeled on three oxygen atoms of β-phosphate
γ-$^{18}O_3$GTP	guanosine 5' triphosphate with ^{18}O labeled on three oxygen atoms of γ-phosphate
GMPPCP	guanyl(β,γ-methylene)-triphosphate
GppNHp	guanosine 5'-(β,γ-imido)-triphosphate
DTT	dithioretol
IPTG	isopropylthiogalactoside
RP-HPLC	reverse phase high performance liquid chromatography

LIST OF TABLES

LIST OF FIGURES

Chapter 1

INTRODUCTION

Guanine nucleotide-binding (GNB) proteins are involved in many cellular processes, such as signal transduction, protein transport and secretion, and polypeptide chain elongation.(Bourne, H. R. et al., 1990, 1991; Gilman, A. G., 1987; Hall, A., 1990). They have several biological properties in common. They all bind GDP (Guanosine Diphosphate) and GTP (Guanosine Triphosphate) each with high affinity and high specificity, so the GNB proteins usually contain bound guanine nucleotides when they are isolated in their native state; and they all have GTPase activities (Miller, D. L. et al., 1970; Ferguson, K. M. et al., 1986, 1987; Poe, M. et al., 1985). GNB proteins are believed to act as molecular switches. In the "ON" or active state, they are complexed to guanosine triphosphate (GTP); and in the "OFF" or inactive state, they are bound to guanosine diphosphate (GDP). In the GTP-bound conformation, they interact with an effector molecule, and the duration of this interaction is regulated either by the effector-mediated or by the intrinsic GTPase activity, which is the rate of cleavage of the terminal phosphate group of GTP, of the protein. Thus, the operational definition of the effector molecule is that it interacts only with active form GNB proteins.

As a member of the GNB protein super family, *ras*-p21 has a molecular weight ~21 kd and is composed of 189 amino acid residues. Point mutations of *ras*-p21 protein have been found in more than 30% of human tumors (Downward, J., 1992). The real functions and the nature of the alterations that follow *ras*-mediated cell transformation are not known; however, *ras*-p21 proteins are believed to be essential switches involved in regulating processes as diverse as cell growth, cell differentiation, and cell fate during development (Cuadrado, A. et al., 1993; Barbacid, M. 1987; Moore, K. J. M. et al., 1993). In general, *ras*-p21 has a GDP molecule bound in a specific site and is biologically inactive in this state. A cytosolic protein, *ras*-GNRF (*ras*-guanine nucleotide-releasing factor) triggers the exchange of GDP to GTP, and thereby alters the protein conformation change, which in turn triggers its biological activities. In the active GTP-bound form, wild type *ras*-p21 interacts with the GTPase activating protein (GAP), and the GTPase activity is enhanced by 10^5 fold as a result of this interaction (John, J. et al., 1990; Rensland, H. et al., 1991). The complex of *ras*-p21 and GAP will rapidly hydrolyze the GTP, and thereby maintain the *ras*-p21 in its inactive GDP-bound state (Figure 1.1). Point mutations at certain positions, such as 12, 35 and 65, of p21 reduce their intrinsic GTPase activity; most important, they lose the ability to interact with GAP pro-

teins (Adari, H. et al., 1988). Consequently the oncogenic proteins are locked in the active GTP-bound state over prolonged time, which promotes the growth signal, resulting in the unregulated cell growth (Langen, R. et al., 1992).

Extensive studies have been carried out on the biological properties of *ras*-p21. Expression of the recombinant *ras*-p21 proteins has resulted in an abundant of sample that has made it feasible to investigate these complete via crystallography, NMR and vibrational spectroscopy. Given the role these proteins play in cell growth, it is thus very important to understand, at an atomic level, how normal and mutant *ras*-p21 proteins interact with GTP and GDP at active and inactive states, as well as how these interactions are involved in the GTP hydrolysis in proteins.

The X-ray structures of wild type and several mutant p21 proteins with complexed with GDP and different GTP analogues have been determined.(Pai, E. F. et al., 1989, 1990; Milburn, M. V. et al., 1990; Schlichting, I. et al., 1990; Krengel, U. et al., 1990, 1991; Tong, L. et al., 1989; de Vos, A. M. et al., 1988). The overall structure of p21 contains a central β-sheet consisting six strands, five helices and nine loops (Figure 1.2). There are three loops which are particularly important for the function of the protein: loop L1 contains Gly12, the residue which is the most frequently mutated residue in the human tumors; loop L2 contains the residues believed to be involved in the interaction with GAP

such as ASP33; loop L4 contains Gln61, the other residue which is highly important for the oncogenic activation of *ras*-p21. In the three-dimensional structure, these three loops comprise the active site of the molecule centered around the γ-phosphate, where the important interactions that can initiate GTPase reaction are observed (Pai, E. F. et al., 1989). X-ray structure studies show several hydrogen bonding interactions between nucleotide and p21 protein, both at the guanine ring moiety and at the phosphate moiety. These strong hydrogen bondinginteractions are attribute to the high affinity and specificity for GDP and GTP. It has been found in the kinetic binding studies, that p21 does not tolerate many substitution of GDP and GTP. The affinity of GMP and ADP for p21 are about six orders of magnitude smaller than that of GDP (John, J. et al., 1990). Loop L4, which contains residues 61 to 65, is found to have the highest temperature factor, which indicated that they are highly mobile or disordered. Gln61 in loop L4 is suspected to be involved in activation of a water molecule, which attacks the terminal phosphate in the transition state, thereby hydrolyzing the GTP (Pai, E. F. et al., 1989). The overall structure of mutant *ras*-p21 proteins is very similar to that of wild type *ras*-p21 protein. Significant effects of the mutations on the three-dimensional structure are confined to the active site around γ-phosphate. We have chosen to study

wild type p21, mutant p21(G12V), p21(G12D) and p21(G12P) in order to understand, at an atomic level, the interactions between these p21 proteins and guanine nucleotides, as well as the differences of the interactions between wild type and mutant p21 proteins. Mutant p21(G12P) is the only non-oncogene protein mutated at position 12, which makes the comparison study very useful.

Vibrational spectroscopy give detailed information on the vibrational motions of atoms in molecules, and because these vibrations are sensitive to chemical changes, the vibrational spectrum can be used as a monitor of molecular chemistry. The conformation of a molecule may be probed and the ionization states of polar groups are easily determined. In addition, vibrational spectroscopy provides a wealth information on protein-ligand interactions, such as hydrogen bondingwhich perturbs a molecule's electronic distribution, and results in modified vibrational force field and vibrational frequency shift. Thus, the changes observed in the vibrational spectrum of a bound ligand is a direct measure of how a protein acts upon it. Our group has succeeded previously in obtaining the classical Raman spectra of a small molecule bound to a protein by difference spectroscopy technique.(Callender, R. H. et al., 1988, 1994; Yue, K. T. et al., 1984; Chen, D. et al., 1987). The changes between a spectrum of a ligand bound in protein and that in solution yield much information about the protein-ligand interactions. The interactions of EF-Tu (Elongation Factor Tu) and

wild type p21 with guanine nucleotides at guanine ring moiety have been previously studied by our group with classical Raman spectroscopy method. Here we continue the study of the interactions between *ras*-p21 proteins and guanine nucleotides at the phosphate moiety, as well as the differences of the interactions between wild type and mutant p21 proteins; and also how these interactions contribute to the hydrolysis of GTP in *ras*-p21 proteins.

Unlike X-ray structure, Raman spectroscopy directly measure the strength of the chemical bond rather than the distance between atoms; Raman spectra are taken at aqueous solution, which are more biologically relevant. In addition, the protein sample is minimally perturbed during the course of experiment. Moreover, the preparation of the sample is simple and the data collection is fast. This is extremely helpful when the sample is not very stable, such as with nucleotide-free *ras*-p21 protein studied in Chapter 8.

The results of the study on the interactions between *ras*-p21 proteins and guanine nucleotides by classical Raman difference spectroscopy are reported here. The hydrogen bondinginteractions and the mechanism of GTP hydrolysis are discussed. We also report the results of the Raman studies on some relevant phosphate model compounds as well as the normal mode analysis of them.

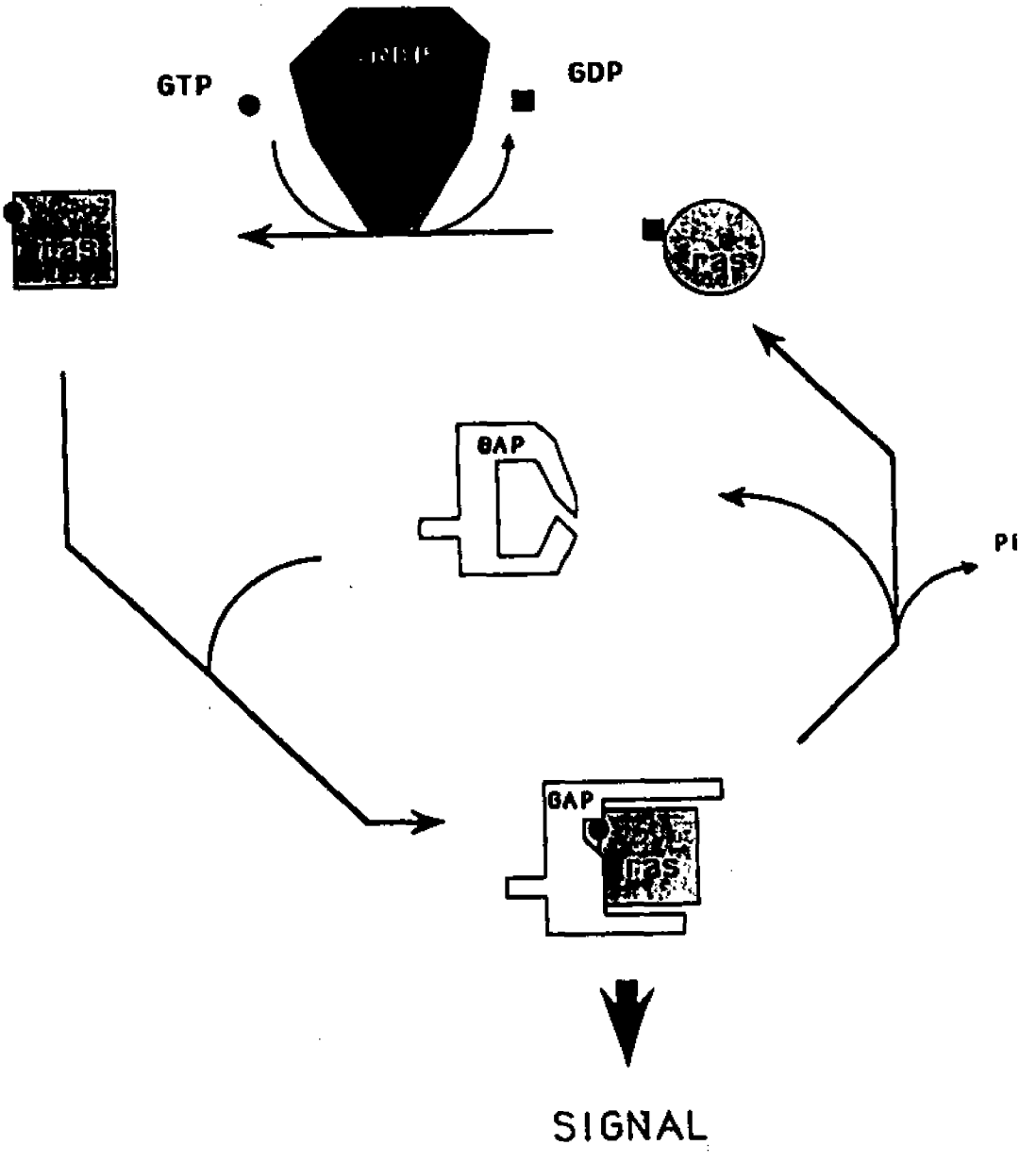

Figure 1.1 Schematic representation of the GTP/GDP cycle of *ras*-p21. The replacement of GDP for GTP is accomplished by receptor activation of *ras*-p21 activated by specific GNRPs. *Ras*-p21 require the presence of specific GAPs for inactivation and probably of their signal transmissions.

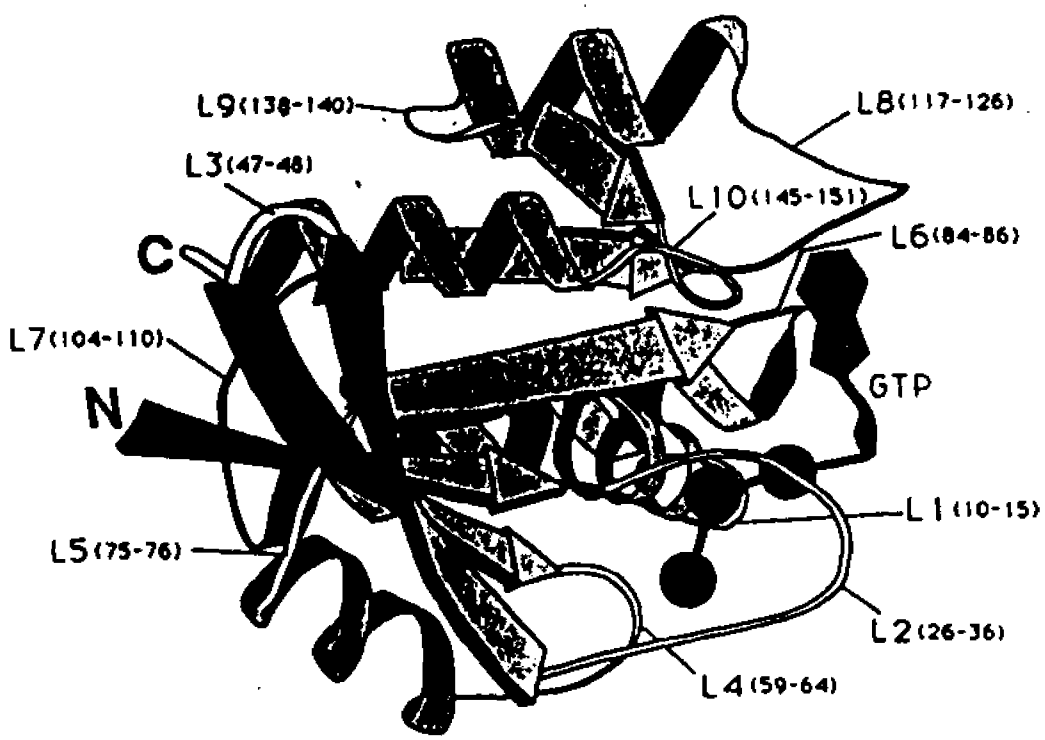

Figure 1.2 Three dimensional structure of *ras*-p21-GppNHp complex (Pai.E.F. et al., 1990). The overall structure contains a central β-sheet consisting six strands, five helices and nine loops. β-strands are drawn as arrows, α-helices as curled ribbons, and loops as double lines. The resolution is 1.35 Å.

Chapter 2

DIFFERENCE RAMAN SPECTROSCOPY

2.1 Theoretical Background of Raman Spectroscopy

2.1.1 Raman Scattering

The Raman effect arises from the interactions of the incident light with the electrons in the illuminated molecules. The frequencies of the scattered light are shifted relative to the incident light by the amounts corresponding to the normal mode frequencies of the molecular vibrations. Raman spectra give detailed information on the vibrational motions of atoms in molecules. Moreover, because these vibrations are sensitive to chemical changes, the vibrational spectra can be used as a monitor of changes in the molecule's structure.

Figure 2.1 shows some of the possible consequences of a photon-molecule interactions from a quantum mechanical point of view. If contributions from molecular rotations and translations are ignored, molecular energy E_{mol} is a sum of electronic energy E_{elec} and vibrational energy E_{vib} (Eq. 2.1). The vibrational energy levels in each electronic state are equally spaced by the amount $h\nu_{vib}$, which reflects the nature of molecular vibrations (Eq. 2.2).

$$E_{mol} = E_{elec} + E_{vib} \qquad \ldots(2.1)$$

$$E_{vib} = (n + 1/2)h\nu_{vib} \qquad n = 0, 1, 2, \ldots \quad (2.2)$$

In this quantum mechanical model, light scattering is depicted as a two-photon process. The first step in this process, indicated by the upward-pointing arrows in Figure 2.1, is the combination of a photon and a molecule to a higher energy state, which may or may not correspond to a quantized energy state of the molecule, with extremely short life time. The second step, indicted by the downward-pointing arrows in Figure 2.1, involves the release of a photon after a very short time interval ($< 10^{-11}$ seconds). For Rayleigh scattering, no change in the frequency of photon occurs; therefore, no information about molecular vibrations is given. For normal Raman scattering, the molecule is brought to a virtual energy state, and then a photon is released. This photon has either a higher energy (anti-Stokes process) or lower energy (Stokes process) than the incoming light, and the difference in light frequency corresponds directly to the ground state vibrational frequency of the molecule, which reflects the vibrational motions of the molecule. Since the anti-Stokes transitions take place when the molecule is in a higher vibrational state ($n > 0$) within the electronic state, and the population of these higher states is governed by a Boltzmann distribution, only a small percentage of molecules are in these higher vibrational states. The ratio of the number of molecules in the n=1 and

n=0 vibrational states in the ground electronic state, which we denote N_1 and N_0 respectively, is

$$N_1/N_0 = \exp(-h\nu_{vib}/kT) \qquad \ldots(2.3)$$

where h is Planck's constant, T is the absolute temperature, and k is Boltzmann's constant. Therefore, the intensity of Stokes line is several orders higher than that of anti-Stokes line, and the feeble anti-Stokes scattering is usually ignored in conventional Raman spectroscopy and only the Stokes spectrum is recorded. For resonance Raman scattering, the molecule is brought to a real electronic excited state, so the intensity of scattered light is greatly enhanced. The pre-resonance Raman scattering is a process between normal and resonance Raman scattering, in which the molecule is brought near but not to the electronic excited state.

2.1.2 Raman Intensity

When a molecule, which is in the molecular state m, is perturbed by an electromagnetic wave of frequency ν_0 and intensity I_0, the total Raman intensity of the scattering light corresponding to the transition from state m to state n is given by

$$I_{mn} = \frac{8\pi}{9c^4} I_0 \omega^4 \sum_{\sigma\rho} |(\alpha_{\sigma\rho})_{mn}|^2 \qquad \ldots(2.4)$$

where

$$(\alpha_{\sigma\rho})_{mn} = \frac{1}{h} \sum_r \left(\frac{\langle n|\mu_\rho|r\rangle\langle r|\mu_\sigma|m\rangle}{\nu_{mr} - \nu_0 + i\Gamma_r} + \frac{\langle n|\mu_\sigma|r\rangle\langle r|\mu_\rho|m\rangle}{\nu_{nr} + \nu_0 + i\Gamma_r} \right) \qquad \ldots(2.5)$$

In these expressions, $(\alpha_{\sigma\rho})_{mn}$ is the component of the polarizability tensor, Γ_r is a damping constant which takes into account the finite life time of each molecular state, and the $\langle n|\mu_r|r\rangle$, etc., are the amplitudes of the electric dipole transition moments, where μ_r is the electric dipole moment operator along direction ρ.

2.1.3 Depolarization Ratio ρ

Polarization characterizes the nature of scattered Raman radiation. The depolarization ratio has proved to be very useful in determining Raman bands. The depolarization ratio is defined as:

$$\rho = \frac{I_{\perp}}{I_{\parallel}} \qquad \ldots(2.6)$$

where $I_{\perp}$ and $I_{\parallel}$ are the intensities of the Raman radiation polarized perpendicular and parallel respectively to the scattering plane, that is, the plane normal to the incident beam.

$$I_{\parallel} = const \times (3g' + 5g'')E_i^2 \qquad \ldots(2.7)$$

$$I_{\perp} = const \times (10g'' + 4g')E_i^2 \qquad \ldots(2.8)$$

where g^0, g^s, and g^a are known as the isotropic, symmetric anisotropic, and antisymmetric anisotropic components respectively.

Detailed calculations show that $\rho = 0.75$ for normal vibrations which do not preserve molecular symmetry during the motion of the nuclei (non-totally-symmetric modes), and $\rho \leq 0.75$ for modes which do preserve molecular symmetry (totally symmetry modes).

2.1.4 Isotopic Substitution

Isotopic substitution can be an invaluable aid in the analysis of vibrational spectra. By making the assumption, which is generally valid, that the force constants are unaltered by isotopic substitution, the shift in observed frequency can be attributed principally to mass effects. Therefore, in a given spectrum, by observing which bands shift and the extent to which they shift on isotopic replacement, it is often possible to gain insight into the participation of the replacement nucleus in the normal mode giving rise to the bands.

For example, in our Raman studies of the phosphate model compounds (Chapter 4), ^{18}O substitution on the oxygen atoms of the phosphate compounds is used to assign the vibrational modes. In general, if a mode is well localized, the Raman frequency of the P-O bond can be expressed as

$$\nu = \frac{1}{2\pi}\sqrt{\frac{k}{\mu}} \qquad \ldots(2.9)$$

where

$$\mu = \frac{m_o m_p}{m_o + m_p} \qquad \ldots (2.10)$$

So the ratio of the P-O mode frequencies between the ^{16}O phosphate compound and its ^{18}O isotopic derivative is:

$$\frac{\nu^*}{\nu} = \sqrt{\frac{\mu}{\mu^*}} = 0.93 \qquad \ldots (2.11)$$

where ν and ν^* are the frequencies of the ^{16}O phosphate compound and its ^{18}O isotopic derivative respectively.

2.2 Theoretical Background of Normal Mode Analysis

2.2.1 Small Vibrations in Classical Mechanics

For a molecular system which has N atoms, it has 3N degrees of freedom. The kinetic energy in Cartesian coordinate is given by

$$T = \frac{1}{2}\sum_{\alpha=1}^{N} m_\alpha \left[\left(\frac{d\Delta x_\alpha}{dt}\right)^2 + \left(\frac{d\Delta y_\alpha}{dt}\right)^2 + \left(\frac{d\Delta z_\alpha}{dt}\right)^2\right] \qquad \ldots (2.12)$$

If we choose mass-weighted Cartesian displacement coordinate $q_1 \ldots q_{3N}$ defined as follow:

$$q_1 = \sqrt{m_1}\Delta x_1, q_2 = \sqrt{m_1}\Delta y_1, q_3 = \sqrt{m_1}\Delta z_1, q_4 = \sqrt{m_2}\Delta x_2, etc \qquad \ldots (2.13)$$

The kinetic energy is then expressed as

$$T = \sum_{i=1}^{3N} \dot{q}_i^2 \qquad \ldots (2.14)$$

For small values of the displacements, the potential energy V can be expressed as a power series in the displacement q_i:

$$V = V_0 + \sum_{i=1}^{3N} f_i q_i + \sum_{i,j=1}^{3N} f_{ij} q_i q_j + \text{higher order terms} \quad \ldots \quad (2.15)$$

Where Vo is the energy of the equilibrium state and is chosen to be zero.

$$f_i = \left(\frac{\partial V}{\partial q_i}\right)_0 \qquad i=1,\ 2,\ \ldots\ 3N \qquad \ldots \quad (2.16)$$

When all atoms are at equilibrium positions, the energy must be minimized. So, $f_i = 0$. For sufficiently small amplitudes of vibration, the high order terms can be neglected and a harmonic oscillator model is chosen. The potential energy is then given by

$$V = \frac{1}{2}\sum_{i,j=1}^{3N} f_{ij} q_i q_j \qquad \ldots \quad (2.17)$$

Where f_{ij} is the force constant given by

$$f_{ij} = \left(\frac{\partial V}{\partial q_i \partial q_j}\right)_0 \qquad \ldots \quad (2.18)$$

by solving Newton's equations of motions

$$\frac{d}{dt}\frac{\partial T}{\partial \dot{q}_i} + \frac{\partial V}{\partial q_i} = 0 \qquad i = 1,2,3,\ \ldots\ 3N \qquad \ldots \quad (2.19)$$

we can get the normal modes of the vibrational motion of a molecule (Wilson, E. B. Jr. 1955).

2.2.2 Internal Coordinates, Generalized Valence Force Constant and GF Formalism

The vibrational motions of a molecule are independent of the translations and rotations of the molecular. Changes

in inter-atomic distances or in the angles between chemical bonds, or both, can be used to provide a set of 3N-6 (or 3N-5 for linear molecules) internal coordinates, which are unaffected by translations or rotations of the molecule as a whole. The internal coordinates are defined as geometrically localized basis coordinates, and are referred as bond stretching, which is the increase of distance between two atoms; valence bending angle, which is the increase in the angle between two valence bonds attached to the same atom; and dihedral angle, which is the angle between a bond and a plane defined between two bonds. Each internal coordinate is considered to have an intrinsic force constant. Coupling among such coordinates produces normal modes and the internal coordinates can be expressed as the linear combination of the normal coordinates.

$$S_t = \sum_{i=1}^{3N} B_{ti} q_i \qquad t = 1,2,3, \ldots, 3N-6 \qquad \ldots (2.20)$$

where S_t is one of the 3N-6 internal coordinates and q_i is one of the 3N Cartesian displacement coordinates. B_{ti} are constants determined by the geometry of the molecule.

By choosing the internal coordinates, we eliminate the rotations and translations from the motion of the molecule, and there are only 3N-6 independent coordinates involved. The force constant defined with internal coordinates, called generalized valence force constants, have clear physical meaning and are often transferable from one molecule to another similar molecule with little modification.

If we construct a G-Matrix as follow:

$$G_{tt'} = \sum_{i=1}^{3N} \frac{1}{m_i} B_{ti} B_{t'i} \qquad t,t' = 1,2,3,\ldots,3N-6 \qquad \ldots (2.21)$$

The kinetic energy and potential energy can be written in terms of internal coordinates in the form:

$$T = \frac{1}{2} \sum_{tt'} (G^{-1})_{tt'} \dot{S}_t \dot{S}_{t'} \qquad \ldots (2.22)$$

$$V = \frac{1}{2} \sum_{tt'} F_{tt'} S_t S_{t'} \qquad \ldots (2.23)$$

where S_t is internal coordinate, $F_{tt'}$ is force constant. Thus the Newton's equations of motion can be written in the form of

$$|GF - E\lambda| = 0 \qquad \ldots (2.24)$$

where G matrix is constructed from the geometry of the molecule and F matrix is constructed from given force constants. The frequencies of vibrations can be calculated from these equations. Therefore, the problem of calculating vibrational frequencies are reduced to find an appropriate set of force constants to fit the observed frequencies with the calculated frequencies by the equation 2.24.

2.2.3 Potential Energy Distribution (PED) and Group Frequency

From observation of the Raman spectra of a number of compounds having a common group of atoms, it is found that, regardless the rest of the molecule, this common group has a

narrow range of frequencies called group frequencies. The PED values give the relative contributions of a specific force constant or a certain chemical function group to a calculated frequency.

Since the discovery of Raman effect (Raman and Krishnan, 1928), a considerable amount of theoretical work has been done on Raman spectroscopy (Williams, R. W. et al., 1995; Snyder, R. G. et al., 1967). Several empirical and semi-empirical methods, such as normal mode calculation and their relative Raman and IR intensity calculations, have been developed to analyze Raman spectra. However, Raman spectra of biological molecules, such as proteins, protein-ligand complexes, or even large ligands themselves, are usually very complicated because of their low symmetry and large number of vibrational modes. For most compounds, some characteristic vibrational frequencies are found to be correlated with certain functional groups. These vibrational modes are called group frequencies. The existence of group frequencies contributes to the fact that the force constant for a given chemical bond is, to a certain degree, transferable from one molecule to another. In order to apply the group frequency concept to a part of a molecule, the motion in a given normal mode must be essentially localized within that group. Group frequencies find their maximum utility when they give rise to intense features, when they occur in a spectral region that is free from other intense features, and when small variations in the group frequency can be cor-

related with conformational and environmental changes. The group frequencies have been used with great success to study hydrogen bondinginteractions. For example, the protein amide I band (which arises from peptide C=O stretch) in the region between 1600 cm^{-1} and 1700 cm^{-1}, and amide III band (which is mostly due to peptide N-H bending) in the region between 1200 cm^{-1} and 1300 cm^{-1} are correlated to the secondary structure of the peptide backbone (Carey, P. R. 1982; Tu, A. T., 1982).

2.3 Instrumentation

Figure 2.2 shows the typical instrumental set-up of our Raman experiment. A laser beam is introduced through the sample. The scattered light is collected at 90 degrees and is focused on the entrance slit of a monochromator. The gratings in the monochromator disperse the incoming light into a spectrum of frequencies. This spectrum is transformed into electronic signals by a detector, and then sent to a computer for analysis.

The laser sources available in our laboratory are a 4-Watt argon ion laser from Spectra Physics (Model 165), a 5-Watt krypton ion laser and a 10-Watt argon ion laser (Coherent Radiation Inc.). The sample holder can hold a double or a triple split cuvette specially designed for measuring several spectra under the same conditions, and each sam-

ple space of the split cell has a dimension of 2.5 x 2.5 mm. The cuvette is set on a computer-controlled stage which can be moved to within 1 μm accuracy. Raman spectra are measured by a Triplemate spectrometer (Spex Industries), equipped with a solid state detector system (Model DIDA-100 water cooled photodiode array and a Model ST-100 detector controller; Princeton Instruments), or a charge coupled device (CCD) system (CCD Model LN/CCD-1152UV liquid nitrogen cooled and a model ST-135 detector controller; Princeton Instruments). Data are acquired, stored, and analyzed on a Macintosh computer (Apple, Cupertino CA). Spectral lines are calibrated against known Raman lines of toluene and are accurate to within $\pm 2 cm^{-1}$. The spectral resolution of the instruments is typically set to 6 cm^{-1} full width at half maximum.

2.4 Difference Raman Spectroscopy

To study protein-ligand interactions, we intend to measure the Raman spectra of bound ligands or other small protein molecular moieties. However, an important experimental constraint needs to be considered in vibrational spectroscopy, the signals from the ligands are generally overwhelmed by background vibrational bands from the protein itself. This difficulty has been largely overcome in recent years using difference Raman spectroscopy (Chen, D. et al.,

1987; Yue, K. T. et al., 1984). The Raman spectrum of protein-ligand complex as well as that of apo-protein (protein itself without bound ligand) are measured under the same conditions, and the protein spectrum is numerically subtracted from the complex spectrum after these measurements. The difference spectrum thus obtained, contains signals of bound ligand, as well as those of protein changes induced by ligand binding. The operation can be represented by:

$$\text{Spectrum (Enzyme•L)} - \text{Spectrum (Enzyme)}$$
$$= \text{Spectrum (L bound in Enzyme)}$$
$$+ \text{Spectrum (protein changes)} \qquad \ldots(2.25)$$

where L represents a cofactor, inhibitor or substrate of the enzyme.

This procedure is not suitable for the studies of the interactions between protein and ligand for the phosphate moieties of GDP and GTP because the signal from phosphate is the same order as that from protein changes, which has a magnitude of 0.5% to 1% of protein amide I intensity in general. An alternative route we have taken to get the difference spectra of these protein-ligand complexes is represented by the following:

$$\text{Spectrum (Protein•L)} - \text{Spectrum (Protein•L*)}$$
$$= \text{Spectrum (L - L* bound in protein)} \qquad \ldots(2.26)$$

where L* is isotopically labeled L at certain positions.

There is no protein changes involved in this approach of the measurement because L and L* have the same chemical properties.

Spectrum (L bound in protein) or Spectrum (L - L* bound in protein) are compared with those collected in solution. The comparison gives information about the protein ligand interactions.

In order to obtain accurate difference spectrum and to avoid artifacts, we used a split cell (Figure 2.2) to measure several samples. The temperature and humidity in the room, where the measurements are taken, are kept nearly constant. Arrangements like these are made to reduce the influences of different optical properties for the different samples, and to control the environmental fluctuations which may affect accuracy of forming the difference spectrum. The long term drift of the optical system can be canceled out if we take the spectra in a sequential way and line up the spectra before adding them. A detailed procedure of the alignment is described as follows: assume sample A is a stable protein-ligand complex, sample B is another stable protein-ligand complex different from A. The spectra of A and B are measured in a $A_1B_1A_2B_2$ .....A_nB_n fashion, with each run taking 10 to 20 minutes. The sets of data are then checked by the subtraction A_n-A_{n-1}, A_n-A_{n-2}, ...,A_n-A_1 and B_n-B_{n-1}, B_n-B_{n-2}, ... B_n-B_1. Every subtraction should give a flat featureless background. All the spectra taken for the same sample are then added together as A or B. To get the difference spectrum, B is subtracted from A. In this study, the sharp protein characteristic band from phenylalanine around 1000

cm^{-1} is used as a reference for the extend of the subtraction.

Figure 2.3 shows some typical results from studies of ligands bound to proteins with difference Raman spectroscopy. Figure 2.3a and Figure 2.3b show the Raman spectra of wild type *ras*-p21•GDP complex and the nucleotide free *ras*-p21 respectively, and Figure 2.3c shows the difference spectrum between these two by subtracting Figure 2.3b from Figure 2.3a. The difference spectrum mainly contains the Raman bands from GDP bound to *ras*-p21.

For the *ras*-p21 proteins studied here, the intensity of the largest nucleotide peak is about 6% of that of the protein amide I peak. With careful measurement, intensity differences as little as 0.1% of the most intense Raman peaks can be detected by our experimental system.

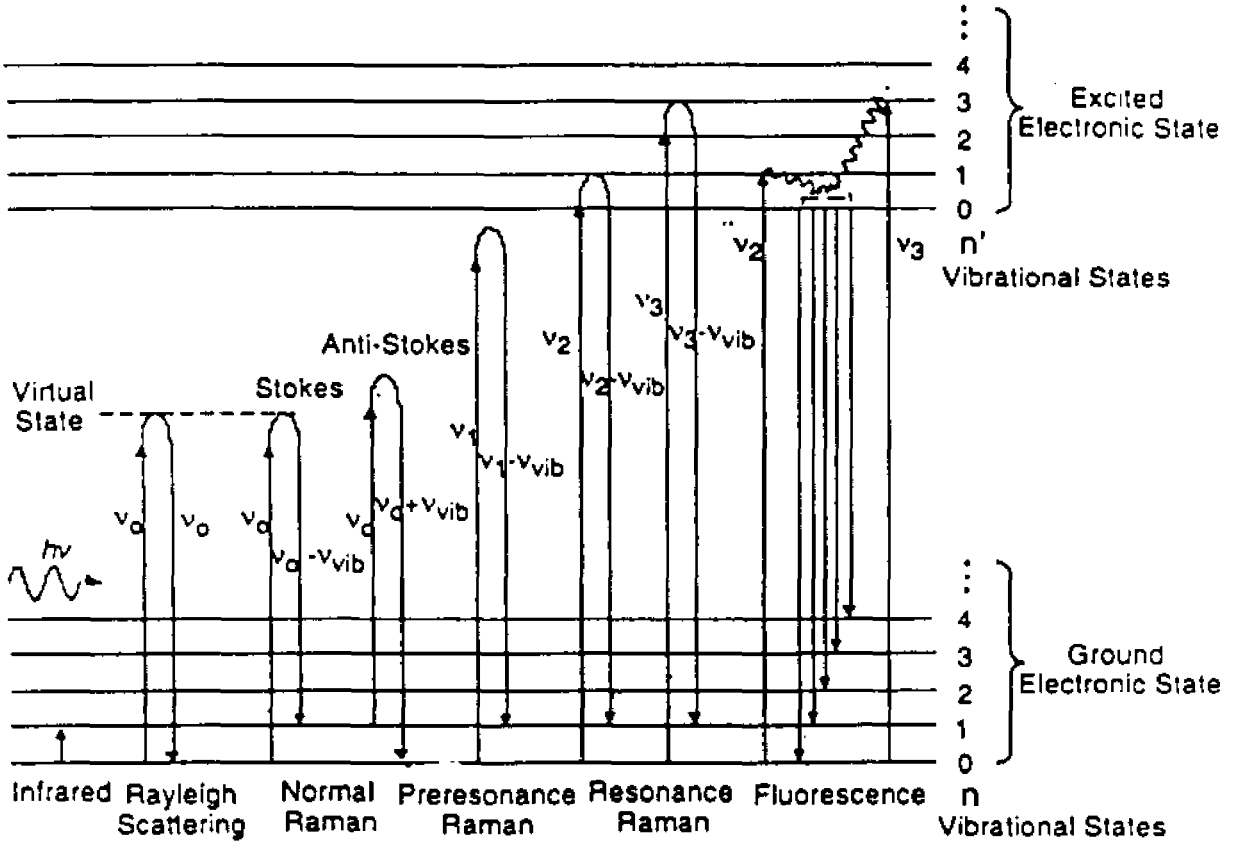

Figure 2.1 The energy diagram of photo-molecule interactions. In infrared process, the molecule absorbs a photon with an energy ν_{vib}; in normal Raman process, the molecule is elevated to an energy difference ν_{vib} (Raman shift); in resonance Raman process, the molecule is elevated to an electronic excited state by a photon and then releases another photon with an energy difference ν_{vib}, and the band intensities are usually orders of magnitude greater.

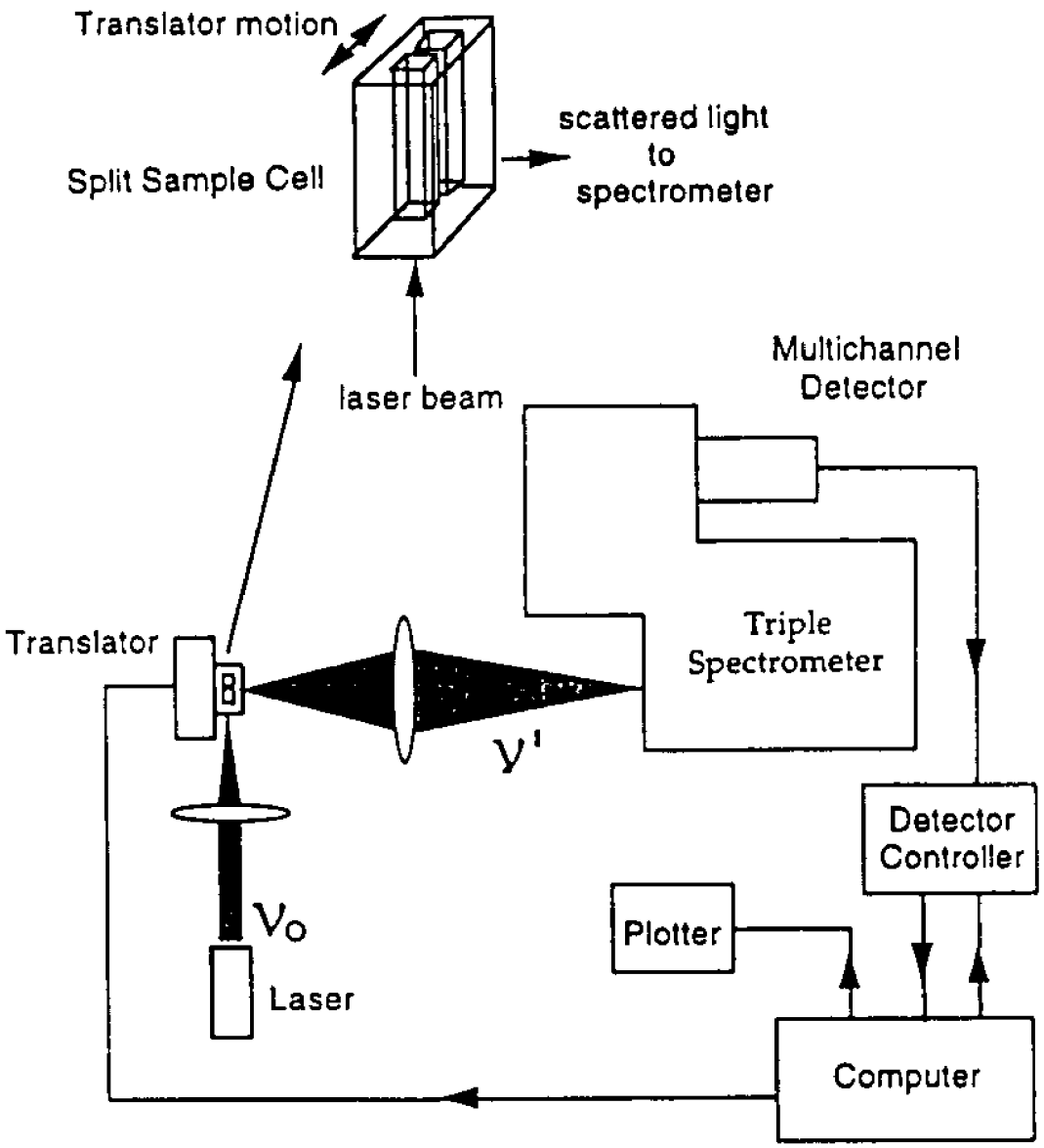

Figure 2.2 A schematic drawing of the instrumental set up for Raman measurement. The monochromatic light emitted from a laser source is introduced through the sample. The scattered light is focused on the entrance slid of a triple spectrometer. The spectrometer disperses the incident light into a frequency spectrum and focuses it on to a detector. The spectrum was converted into electrical signals by a charge coupled device, and transferred to a computer for analysis.

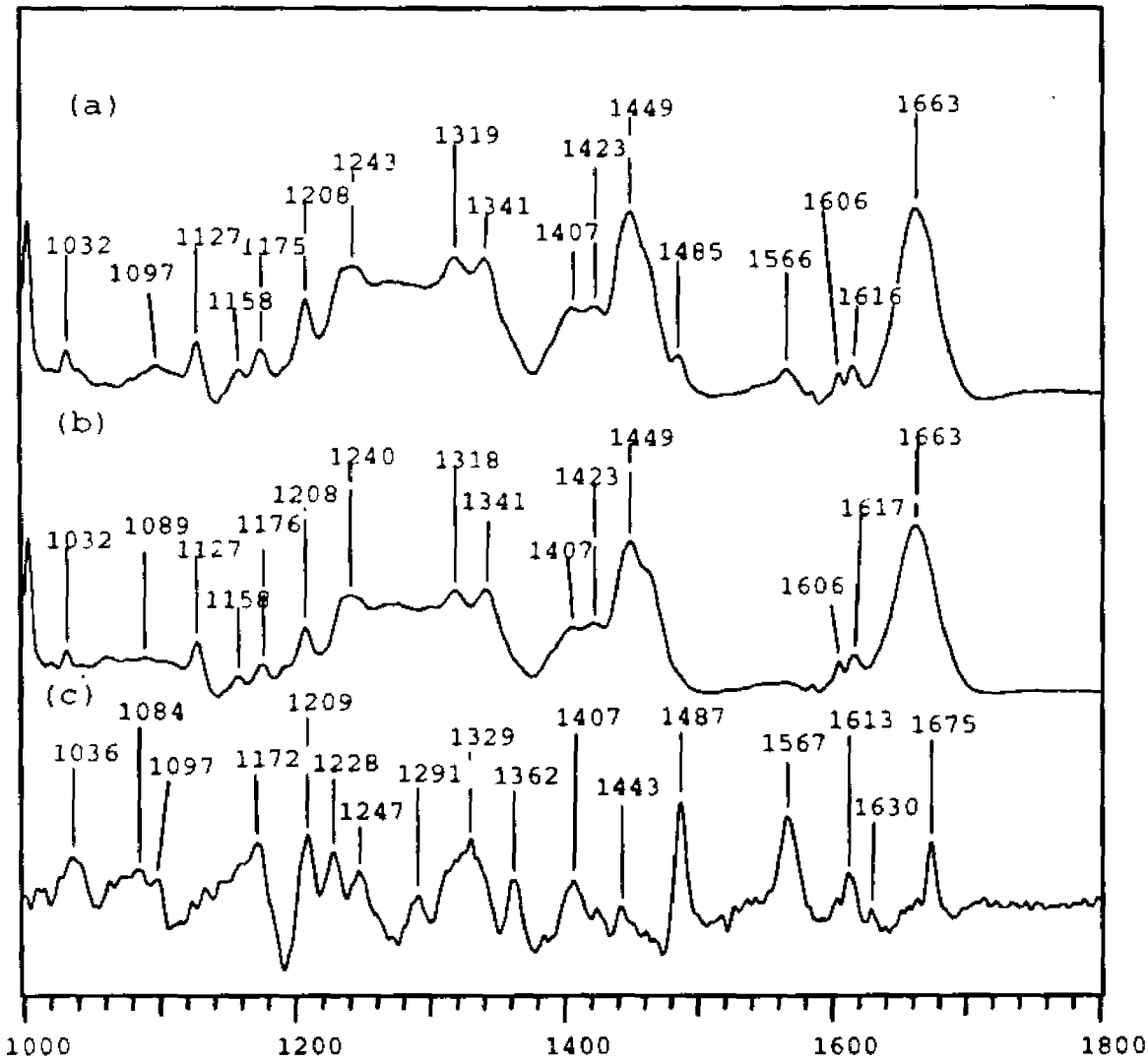

Figure 2.3 Raman spectra of wild type p21.
(a) p21-GDP complex, 3mM, pH 7.5.
(b) Nucleotide-free p21, 3mM, pH 7.5.
(c) Difference spectrum between p21-GDP and apo-p21.
Laser excitation: 568. 2 nm, 150 mW.

Chapter 3

SAMPLE PREPARATION

3.1 Nucleotides

GMP, GDP, GTP, IDP, and GMPPCP were purchased from Sigma or Boerhinger Mannheim and used without further purification. ^{3}H-GDP (12 Ci/mmole) was purchased from Amersham. All other chemicals were purchased from Sigma.

6-^{18}O-GDP and 8D-GDP were synthesized by C. X. Chen (Chemistry Department, City College of CUNY). ^{18}O-GDP and ^{18}O-GTP were synthesized by Dr. M. Webb (London). The ^{18}O-GDP and ^{18}O-GTP samples from Dr. M. Webb were treated with biobeads (SM-2, 20-50 Mesh, Bio-Rad) to remove the fluorescence impurities: 0.5 ml of 30 mM ^{18}O-GDP or ^{18}O-GTP was added to ~ 0.5 ml of biobeads in a 1.5 ml Eppendorf tube, and the mixture was shaken at 4°C for ~ 2 hours before it was centrifuged at 2000 r.p.m. with table top centrifuge (Jouan Model MR1812) for approximately 20 minutes. The ^{18}O-GDP or ^{18}O-GTP solution was then separated from the biobeads by pipetting. The remaining biobeads were then washed with 1 ml H_2O several times to insure all the nucleotides had been collected.

3.2 Wild Type and Mutant ras-p21 Proteins

3.2.1 Isolation of Plasmid

c-Ha-*ras* gene was expressed in *Escherichis coli*. strain RRIDM 15 under the control of the tac promoter (Turcker, J. et al., 1986). The cloned *E•coli*. strain was obtained from Prof. A. Wittinghofer (Heidelberg, Germany). The gene was checked to its plasmid DNA content. The extraction procedures are described as follows:

Cells from 5 ml overnight culture were centrifuged at 6000 r.p.m. for 10 minutes with table top centrifuge, and the pellet of the cells was resuspended in 50 µl of 25% sucrose in H_2O. 300 µl of M-STET (5% triton X-100; 5mM EDTA; 50 mM Tris, pH 8.0; 5% sucrose) was added and mixed well. The mixture was transferred to 1.5 ml Eppendorf tube and 25 µl of 10 µg/ml lysozyme was added to it. The tube was heated in boiling water bath for 1 minute and immediately chilled on ice. It was then centrifuged at 6,000 r.p.m. for 15 minutes with table top centrifuge, and the supernatant (about 200 µl) was transferred to a new Eppendorf tube before 200 µl of ice-cold iso-propanal was added to it to precipitate nucleic acids. The tube was frozen in a dry ice ethanol bath for 20 minutes before it was centrifuged at 6,000 r.p.m. for 15 minutes, and the supernatant was drained on paper towel. After the pellet was dried in vacuum system, it was resus-

pended in 200 µl TE buffer (10mM Tris, pH7.4; 1mM EDTA), and was run on 0.7% agarose gel. The gene with the right plasmid was transferred to a recipient bacterium which was from a LB plate (5 grams of NaCl; 10 grams of Kryptone; 5 grams of Yeast Extract; 15 grams of Agar; 1 liter H_2O) containing 50 µg/ml ampicillin for future cell growth.

3.2.2 Cell Culture

The cloned *E•coli.* cells were grown in large quantities in a high density fermentor (Lab-line Instruments, Inc.). The procedures for cell growing are described as follows:

Medium A (43 grams of Tryptone; 93 grams of Yeast extract; 20 ml of Glycerol; 20 grams of NaCl and 3 liters of H_2O) and medium B (7.19 grams of KH_2PO_4; 60.48 grams of K_2HPO_4; 1 liter of H_2O; pH 7.6) were autoclaved separately and mixed together after they cooled down. 20 ml of $CaCl_2$ (0.1 M), 20 ml of $MgSO_4$ (1M) and ampicillin (50 µg/ml) were filter-sterilized and added to the mixed cell culture. Inoculum was grown in 500 ml medium overnight and then added to the fermentor with the rest of media. The fermentation conditions were set to: temperature at 37°C, air pressure at 15 psi, speed of the rotation of the fermentor at 250 r.p.m. After 2 hours of cell growth, the cells were induced by the addition of 50 µM IPTG, 50 µg/ml of ampicillin and 50 ml of 50% glycerol. A small amount of cell sample was taken out

every hour, and the UV absorption of the sample (at 560 nm) was measured accordingly. The growing curve (Figure 3.1) of the absorption of the cells at 560 nm vs. growing time was used to monitor the cell growth. The cells were harvested when cell growth stopped (normally around 10-12 hours). Harvested cells were pelleted down by centrifugation at 10,000 r.p.m. with GSA rotor, washed with buffer A (50 mM Tris-HCl; 1mM NaN_3; 0.5 mM DTE; pH 7.6) three times ,and stored at -80°C in freezer.

3.2.3 Column Chromatography

Approximately 100 grams of frozen cells were suspended in 500 ml of buffer A (50 mM Tris-HCl; 1mM NaN_3; 0.5 mM DTE; pH 7.6). PMSF (0.01 mM), benzamidine (0.01 mM), 1ml EDTA (0.5 M; pH7.6), 200 µg lysozyme and 20 µg of DNase I were added to the cell suspension. The cells were homogenized and the mixture was incubated at 4°C for 30 minutes, during which it was stirred. 5 ml of $MgCl_2$ (1 M) and 2.5 ml 4% of DOC (Sodium Deoxycholate) were then added. After further incubation with stirring at 4°C for another 30 minutes, the mixture was centrifuged at 10,000 r.p.m. at 4°C for 60 minutes with a Sorvall GSA rotor to remove cell debris. The supernatant was applied to a column (5 x 30 cm) of DEAE-Sepharose CL-6B (from Pharmacia) equilibrated with buffer B (buffer A with 10 mM $MgCl_2$). The column was washed with 500 ml of buffer B and then developed with a 5,000 ml linear

gradient of 0-0.3 M NaCl in buffer B. The flow rate was controlled at 3.6 ml/min and 20 ml-fractions were collected. The elution was checked by UV absorption at 280 nm , radioactive binding assay and SDS-PAGE. The fractions containing p21 were pooled and brought to 60% saturation with ammonium sulfate. The precipitation recovered by centrifugation was dissolved in 15 ml of buffer C (buffer B with 0.05 mM GDP and 200 mM NaCl), and was applied to a system of two columns (one AcA54, 25 x 100 cm and one AcA44, 25 x 100 cm). The columns were developed with buffer C at a flow-rate of 1.2 ml/min and 9ml-fractions were collected. The portion containing pure p21, which had been checked by UV-absorption, radioactive binding assay, and SDS-PAGE, was poured together and brought to 70% saturation with ammonium sulfate. The precipitate was collected by centrifugation and the pellet was dialyzed against buffer C to remove the ammonium sulfate. The p21 protein samples were then stored at -80°C in freezer.

3.2.4 Radioactive Binding Assay and SDS-PAGE

The procedures of radioactive binding assay are described as follows:

The radioactive mix contained [250 µl of ^{3}H-GDP (1.0 mCi/ml, from Amersham); 187 µl of 1 mM GDP; 7.814 ml of H_2O and 1.5 ml of absolute ethanol. Absorption of the mix at 260 nm is approximately 0.25 OD]. Binding buffer [0.2 M

$(NH_4)_2SO_4$; 0.2 M Tris-HCl, pH 7.4; 5 mM DTT; 1 mM NaN_3; 3 mM EDTA] and washing buffer [40 mM Tris-HCl, pH 7.4; 40 mM $(NH_4)_2SO_4$; 10 mM DTT; 10 mM $MgCl_2$ and 1 mM NaN_3) were prepared. Cellulose nitrate filters (25 mm diameter, type HA) were bought from Millipore Corp. 20 µl of protein sample (concentration to ~ 50 µM) was added to a 10 x 50 mm test tube in a total volume of 200 µl, which contains 50 µl binding buffer, 20 µl radioactive mix. The reaction mixture was allowed to equilibrate for 30 minutes at room temperature, and was then diluted with 2 ml of washing buffer, filtered and washed three times with 3 ml of the same buffer. The filters are immersed in 4 ml of scintillation fluid (Filtron-X, National Diagnostic Inc.), and radioactivity is measured in a scintillation counter.

The SDS Gel was prepared and used as follows:

The running gel solution [15 ml of 40% Acrylamide; 1.4 ml of 2% Methylenebisacrylamide; 13.6 ml of 1M Tris, pH 8.8; 9.5 ml of H_2O; and 0.4 ml of 10% SDS (sodium dodecyl sulfate)] and stacking gel solution (2.5 ml of 40% Acrylamide; 1.3 ml of 2% Methylenebisacrylamide; 1.3 ml of 1M Tris, pH 6.8; 14.5 ml of H_2O; 0.2 ml of 10% SDS; 5 µl of Phenol red) were prepared. A gel rack (Hoffer Scientific Instruments; Model SE 250 unit) was set up with spacers between glass and aluminum plates. 0.2 ml of ammonium peroxodisulphate and 31 µl of tetramethylrthylenediamine were added to the running

gel solution and the solution was then well mixed. The mixed running gel solution was immediately poured into the gel rack. Care was taken to prevent the formation of bubbles. The rack was filled to ~ two-thirds capacity. The running gel inside the rack was dried at room temperature for about 1 hour. 0.1 ml of ammonium peroxodisulphate and 10 µl of tetramethylrthylenediamine were added to stacking gel solution and then the solution was well mixed. The mixed stacking gel solution was then poured into the gel rack on top of the running gel until it filled up the top of the rack. Well combs were then placed on the top of the gel rack to make the sample wells. After 1 hour, the gels were removed from the rack and put on the gel holder. Electrophoresis buffer was poured into the gel holder and fully filled up to the space between the gel holder and the gel. At the same time, 10 µl of protein samples, from each test tubes, were transferred to 1.5 ml Eppendorf tubes, where 10 µl of blue dye (Briliant Blue) was added to each sample tube before they were heated in a boiling water bath for 1 minute. 10 µl of protein samples from each tube, as well as the molecular weight marker, were then loaded to each sample wells. The gel was run under 20 mA constant current until the line of blue dye reach the end of the gel. The gel was taken out and put into stain solution (500 ml of 1% Comastic Briliant Blue solution; 500 ml of methanol; and 200 ml of acetic acid). After 1 hour, the gel was transferred to destain solution

(300 ml of methanol; 100 ml of acetic acid; and 600 ml of H_2O) for approximately 2-4 hours until the gel became clear.

The same methodology applies to the purification of all the mutant p21 proteins, such as, p21(G12V), p21 (G12D) and p21(G12P).

3.3 Nucleotide Free *ras*-p21 Protein

Studies show that SO_4^{2-} ion can dramatically increase the dissociation rate of GDP (Hall, A. et al., 1986; Mistou, M. et al., 1992). Removal of Mg^{2+} ion may increase the dissociation constant of GDP to p21 by a factor of 10. Therefore, excess Mg^{2+} was removed from the preparation: 1 ml of protein solution (20 mg/ml) was applied to a 9-ml Sephadex PD-10 G-25 column, and eluted with 5ml of Mg^{2+}-free buffer I [200 mM Tris-HCl; 200 mM $(NH_4)_2SO_4$; 0.5 mM DTE; and 0.5 mM NaN_3 at pH 7.5). The collected fractions were concentrated by centrifugation with Centricon 10 (from Amicon) at 8,000 r.p.m. At room temperature, the concentration of p21 was adjusted to about 100 μM with buffer I, and GMPPCP was added in equi-molar concentration with p21. Alkaline phosphate acrylic beads (Boehringer Mannheim) were added to a concentration of 2 units/mg p21. The degradation of GDP was monitored by HPLC on a RP-C18 column under ion-pairing conditions with HPLC buffer [80 mM potassium phosphate; 10 mM

TEAB (Tetrabutylammonium Bromide); 0.2 mM NaN_3; 5% acetonitrile; pH7.5). Figure 3.2 shows the enzyme reaction monitored by RP-HPLC. When all of the GDP had been converted to guanosine (about 1 hour), the protein sample was cooled down to 4°C, and alkaline phosphate acrylic beads were removed by filtering the mixture through a low protein affinity filter (Millpore HVLP 013). P21•GMPPCP was immediately concentrated in Centricon 10 tubes (from Amicon) at 8,000 r.p.m, and brought to the final concentration to about 0.5 mM. Snake venom phosphodiesterase was added to a concentration of 20 μg/mg of p21. The degradation of GMPPCP was monitored by RP-HPLC (Jacob, J., et al., 1990). After this process was complete (about 1 hour), the protein sample, together with the snake venom phosphodiesterase, was filtered with Centricon 100 (from Amocon) at 3000 r.p.m. for about 2 hours. The portion of the solution which passed through the Centricon 100 was collected and was passed through a Sephadex PD-10 G-25 column to remove the guanosine.

3.4 Protein and Guanine Nucleotide Complex

Isotopically-labeled guanine nucleotides help establish assignments for the bands in the vibrational spectrum; however, isotopically-labeled guanine nucleotides have the same chemical properties as natural abundance nucleotides. Isotopically-labeled GDP or GTP was prepared as follows for the

p21•GMPPCP complex: p21•GMPPCP was first obtained by the method described in the previous section. 5 molar excess of isotopically labeled GDP or GTP was added to the protein sample, and the protein nucleotide mixture was incubated in buffer I with 0.6 mM EDTA at room temperature for about 45 minutes. For Raman the experiment, the sample was then washed three times with buffer T (20 mM Tris-HCl; 10 mM $MgCl_2$; 0.5 mM NaN_3; pH7.5) by Centricon 10 at 8,000 r.p.m..

The concentration of protein or nucleotide samples was determined spectroscopically by monitoring at 280 nm for p21 (ϵ, extinction = 18,450 $M^{-1}cm^{-1}$) and at 254 nm for GDP/GTP (ϵ, extinction = 13,700 $M^{-1}cm^{-1}$) (Miller, D. L. et al., 1974; Tucker, J. et al., 1986). Figure 3.3 shows the UV absorption of p21•GDP complex, GDP and IDP in solution. Prior to Raman measurements, protein samples were washed three times with buffer T using Centricon 10 at 8,000 r.p.m., and the final concentration of protein was brought to 2-6 mM. Samples for the difference Raman Spectroscopy, in which two or three samples were measured together, were prepared at the same time with the same method to ensure identical conditions for all these samples.

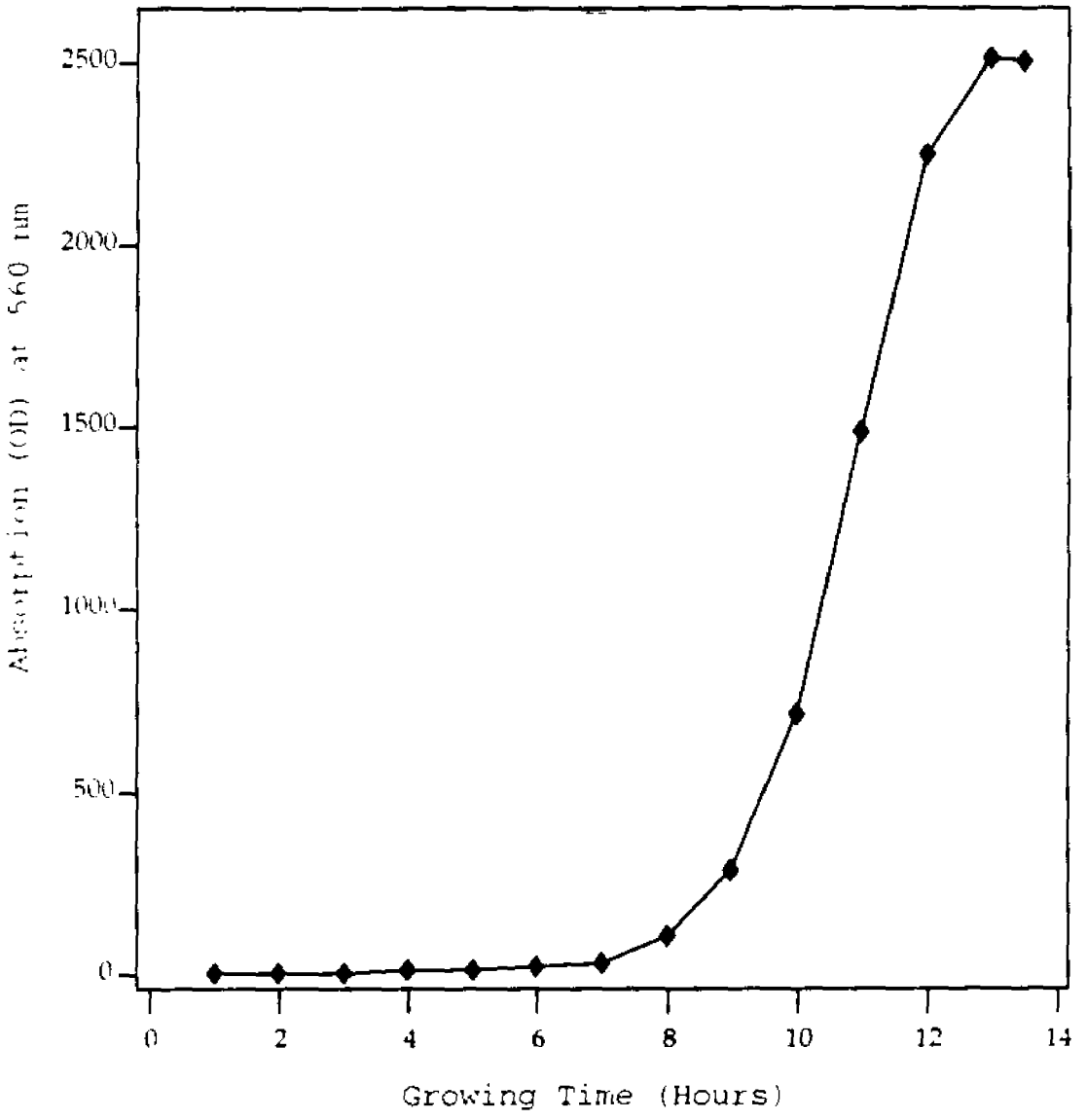

Figure 3.1 Growing Curve of *E•coli*.

E•coli. cells were grown in a high density fermentor at 37 °C. Media was supplemented with 50 μM IPTG and 50 μg/ml ampicillin after 2 hours of growth. The concentration of cells was monitored by the absorption at 560 nm. Cells were harvested normally after 12 hours of growing.

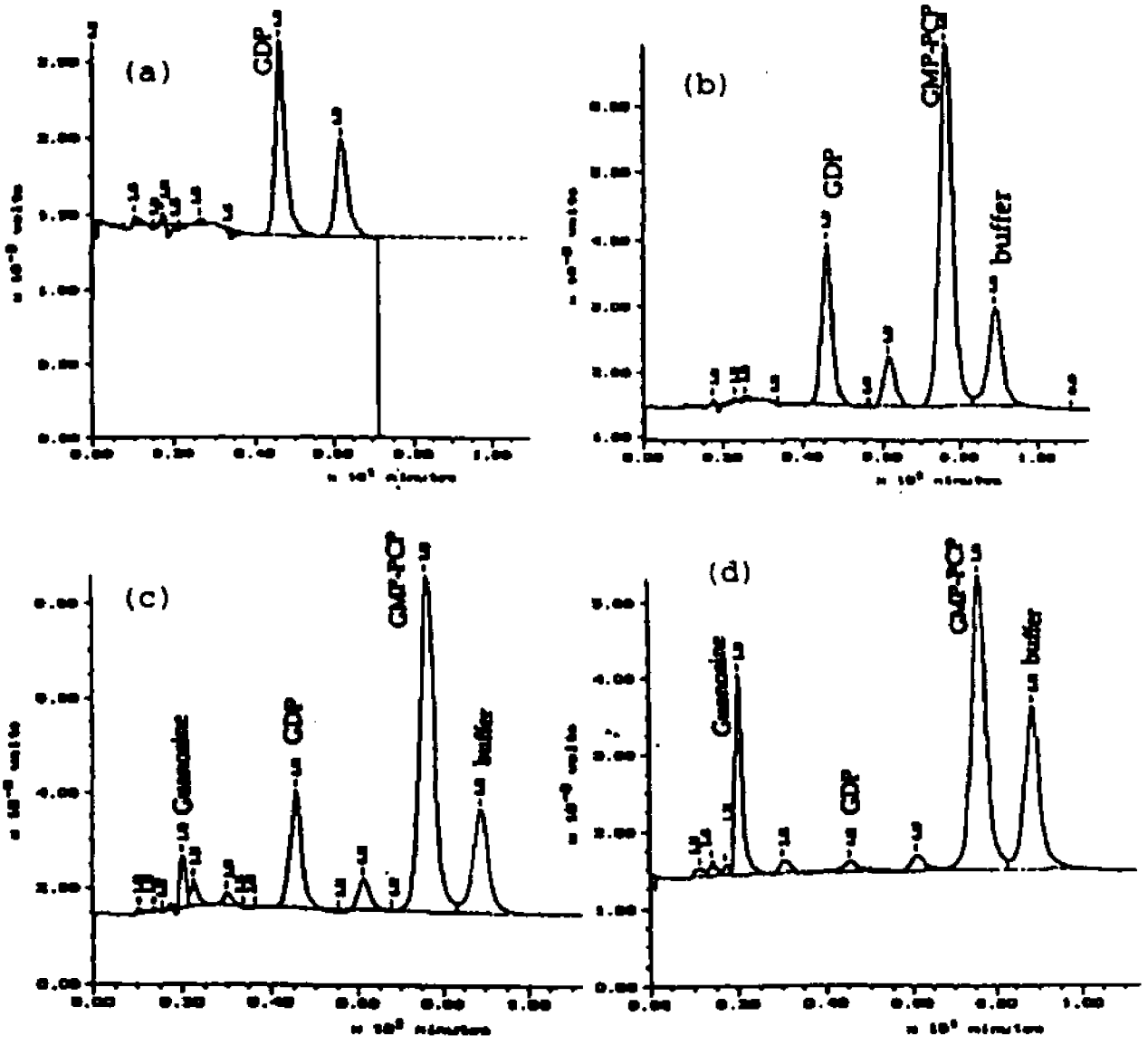

Figure 3.2 HPLC chromatography on making p21·GMPPCP complex. (a) p21·GDP; (b) p21·GDP plus GMP-PCP and alkaline phosphotase at t=0 min; (c) Enzyme reaction at t=15 min; (d) Enzyme reaction at t=45 min when all GDP are converted to GMP.

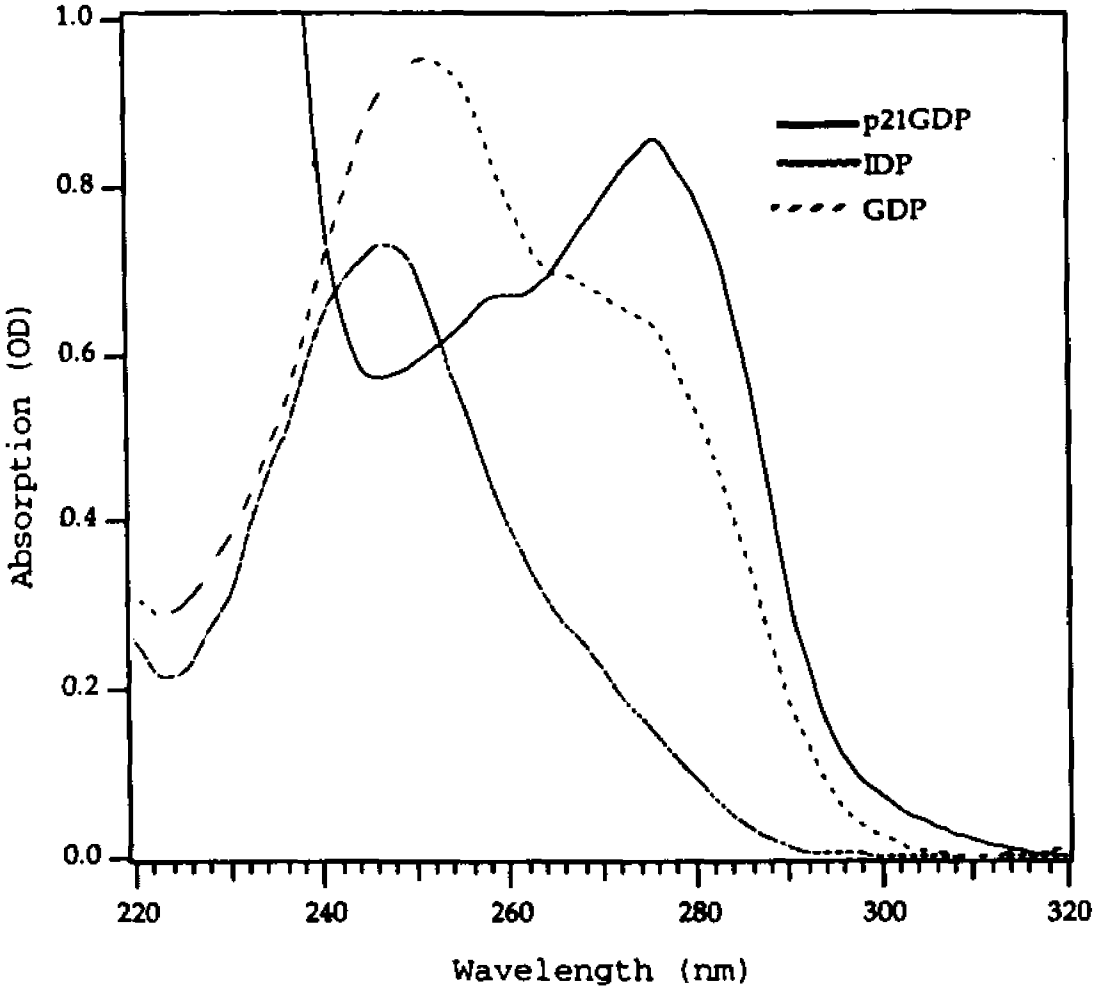

Figure 3.3 UV Absorption of ras-p21•GDP, GDP and IDP. The extinction coefficients are:

18,450 $M^{-1}cm^{-1}$ at 280 nm for ras-p21;

13,7000 $M^{-1}cm^{-1}$ at 254 nm for GDP;

12,4000 $M^{-1}cm^{-1}$ at 242 nm for IDP.

Chapter 4

RAMAN STUDIES OF PHOSPHATE COMPOUNDS

A clear knowledge of the chemical properties of phosphate is of great importance in studies of biological reaction involving phosphate groups. Studies on nucleic acid model compounds, nucleotides and oligonucleotides have been extensively carried out by many different methods due to their biological importance (Brown, E. B. et al., 1965; Taga, K. et al., 1988; Van Der Veken, B. J., et al., 1986; Matthies, M. et al., 1979). The conformational structure of phosphate backbones, for example, are important in biological systems in the nature of the nucleic acids and phospholipids. ATP is an energy transfer agent in biological systems. In order to understand the nature and mechanism of ATP hydrolysis and energy transfer, it is important to know the interactions involved in the phosphate moiety of ATP (Lane, M. J., 1979; White, J. C. et al., 1987; Lanir, A. et al., 1979; Lewis, A. et al., 1975; Zhelyyaskov, V. et al., 1992). As discussed in Chapter 1, G proteins play an important role in signal transduction, and they are tightly regulated by the nature of guanine nucleotides. As such, it is very important to study the specific chemical properties of phosphate of guanine nucleotides in order to understand the mechanism of GTP hydrolysis.

In pursuit of this goal, both experimental and theoretical approaches have been used to investigate the structure of different phosphate model compounds (Ramia, L. et al., 1969; Heyde, M. E. et al., 1971; Tajmir-Riahi, H. A. et al., 1984, 1988). X-ray diffraction is successfully applied to a number of biological polymers to yield the detailed molecular structures of these materials with fine information about their structures. An enzyme, for example, and its functioning as a catalyst of a biochemical reaction can be elucidated in more definite fashion than can be done in absence of such information. However, there are two practical limitations to the X-ray crystallographic approach: firstly, it is a time-consuming and complicated procedure and, secondly, it can be applied only to crystallizable systems. For some biological compounds, the structural differences between aqueous solution state and crystalline state may be significant. Vibrational spectroscopy has been successfully used to solve this latter problem giving the structural information in aqueous solution.

Here we present Raman studies on a series of phosphate model compounds. The goal of this investigation is to establish the correlation between vibrational spectra and specific structural features of nucleotides and other phosphate compounds.

4.1 Raman Spectra of Mono-phosphate Compounds

4.1.1 Raman Spectra of PO_4^{3-}, HPO_4^{2-}, $H_2PO_4^-$ and H_3PO_4 in Solution

Figures 4.1 and 4.2 show the parallel and perpendicular components of the polarized Raman spectra of PO_4^{3-}, HPO_4^{2-}, $H_2PO_4^-$ and H_3PO_4 respectively. Figures 4.3 and 4.4 show the similar spectra while the oxygen atoms are replaced by ^{18}O.

Most of phosphate bands appear in the region 200 cm^{-1} - 1200 cm^{-1}. Due to the strong Raleigh scattering, we can not take the Raman spectrum lower than 300 cm^{-1} in solution.

In Figure 4.1a and Figure 4.2a, the band at 937 cm^{-1}, which is polarized, is assigned to the P=O symmetric stretching mode of PO_4^{3-} group. This mode shifts down 52 cm^{-1} to 885 cm^{-1} when ^{16}O atoms are replaced by ^{18}O (Fig. 4.3a, Fig. 4.4a). The band at 1010 cm^{-1}, which is depolarized, is assigned as a degenerate asymmetric P=O stretching mode. In principle, PO_4^{3-} has T_d symmetry, so one symmetric mode and one degenerate asymmetric P=O stretching mode are expected. In practice, however, the degenerate modes are often inequivalent and can give rise to three closely spaced Raman bands, all of which are depolarized (Guan, Y. et al., 1994; Van Der Veken, B. J. et al., 1986). This may account for the broadness of the observed degenerate band to the PO_4^{3-} spectra. This band shifts down to 978 cm^{-1} due to the heavier mass of the ^{18}O labeling (Fig. 4.3a, Fig. 4.4a). Because of the tetrahedral symmetry of PO_4^{3-}, there are one three-fold

and one two-fold degenerate deformation modes, which appear at 553 cm^{-1} and 418 cm^{-1} (Fig. 4.1a, Fig. 4.2a) respectively. They shift down to 534 cm^{-1} and 398 cm^{-1} respectively, in ^{18}O labeling spectra in Figure 4.3a and Figure 4.4a.

Figures 4.1b, 4.2b, 4.3b, and 4.4b show the spectra of HPO_4^{2-} and $HP^{18}O_4^{2-}$ at pH 9.5 when one oxygen atom is protonated. The band at 989 cm^{-1} (Fig 4.1b, 4.2b), which is polarized, is assigned to symmetric P=O stretching mode of PO_3^- group. This group has a local C_{3v} symmetry and we expect another degenerate mode above this band. The band at 1084 cm^{-1}, which is depolarized, is assigned to this degenerate P=O stretching mode. The bands at 393 cm^{-1} and 533 cm^{-1} are assigned to the two-fold degenerate O-P=O deformation mode and the symmetric O=P=O deformation mode overlapping with another two-fold degenerate O=P=O deformation mode respectively. The band at 858 cm^{-1} is assigned to P-O single bond stretching mode. All these modes have large shifts upon the ^{18}O labeling (Figures 4.3b and 4.4b). The symmetric and degenerate P=O stretching modes at 990 cm^{-1} and 1084 cm^{-1} shift down to 950 cm^{-1} and 1052 cm^{-1} respectively. The two degenerate deformation modes of PO_3^{2-} group at 533 cm^{-1} and 393 cm^{-1} shift down to 512 cm^{-1} and 377 cm^{-1}, respectively, upon ^{18}O replacement.

Raman spectra of $H_2PO_4^-$ and $H_2P^{18}O_4^-$ at pH 4.5 are shown in Figures 4.1c, 4.2c, 4.3c and 4.4c. P=O stretching modes of the PO_2^- group are expected to occur in the region of 1000-1200 cm^{-1} (Guan, Y. et al., 1994). The band at 1077 cm^{-1}

$^{-1}$, which has polarization ratio less than 0.75, is assigned to the symmetric P=O stretching mode of the PO_2^- group. The depolarized band at 1162 cm^{-1} is assigned to the asymmetric P=O stretching mode. These two modes shift down to 1040 cm^{-1} and 1136 cm^{-1} respectively due to ^{18}O labeling (Fig. 4.3c, 4.4c). P-O stretching vibrations of the H-O-P-O-H group are expected to occur in the 800-1000 cm^{-1} region. The bands at 878 cm^{-1} and 944 cm^{-1} are thus assigned to the symmetric stretching mode and the asymmetric stretching modes of O-P-O group. These two modes shift down to 838 cm^{-1} and 918 cm^{-1} respectively in the spectra of ^{18}O labeled $H_2PO_4^-$. The deformation modes are in the 300-600 cm^{-1} region. The band at 516 cm^{-1} is assigned to bending mode of PO_2^- group, and bands at 390 cm^{-1} and 377 cm^{-1} are assigned to be the twist modes of PO_2^- and bending mode of O-P-O group, these modes shift down to 495 cm^{-1}, 371 cm^{-1} and 354 cm^{-1} respectively upon the ^{18}O substitution.

Figures 4.1d, 4.2d, 4.3d, and 4.4d show the Raman spectra of H_3PO_4 and $H_3P^{18}O_4$. The band at 1177 cm^{-1} is assigned to the P=O stretching mode. The band at 890 cm^{-1} is assigned to P-O symmetric stretching mode of $(POH)_3$ group, and the band at 1010 cm^{-1} is assigned to degenerate asymmetric stretching mode of this group. These bands shift down to 1143 cm^{-1}, 849 cm^{-1} and 980 cm^{-1} respectively in ^{18}O substitution Raman spectra (Fig. 4.3d, 4.4d). The band at 500 cm^{-1} is assigned to the O-P=O deformation mode, and the band at 375 cm^{-1} with two shoulders at 357 cm^{-1} and 392 cm^{-1} are assigned to those

O-P-O deformation modes. These modes shift down to 483 cm^{-1}, 374 cm^{-1} and 350 cm^{-1}, respectively upon 18O labeling (Figure 4.3d and Figure 4.4d).

Table 4.1 shows the summary of the assignments of PO_4^{3-}, HPO_4^{2-}, $H_2PO_4^-$, H_3PO_4 and their ^{18}O substitution compounds.

4.1.2 Raman Spectra of Methyl Phosphate and its Isotopomers in Solution

Figures 4.5 and 4.6 show the parallel and perpendicular components of $CH_3OPO_3^{2-}$ (MP), $CH_3{}^{18}OPO_3^{2-}$ (MOP), $CH_3OP^{18}O_3^{2-}$ (MPO) and $CD_3OPO_3^{2-}$ (MDP) respectively. The ($-PO_3^{2-}$) group has a local C_{3v} symmetry. So we expect a symmetric mode and a degenerate stretching mode for this group. The polarized band at 984 cm^{-1} in $CH_3OPO_3^{2-}$ shifts down to 949 cm^{-1} in $CH_3OP^{18}O_3^{2-}$ and remains in almost the same position in $CH_3{}^{18}OPO_3^{2-}$ and $CD_3OPO_3^{2-}$. This band is assigned to P=O symmetric stretching mode of the PO_3^{2-} group. The broad, depolarized band around 1100 cm^{-1} (Figure 4.6a) in $CH_3OPO_3^{2-}$ is thus assigned to the degenerate mode of the PO_3^{2-} group, and shifts down to ~ 1080 cm^{-1} in $CH_3OP^{18}O_3^{2-}$, where it overlappes with the 1054 cm^{-1} band. The band at 1055 cm^{-1} is assigned to C-O stretching mode, and shifts down to 1025 cm^{-1} in $CH_3{}^{18}OPO_3^{2-}$. The band at 761 cm^{-1} in $CH_3OPO_3^{2-}$ shifts down to 745 cm^{-1} in $CH_3{}^{18}OPO_3^{2-}$. This band is assigned to a P-O single bond stretching mode. It also shifts down to 757 cm^{-1} and

728 cm^{-1} respectively in $CH_3OP^{18}O_3^{2-}$ and $CD_3OPO_3^{2-}$ due to the coupling between the PO_3^{2-} group and the CH_3 group

Because of the local C_{3v} symmetry of $-PO_3^{2-}$ group, two two-fold deformation modes and one symmetric deformation mode are expected to occur in the region between 300 cm^{-1} and 600 cm^{-1}. The band at 398 cm^{-1} in $CH_3OPO_3^{2-}$ is assigned to one two-fold O-P=O deformation mode of $-PO_3^{2-}$ group (Fig 4.5, 4.6). It shifts down to 392 cm^{-1}, 387 cm^{-1} and 390 cm^{-1} respectively in $CH_3{}^{18}OPO_3^{2-}$, $CH_3OP^{18}O_3^{2-}$ and $CD_3OPO_3^{2-}$. The band at 519 cm^{-1} in $CH_3OPO_3^{2-}$ is assigned to the symmetric $-PO_3^{2-}$ bending mode, and shifts down to 510 cm^{-1}, 502 cm^{-1}, and 515 cm^{-1} respectively in $CH_3{}^{18}OPO_3^{2-}$, $CH_3OP^{18}O_3^{2-}$ and $CD_3OPO_3^{2-}$. The band at 559 cm^{-1} in $CH_3OPO_3^{2-}$ is assigned to the other two-fold degenerate O=P=O deformation mode of $-PO_3^{2-}$ group. It shifts down to 550 cm^{-1}, 550 cm^{-1} and 548 cm^{-1} respectively in $CH_3{}^{18}OPO_3^{2-}$, $CH_3OP^{18}O_3^{2-}$ and $CD_3OPO_3^{2-}$. These two-fold degenerate deformation modes of the $-PO_3^{2-}$ group are depolarized, while the symmetric deformation mode is polarized.

The depolarized bands at 1162 cm^{-1} and 1189 cm^{-1} in $CH_3OPO_3^{2-}$ shift down to 902 cm^{-1} and 939 cm^{-1} respectively in $CD_3OPO_3^{2-}$, and exhibit virtually no shift in $CH_3{}^{18}OPO_3^{2-}$ and $CH_3OP^{18}O_3^{2-}$. Therefore, these bands are assigned to asymmetric CH_3 rocking modes. The bands at 1450 cm^{-1} and 1464 cm^{-1} in $CH_3OPO_3^{2-}$ (Fig. 4.7) are assigned to the symmetric and degenerate CH_3 deformation vibrations. These mode are expected to shift down to a region around 1100 cm^{-1} in $CD_3OP_3^{2-}$, where

they overlap with the C-O stretching and degenerate PO_3^- stretching modes.

The region between 2950-3100 cm^{-1} of the Raman spectra of $CH_3OPO_3^{2-}$ and $CD_3OPO_3^{2-}$ (Fig. 4.9) show the typical five-band pattern expected for C-H stretching vibrations of the methyl group (Bellamy, L. J. 1968). The depolarized band at 3006 cm^{-1} is assigned to the degenerate C-H stretching vibrations. It shifts down to 2254 cm^{-1} in $CD_3OPO_3^{2-}$. The bands at 2954 cm^{-1} and 2849 cm^{-1} exhibit nearly equivalent intensities and both are polarized, contrary to the expectation of having only one intense and polarized Raman band, due to the CH_3 symmetric stretching mode. These two polarized bands are assigned as a Fermi doublet. They shift down to 2227 cm^{-1} and 2141 cm^{-1} respectively in $CD_3OPO_3^{2-}$ (Guan, Y. et al., 1994; Colthup, N. B. et al., 1990).

Table 4.2 shows the assignments of the Raman bands of methyl phosphate and its isotopomers.

4.1.3 Raman Spectra of Methyl Phosphate and its Isotopomers in Crystal

Figure 4.10 shows the Raman spectra of crystalline $CH_3OPO_3^{2-}$, $CH_3{}^{18}OPO_3^{2-}$, $CH_3OP^{18}O_3^{2-}$, and $CD_3OPO_3^{2-}$. In general, the Raman bands in crystal are sharper than those in solution. The positions of the crystal form phosphate bands are somewhat altered because of the crystal packing and different hydrogen bondingenvironment compared to solution. Most

important, the two broad bands from degenerate modes in 300-600 cm^{-1} region in solution spectra are resolved and appear as several sharper bands here in crystal. The broad band at 519 cm^{-1} in the solution spectrum of $CH_3OPO_3^{2-}$ splits into three bands at 512 cm^{-1}, 536 cm^{-1} and 550 cm^{-1} in crystal. The band at 512 cm^{-1} is assigned to symmetric deformation of PO_3^{2-} group and the band at 536 cm^{-1} and 550 cm^{-1} are assigned to the asymmetric deformation vibrations of this group. The band at 398 cm^{-1} in solution of $CH_3OPO_3^{2-}$ splits into two bands at 386 cm^{-1} and 411 cm^{-1} in the crystal form spectra respectively, and these bands are assigned to asymmetric rock vibrations of PO_3^{2-} group. All these modes have large down shifts in $CH_3OP^{18}O_3^{2-}$, and have less changes in $CD_3OPO_3^{-}$ and $CH_3{}^{18}OPO_3^{2-}$. In the Raman spectra of $CH_3{}^{18}OPO_3^{2-}$ in crystal, the PO_3^{2-} symmetric stretching band is split to two bands at 968 cm^{-1} and 959 cm^{-1}. This may be due to the inhomogeneous of the crystal, which changes the symmetry of the compound. We have observed the same effect in some other phosphate compound crystal or powder spectra.

4.1.4 The Relationship between P=O Bond Order and pK_a of the Leaving Group

It is interesting to know whether the P-O bond order of R-O-P group in R-O-PO_3^{2-} type compounds is related with the pK_a of the corresponding R-O-H compounds. As we have discussed above, Raman spectroscopy can directly measure the

P=O vibrational frequencies, which is directly related with the bond order of the P=O bond. We take the Raman spectra of a series of R-O-PO_3^{2-} compounds corresponding to R-O-H compounds with different Pk_a values, and we can get the relationship between the Pk_a of the corresponding R-O-H compounds and the P=O bond orders from the relative positions of Raman frequencies.

Figures 4.11 and 4.12 show the Raman spectra of acetic phosphate, phenyl phosphate and 4-nitrophenyl phosphate at unprotonated state and protonated state of PO_3^{2-} group respectively. The Pk_a values of corresponding compounds (Acetic Acid, Phenol, and 4-Nitrophenol) are 4.7, 10.0 and 7.15 respectively. Comparing Figure 4.11 with Figure 4.12, we have found that the band at 984 cm^{-1} in acetic phosphate in unprotonated state of the PO_3^{2-} group (Figure.4.11a) disappears in the protonated state of the PO_3-H group (Fig.4.12a). We thus assigned this band as the symmetric P=O stretching vibration of the PO_3^{2-} group. The band at 984 cm^{-1} remains at the same position in acetic phosphate, phenyl phosphate and 4-nitrophenyl phosphate. This suggests that all these three compounds have the same symmetric stretching vibrational frequency, thus the P=O symmetric stretching vibrational frequencies are not related with the pK_a of the corresponding R-O-H compounds.

Figure 4.24 shows the IR spectra of methylphosphate (corresponding R-O-H compound, methanol, has a pK_a around 15.5), acetic phosphate, phenyl phosphate and 4-nitrophenyl

phosphate in unprotonated state. The broad bands around 1100 cm^{-1} are assigned to be the double degenerate P=O asymmetric stretching vibrational modes for these phosphate compounds. Two bands appear at 1090 cm^{-1} and 1110 cm^{-1} in methylphosphate vibrational spectrum, and we take an average of 1100 cm^{-1} for the double degenerate P=O asymmetric vibrational frequencies of methyl phosphate. The sharp band at 1115 cm^{-1} in 4-nitrophenyl phosphate vibrational spectrum is not from phosphate moiety. We take an average of 1121 cm^{-1} for the double degenerate P=O asymmetric vibrational frequencies of 4-nitrophenyl phosphate. The P=O asymmetric vibrational frequencies of these phosphate compounds decrease when the pK_a of their corresponding R-O-H compounds increase. We use the average of the P=O symmetric frequency [ν_s(P=O)] and the P=O asymmetric frequencies [ν_a(P=O)] to represent the P=O stretching vibrational frequency [ν(P=O)], which is

$$\nu^2(P=O) = [\nu_s^2(P=O) + 2\nu_a^2(P=O)]/3 \quad \ldots (4.1)$$

The square of ν(P=O) is linearly related with the pK_a of their corresponding R-O-H compounds. Figure 4.25 shows the curve fitting of the square of ν(P=O) of the phosphate compounds versus the pK_a of their corresponding R-O-H compounds.

Since the P=O bond order is directly related with the P=O force constant, which is directly proportional to the square of P=O vibrational frequency, the P=O bond order of

these phosphate compounds is also linearly related with the pK_a of their corresponding R-O-H compounds.

We can estimate the P-O bond order from the P=O bond order by using an empirical rule, which is the sum of PO bond order of $O\text{-}PO_3^{2-}$ group (i.e. the sum of the P-O single bond order and three P=O double bond orders), remains as close as possible to 5 vu. (Deng, H. et al., 1993; Ray, J. et al., 1993). So the -O-P- bond order of these phosphate compounds is also linearly related with the pK_a of their corresponding R-O-H compounds.

However, the observed P-O vibrational frequencies of these phosphate are not linearly related with the pK_a of their corresponding R-O-H compounds. The P-O vibrational frequencies of methyl phosphate, acetic phosphate, phenyl phosphate and 4-nitrophenyl phosphate in unprotonated state are 761 cm^{-1}, 735 cm^{-1}, 727 cm^{-1} amd 734 cm^{-1}, respectively. This is due to the fact that the P-O vibrational mode is coupled with the C-O-P vibrational mode. The coupling effect, rather than the change of force constant or P-O bond order, changes the P-O vibrational frequencies. This result is confirmed by the normal mode analysis in Chapter 5.

4.2 Raman Spectra of Diphosphate Compounds

Figures 4.13 and 4.14 show the Raman spectra of ADP, GDP and IDP at pH 7.5 and pH 5 respectively. The terminal

PO_3 group is unprotonated at pH 7.5 and is protonated at pH 5 because the pK_a of the terminal phosphate PO_3 group is around 6.3. The bands at 943 cm^{-1} in all three spectra in Figure 4.13 disappear in the corresponding spectra shown in Figure 4.14 when the terminal PO_3^{2-} groups are protonated. We thus assign these band as the P=O symmetric stretching vibration of PO_3^{2-} groups. The bands at 1087 cm^{-1} at pH 7.5, shift up to 1108 cm^{-1} at pH 5. These bands at 1087 cm^{-1} at pH 7.5 are assigned to α-PO_2^- symmetric stretching, and the bands at 1108 cm^{-1} at pH 5 are assigned to α-PO_2^- and β-PO_2^- in-phase symmetric stretching vibration. (Heyde, M. E. et al., 1971; Raimai, L. et al., 1969; Takeuchi, H. et al., 1988). These assignment are confirmed by ^{18}O labeling Raman difference spectra of GDP.

Figures 4.17 and 4.18 show the spectra of GDP, β-$^{18}O_3$-GDP and their difference spectrum at pH 7.5 and pH 5 respectively. In the difference spectrum between GDP and β-$^{18}O_3$-GDP at pH 7.5 (Fig. 4.17c), there are two major derivative-like bands. One has a positive peak at 945 cm^{-1} and a negative peak at 921 cm^{-1}, and the other has a positive peak at 1095 cm^{-1} and a negative peak at 1071 cm^{-1}. The former derivative-like band is assigned to the P=O symmetric stretching vibration of PO_3^{2-} group, which disappears in the spectra at pH 5 (Fig. 5.17c); while the other is assigned to the α-PO_2^- symmetric stretching vibration. At pH 5, the derivative-like

band with a positive peak at 1111 cm^{-1} and a negative peak at 1097 cm^{-1} is thus assigned to the in-phase symmetric stretching vibrations of α-PO_2^- and β-PO_2^- groups.

Mg^{2+} remains at a relatively high concentration level in living cells and has a high affinity for GDP, GTP and other phosphate compounds. It is involved in the enzymatic hydrolysis of GDP and GTP, serving as a cofactor. Interactions of ATP with Mg^{2+} in aqueous solution have been studied intensively by spectroscopic methods, which have commonly shown that the adenine ring of ATP is not, or only negligibly, involved in the interaction with Mg^{2+}, but the triphosphate moiety interacts with the cation (Takeuchi, H. et al., 1988).

Figures 4.15 and 4.16 show the Raman spectra of ADP, GDP and IDP with 1:1 Mg^{2+} at pH 7.5 and pH 5. At pH 7.5, the bands at 943 cm^{-1} in Figure 4.13, which are assigned to the P=O symmetric stretching vibration of the terminal PO_3^- group, have almost no changes in the presence of Mg^{2+} in Figure 4.15. This may suggest that Mg^{2+} has little effect on the P=O symmetric stretching mode. Takeuchi and his colleague reported that the asymmetric P=O stretching vibrational mode of the terminal PO_3^{2-} group shifts up about 9 cm^{-1} due to the binding of Mg^{2+} in their IR studies of ATP. This suggests that the binding of Mg^{2+} only influence the P=O asymmetric vibrational mode, Which is not observed in our Raman spectra due to the less Raman effect of the asymmetric

band, while has little effect on the P=O symmetric vibrational mode. We have observed similar situation in our Raman studies of monophosphate (Section 4.1.4) that the P=O asymmetric mode changes while the P=O symmetric mode remains the same. The band at 1087 cm^{-1}, which are assigned to α-PO_2^- symmetric stretching vibrations, shift up to 1094 cm^{-1} in the presence of Mg^{2+} due to the interactions between α-PO_2^- groups and Mg^{2+}. At pH 5, the corresponding bands at 1108 cm^{-1} have little changes in the presence of Mg^{2+}. This suggests that the interactions between GDP and Mg^{2+} is stronger at pH 7.5 than that at pH 5. This conclution is similar to the result from the Raman and IR studies of ADP and ATP (Takeuchi, H. et al. 1988; Tajmir-Riahi, H. A. et al. 1988).

4.3 Raman Spectra of Triphosphate Compounds

Figures 4.19 and 4.20 show the Raman spectra of GTP, β-$^{18}O_3$-GTP and their difference spectrum at pH 7.5 and pH 5 respectively. The terminal phosphate is unprotonated at pH 7.5, and it is protonated at pH 5. The large derivative-like band with a positive peak at 1117 cm^{-1} and a negative peak at 1100 cm^{-1} at pH 7.5 is assigned to the in-phase symmetric stretching vibrations of α-PO_2^- and β-PO_2^- group. The corresponding band at pH 5, which has a positive peak at 1124 cm^{-1} and a negative peak at 1106 cm^{-1}, is assigned to the in-

phase symmetric stretching vibration of α-PO_2^-, β-PO_2^- and γ-PO_2^- group (Raimai, L. et al., 1969; Takeuchi, H. et al., 1988). The small derivative-like band, which has a positive peak at 704 cm^{-1}, and a negative peak at 684 cm^{-1} is assigned to the vibration involved with P_β-O-P_γ linkage.

Figures 4.21 and 4.22 show the Raman spectra of GTP, γ-$^{18}O_3$-GTP and their difference spectrum at pH 7.5 and pH 5. The derivative-like band at pH 7.5, which has a positive peak at 927 cm^{-1} and a negative peak at 901 cm^{-1}, is assigned to the P=O symmetric stretching vibration of the terminal PO_3^{2-} group. This peak vanishes in the spectra at pH 5. The derivative-like band with a positive peak at 1127 cm^{-1} and a negative peak at 1115 cm^{-1} at pH 5, is assigned to the in-phase symmetric stretching of α-PO_2^-, β-PO_2^- and γ-PO_2^- groups. This band appears at a position close to that in the difference spectra between GDP and β-$^{18}O_3$GTP at pH 5.

Figure 4.23 shows the spectra of GTP, β-$^{18}O_3$GTP, γ-$^{18}O_3$GTP, the difference spectrum between GTP and β-$^{18}O_3$GTP ,and the difference spectrum between GTP and γ-$^{18}O_3$GTP with 1:1 $MgCl_2$ at pH 7.5 respectively. In the difference spectrum between GTP and γ-$^{18}O_3$GTP with Mg^{2+}, the frequency of the P=O symmetric stretching mode of the PO_3^{2-} group remains at almost the same places as that in the spectrum without Mg^{2+}, but a new band with a positive peak at 1121 cm^{-1} and a nega-

tive peak at 1105 cm^{-1} appears (at least the intensity increases). This band is close to the position of the in-phase symmetric stretching vibration of the $-PO_2^-$ groups, and appears when GTP is protonated at pH 5. This may suggest that the interaction between Mg^{2+} and the terminal phosphate group PO_3^{2-} of GTP may have some degree of protonated effect. In the difference spectrum between GTP and β-$^{18}O_3$GTP with Mg^{2+}, the frequency of the in-phase symmetric stretching mode of α-PO_2^- and β-PO_2^- groups shifts up about 7 cm^{-1} due to the interactions between these groups and Mg^{2+} ion.

The P=O symmetric stretching mode of the PO_3^{2-} group in all the mono-phosphate compounds we studied appears in the region around 990 cm^{-1}. However, this mode has lower frequency in the di-phosphate and tri-phosphate compounds (around 943 cm^{-1} in GDP and 921 cm^{-1} in GTP). As normal mode calculation predict in Chapter 5, the frequency of the P=O stretching mode are largely affected by the coupling between different phosphate modes. So the downshift of the P=O symmetric stretching frequency in GDP and GTP may be due to the coupling between the terminal phosphate PO_3^{2-} group and the α-PO_2^- group, or the β-PO_2^- group, or both in GDP or GTP.

Table 4.1 Assignment of Raman bans in PO_4^{3-}, HPO_4^{2-}, $H_2PO_4^-$, H_3PO and their ^{18}O isotopic derivatives.

MODE	ν(cm-1) (non-labeled)	ν(cm-1) (^{18}O labeled)
(For PO_4^{3-})		
P=O symmetric stretch	937	885
P=O asymmetric stretch	1010	978
O=P=O bending (triple degenerate)	553	534
O=P=O bending (double degenerate)	418	398
(For HPO_4^{2-})		
P=O symmetric stretch	989	950
P=O asymmetric stretch	1084	1052
P-O stretch	858	833
O=P=O symmetric bending	533	512
O=P=O bending (double degenerate)	533	512
O-P=O bending (double degenerate)	393	377
(For $H_2PO_4^-$)		
P=O symmetric stretch	1077	1040
P=O asymmetric stretch	1162	1136
P-O symmetric stretch	878	838
P-O asymmetric stretch	944	918
O=P=O bending	516	495
O-P=O twist	390	371
O-P-O bending	377	354
(For H_3PO_4)		
P=O stretch	1177	1143
P-O symmetric stretch	890	849
P-O asymmetric stretch	1010	980
O-P=O bending	500	483
O-P-O bending	392	374
O-P-O bending	375	350
O-P-O bending	357	350

Table 4.2 Assignment of Raman bands of methyl phosphate and its ^{18}O labeled componds.

MODE	$\nu(cm^{-1})$ (MP)	$\nu(cm^{-1})$ (MOP)	$\nu(cm^{-1})$ (MPO)	$\nu(cm^{-1})$ (MDP)
P=O symmetric stretch	984	980	949	984
P=O asymmetric stretch	1100	1100	1080	1113
P-O stretch	761	745	757	728
O=P=O bending (double degenerate)	559	550	545	548
O=P=O symmetric bending	519	510	502	515
O-P=O bending (double degenerate)	398	392	387	390
C-O stretch	1055	1025	1054	1049
C-H rock	1162	1159	1162	902
C-H rock	1189	1182	1189	939
C-H bending	1450	1450	1450	---
C-H bending	1464	1464	1464	---
C-H symmetric stretch (Fermi doublet)	2954	---	---	2227
C-H symmetric stretch (Fermi doublet)	2849	---	---	2141
C-H asymmetric stretch	3006	---	---	2254

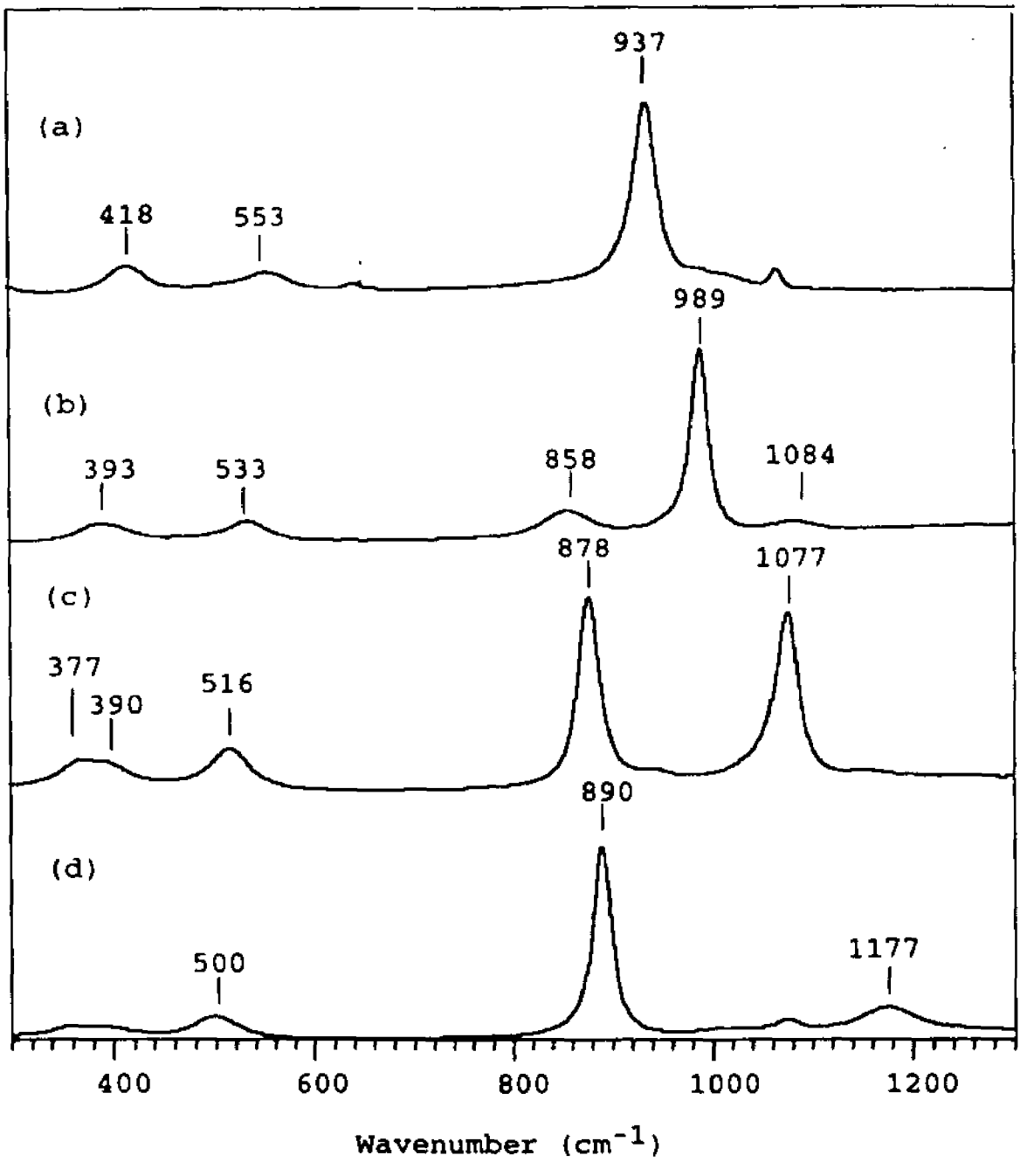

Figure 4.1 Parallel components of Raman spectra of (a) PO_4^{3-}; (b) HPO_4^{2-}; (c)$H_2PO_4^-$; (d) H_3PO_4 . Sample concentration: 0.5 M. Laser excitation: 514.5 nm, 200 mW. Room temperature.

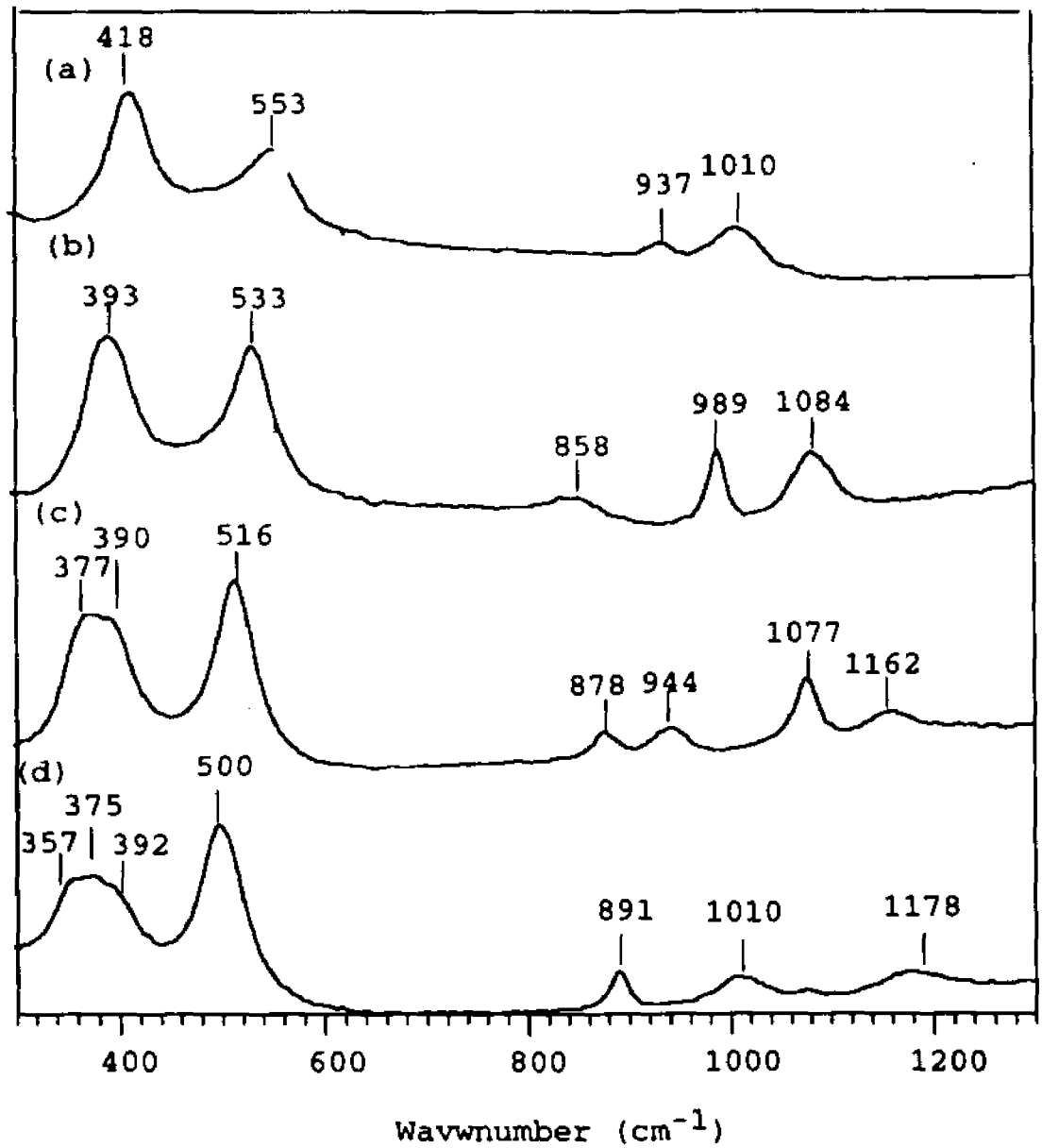

Figure 4.2 Perpendicular components of Raman spectra of (a) PO_4^{3-}; (b) HPO_4^{2-}; (c) $H_2PO_4^-$; (d) H_3PO_4. Sample concentration: 0.5 M. Laser excitation: 514.5 nm, 200 mW. Room Temperature.

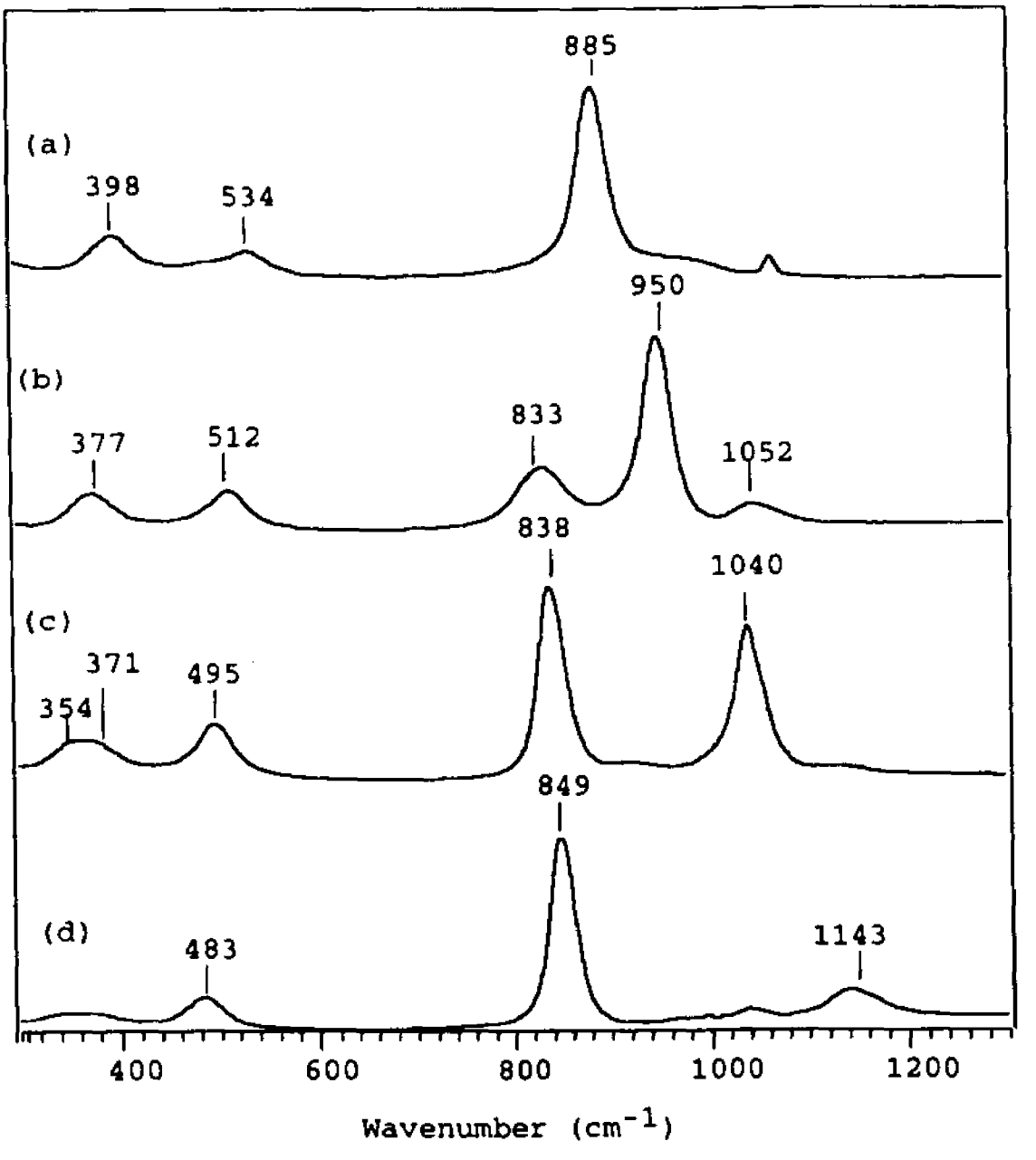

Figure 4.3 Parallel components of Raman spectra of (a) $P^{18}O_4^{3-}$; (b) $HP^{18}O_4^{2-}$; (c) $H_2P^{18}O_4^{-}$; (d) $H_3P^{18}O_4$.

Sample concentration: 0.5 M. Laser excitation: 514.5 nm, 200 mW. Room temperature.

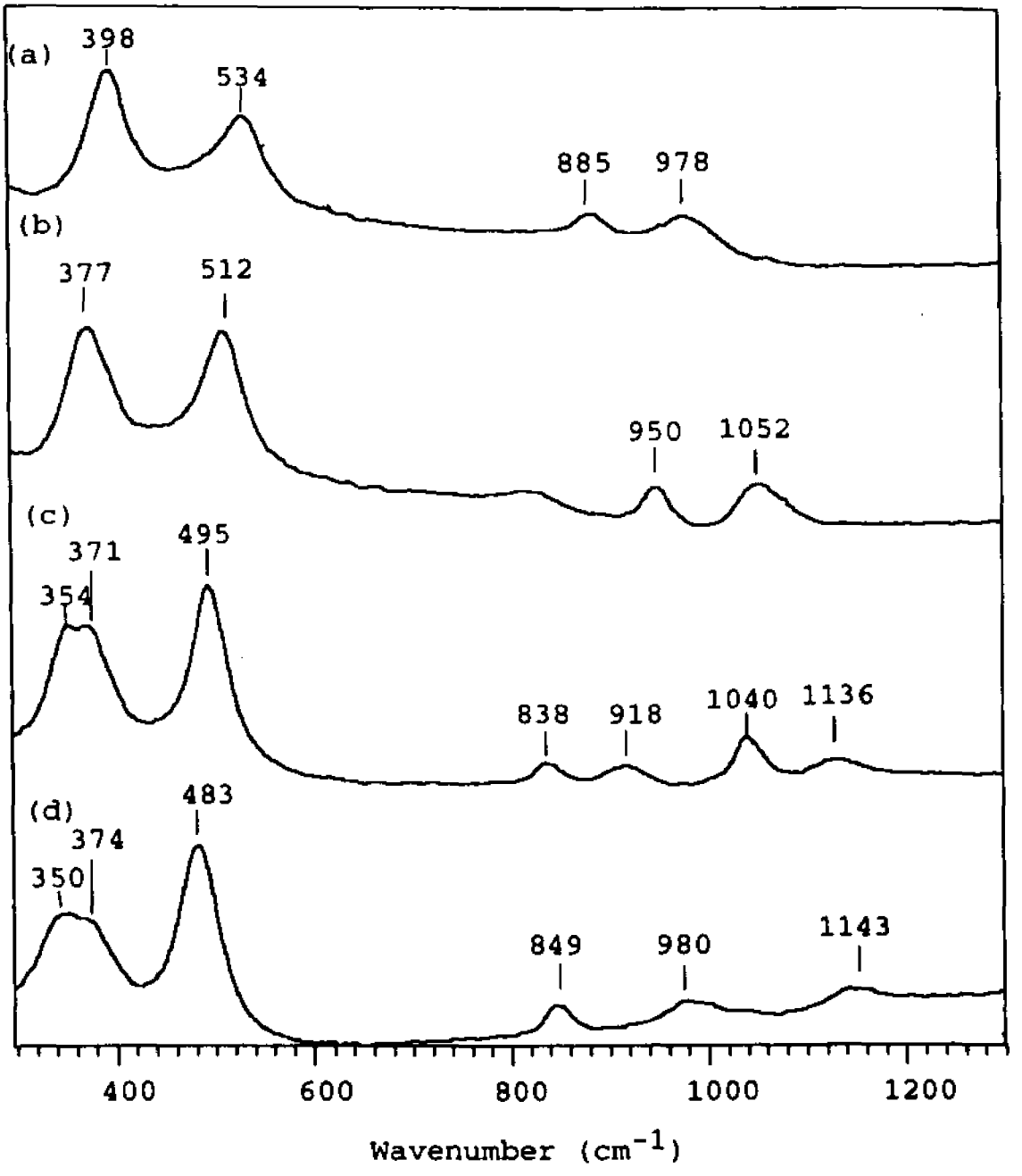

Figure 4.4 Perpendicular components of Raman spectra of (a) $P^{18}O_4^{3-}$; (b) $HP^{18}O_4^{2-}$; (c) $H_2P^{18}O_4^{-}$; (d) $H_3P^{18}O_4$.

Sample concentration: 0.5 M. Laser excitation: 514.5 nm, 200 mW. Room temperature.

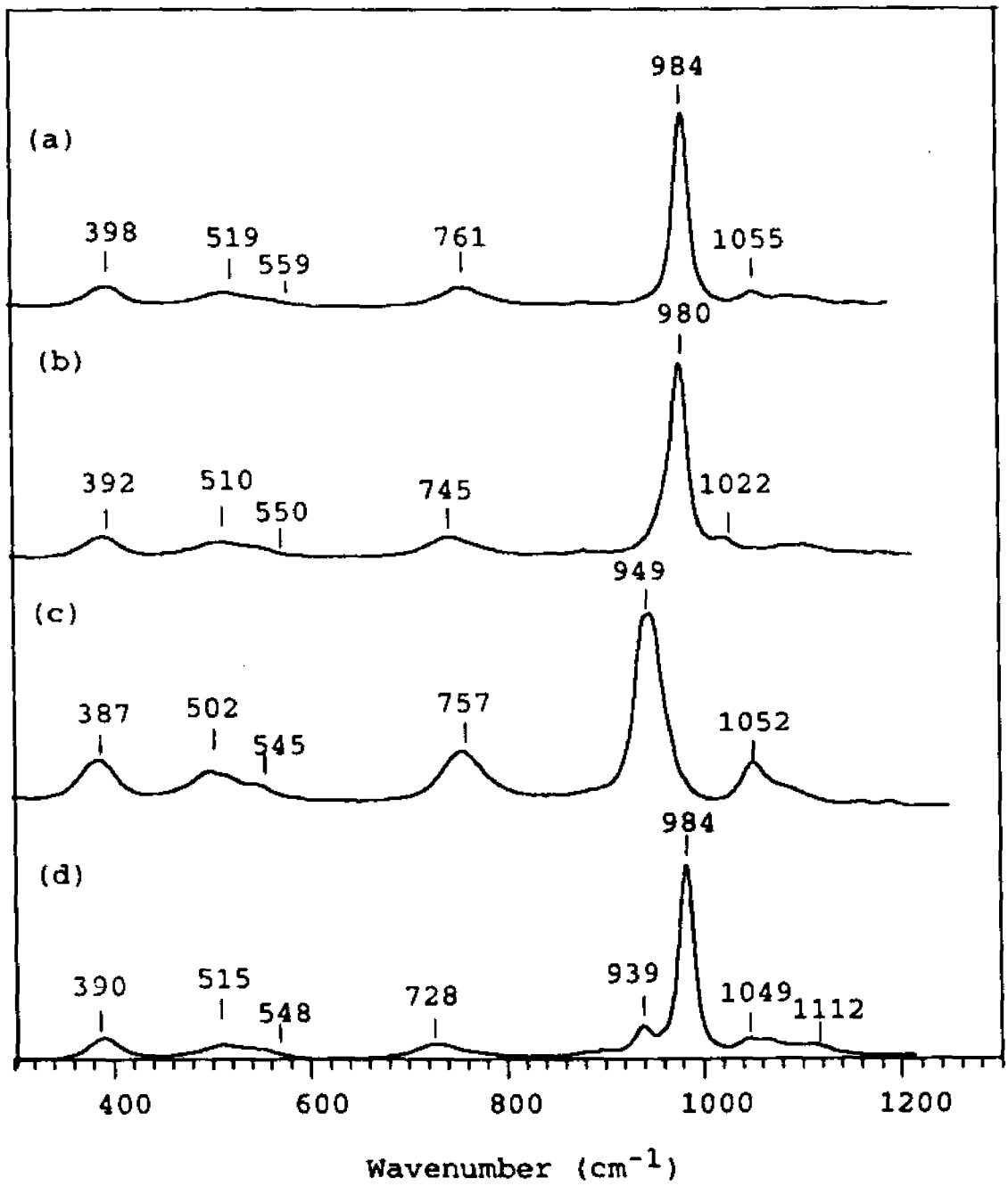

Figure 4.5 Parallel components of Raman spectra of (a) MP; (b) MOP; (c) MPO; (d) MDP. Sample concentration: 0.5 M. Laser excitation: 514.5 nm, 200 mW. Room temperature.

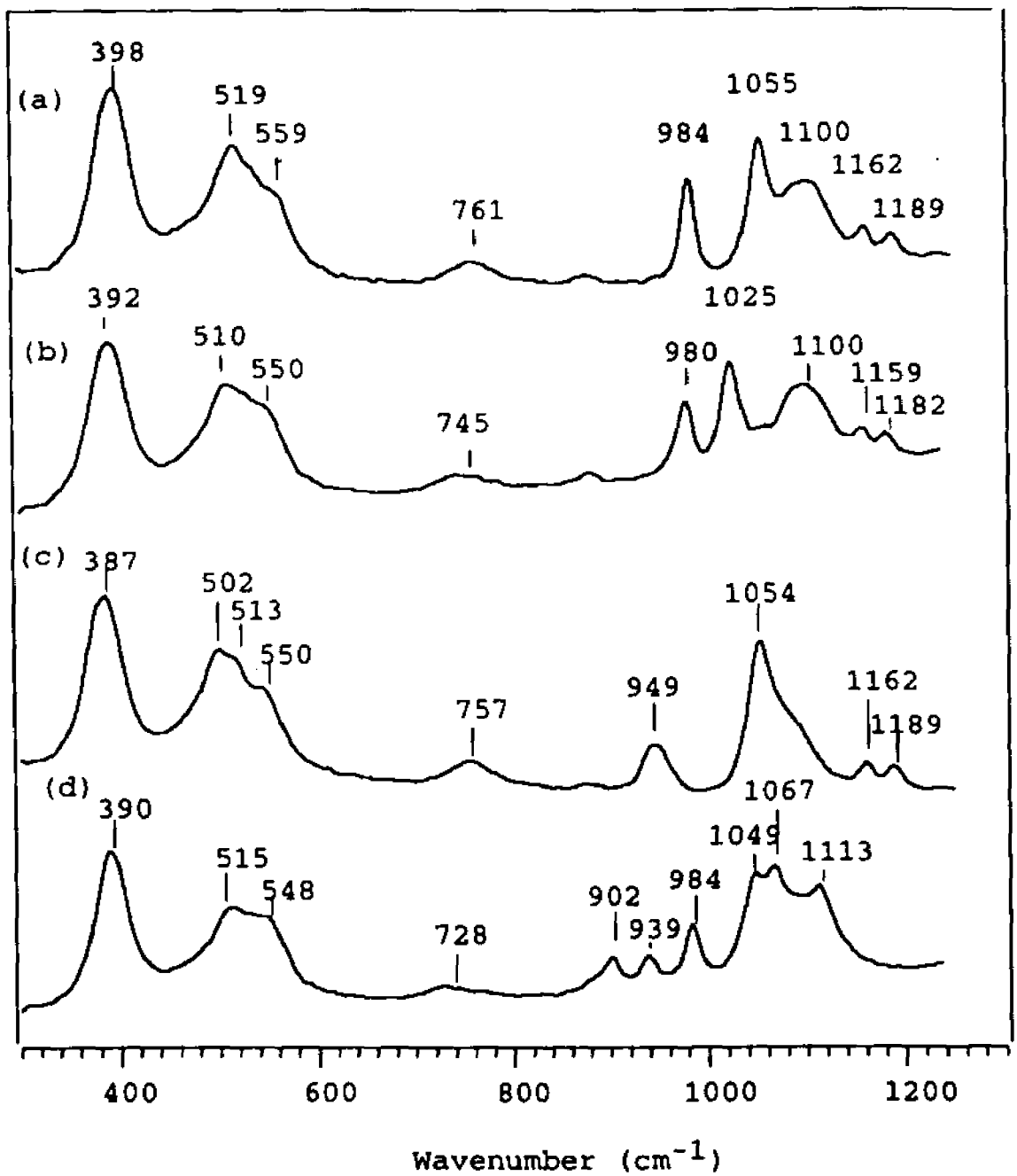

Figure 4.6 Perpendicualr components of Raman spectra of (a) MP; (b) MOP; (c) MPO; (d) MDP. Sample concentration: 0.5 M. Laser excitation: 514.5 nm, 200 mW. Room temperature.

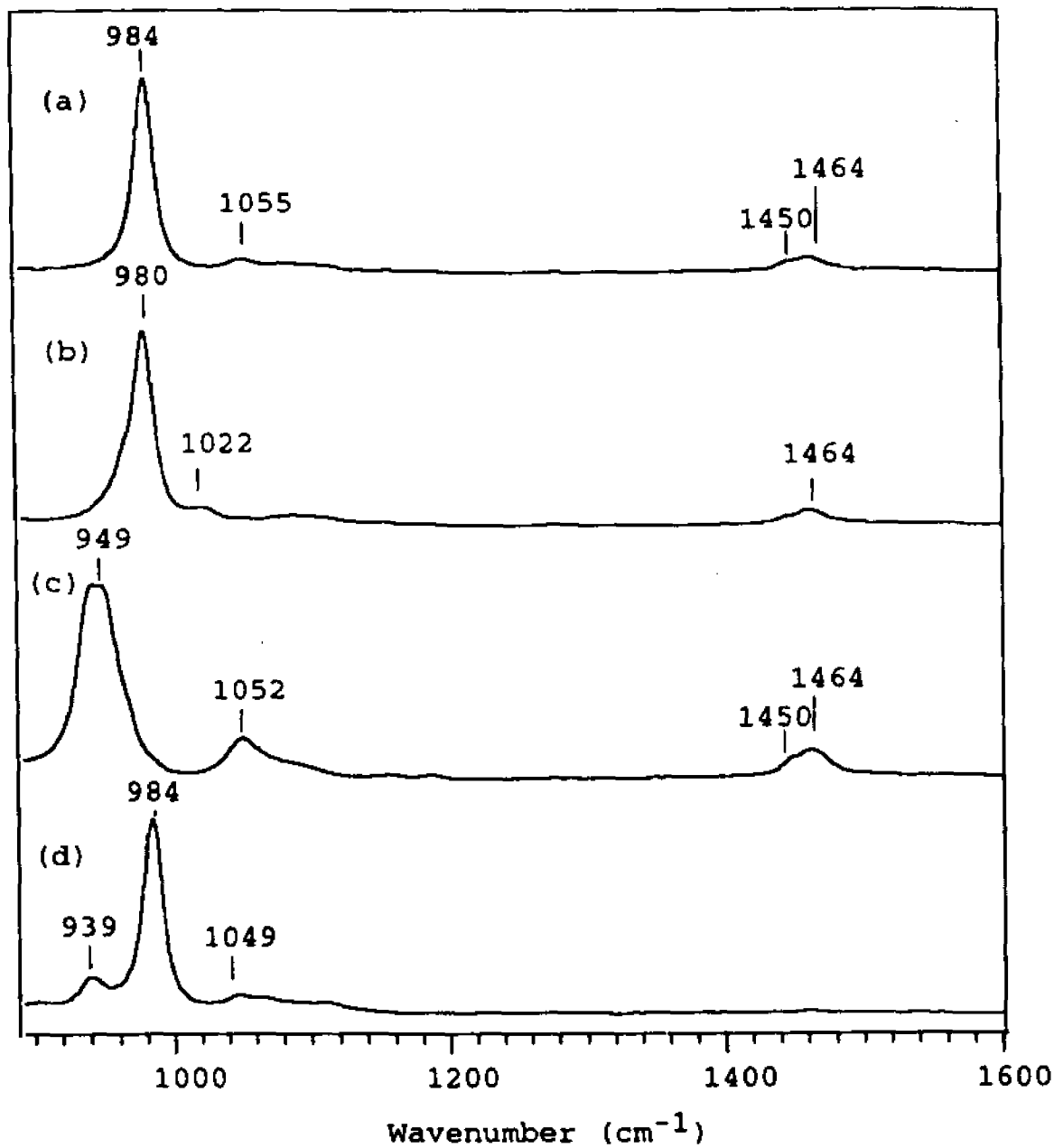

Figure 4.7 Parallel components of Raman spectra of (a) MP; (b) MOP; (c) MPO; (d) MDP. Sample concentration: 0.5 M. Laser excitation: 514.5 nm, 200 mW.

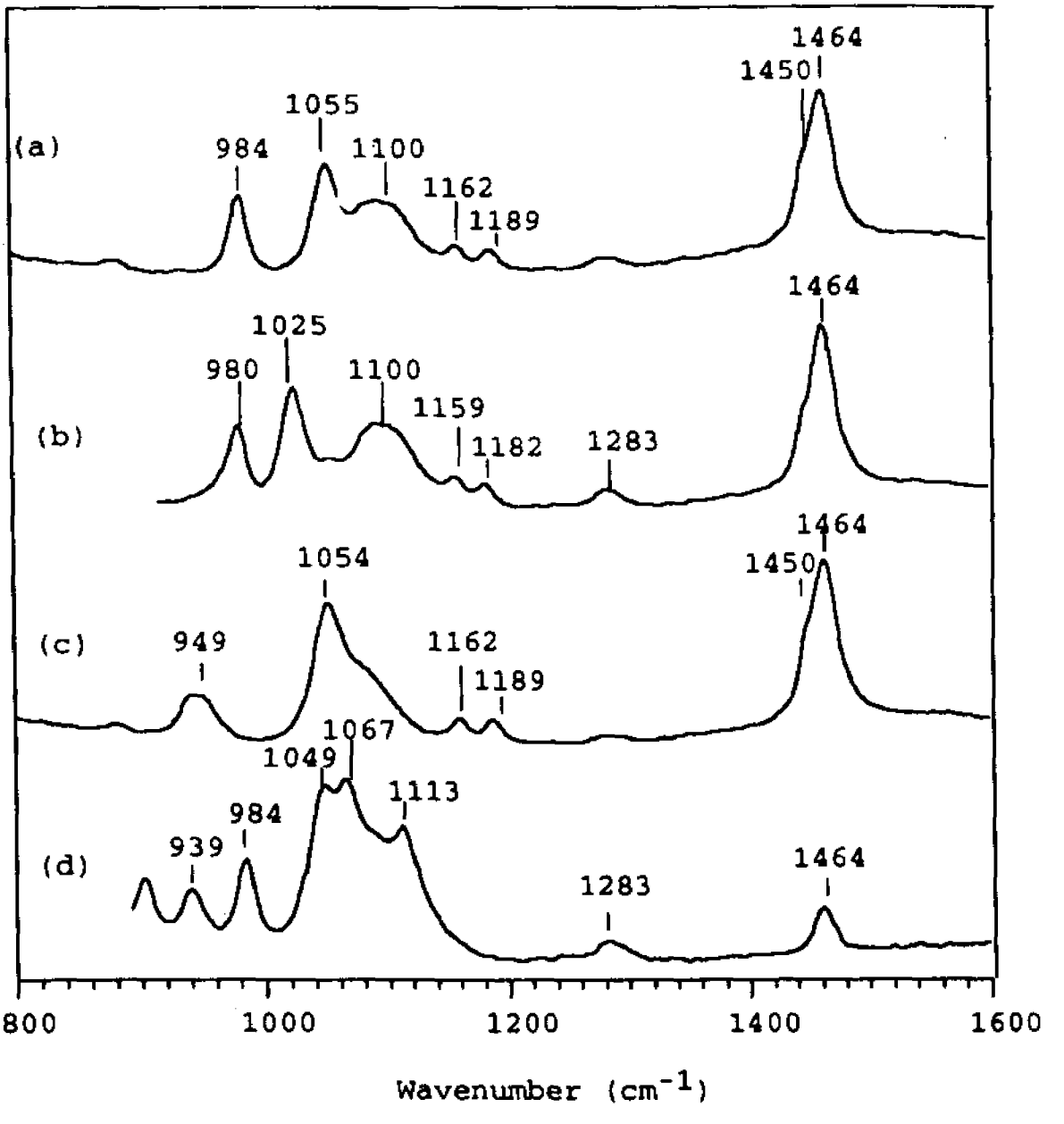

Figure 4.8 Perpendicular components of Raman spectra of (a) MP; (b) MOP; (c) MPO; (d) MDP. Sample concentration: 0.5 M. Laser excitation: 514.5, 200 mW.

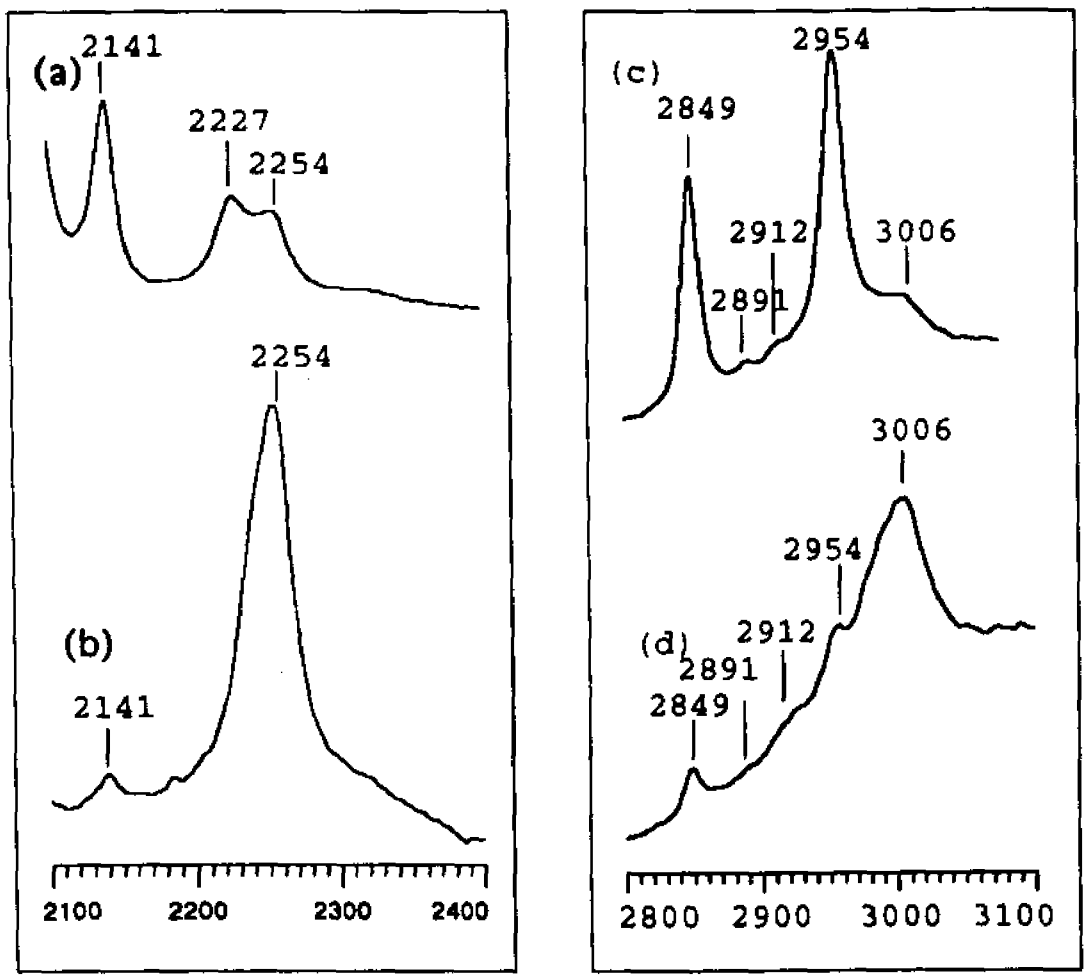

Figure 4.9 (a) Parallel and (b) perpendicular components of MDP; (c) Parallel and (d) perpendicular components of MP. Laser excitation: 514.5 nm, 200 mW.
Sample concentration: 0.5 M.

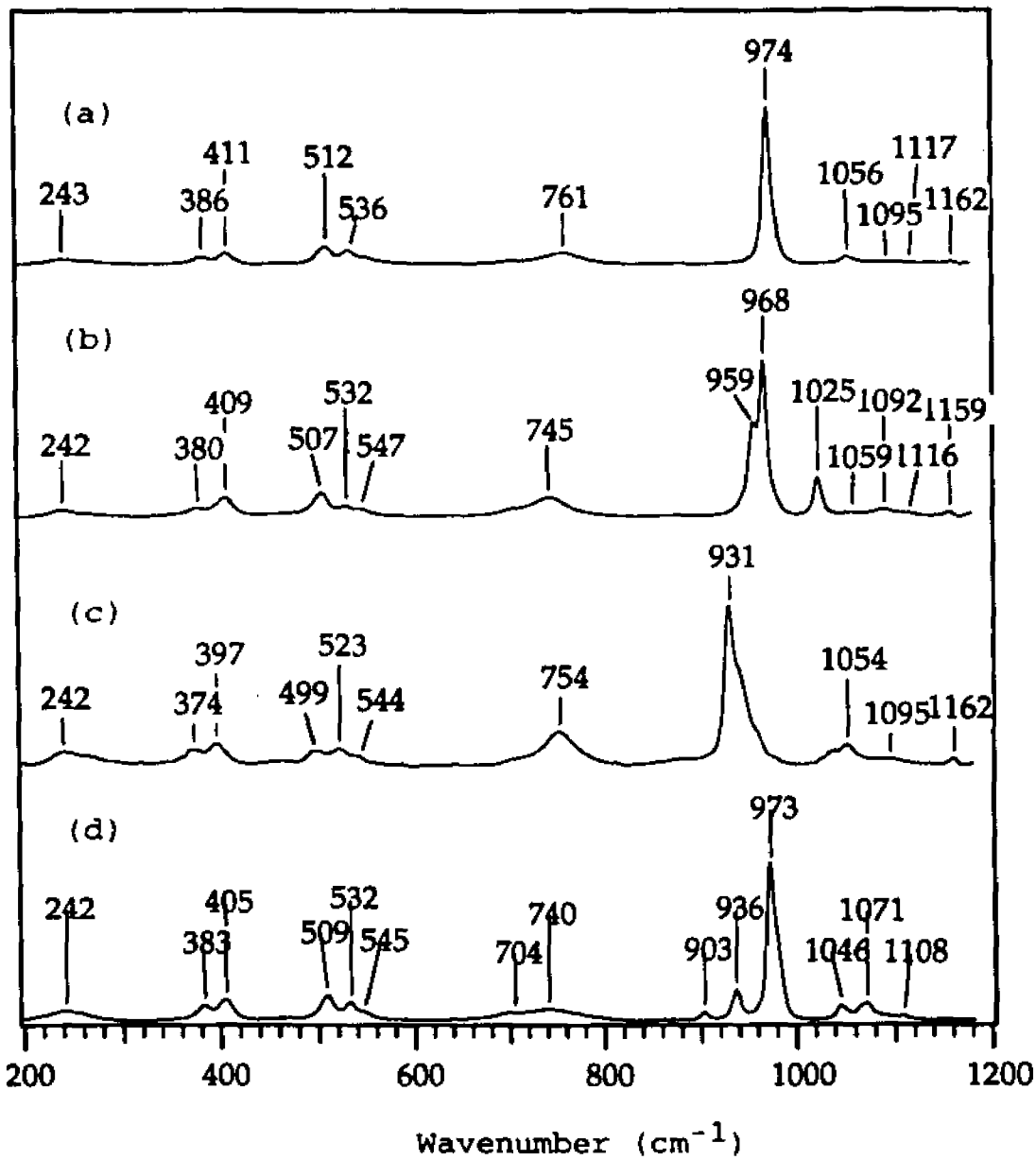

Figure 4.10 Raman spectra of (a) MP; (b) MOP; (c)MPO (d) MDP; in crystal. Laser excitation: 568.2 nm, 100 mW. Room temperature.

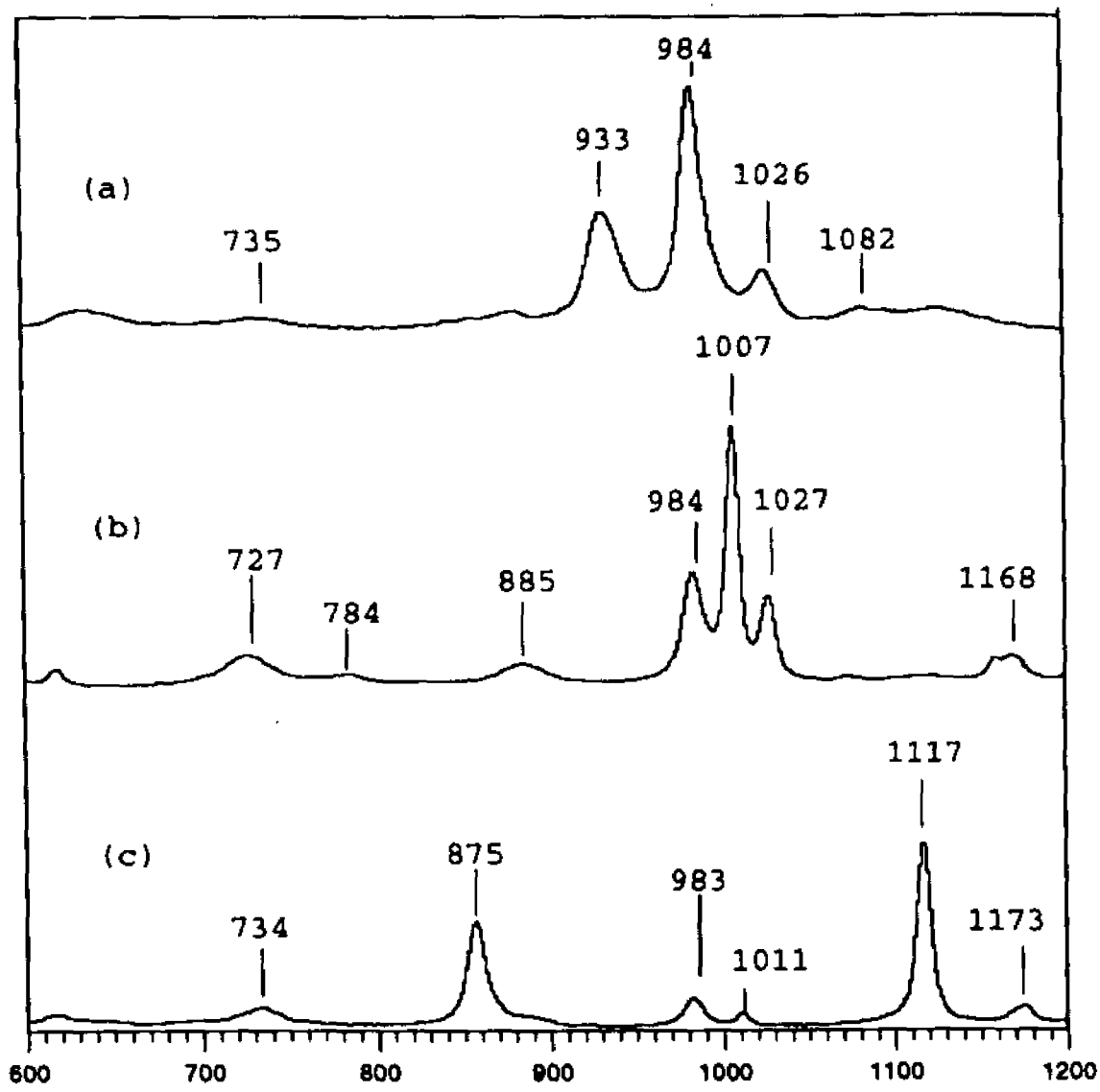

Figure 4.11 Raman spectra of (a) Acetyl phosphate, pH 7.5; (b) Phenyl phosphate, pH 10.0; (c) 4-Nitrophenyl phosphate, pH 7.5 in solution. Sample concentration: 0.5 M. Laser excitation: 514.5 nm, 200 mW. Room Temperature.

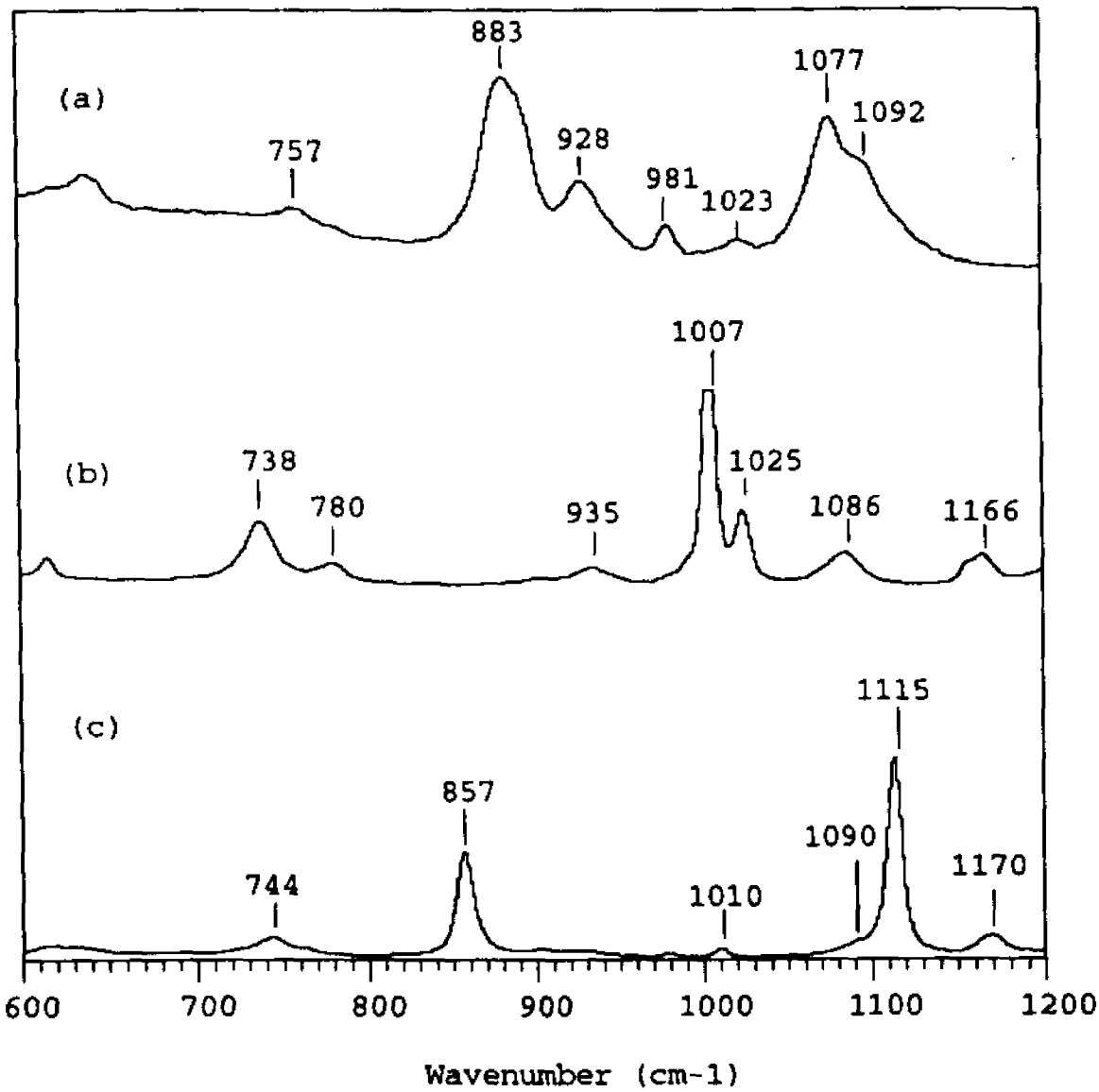

Figure 4.12 Raman spectra of (a) Acetyl phosphate; (b) Phenyl phosphate; (c) 4-Nitrophenyl phosphate at pH 4 in solution. Sample concentration: 0.5 M. Laser excitation: 514.5 nm, 200 mW. Room Temperature.

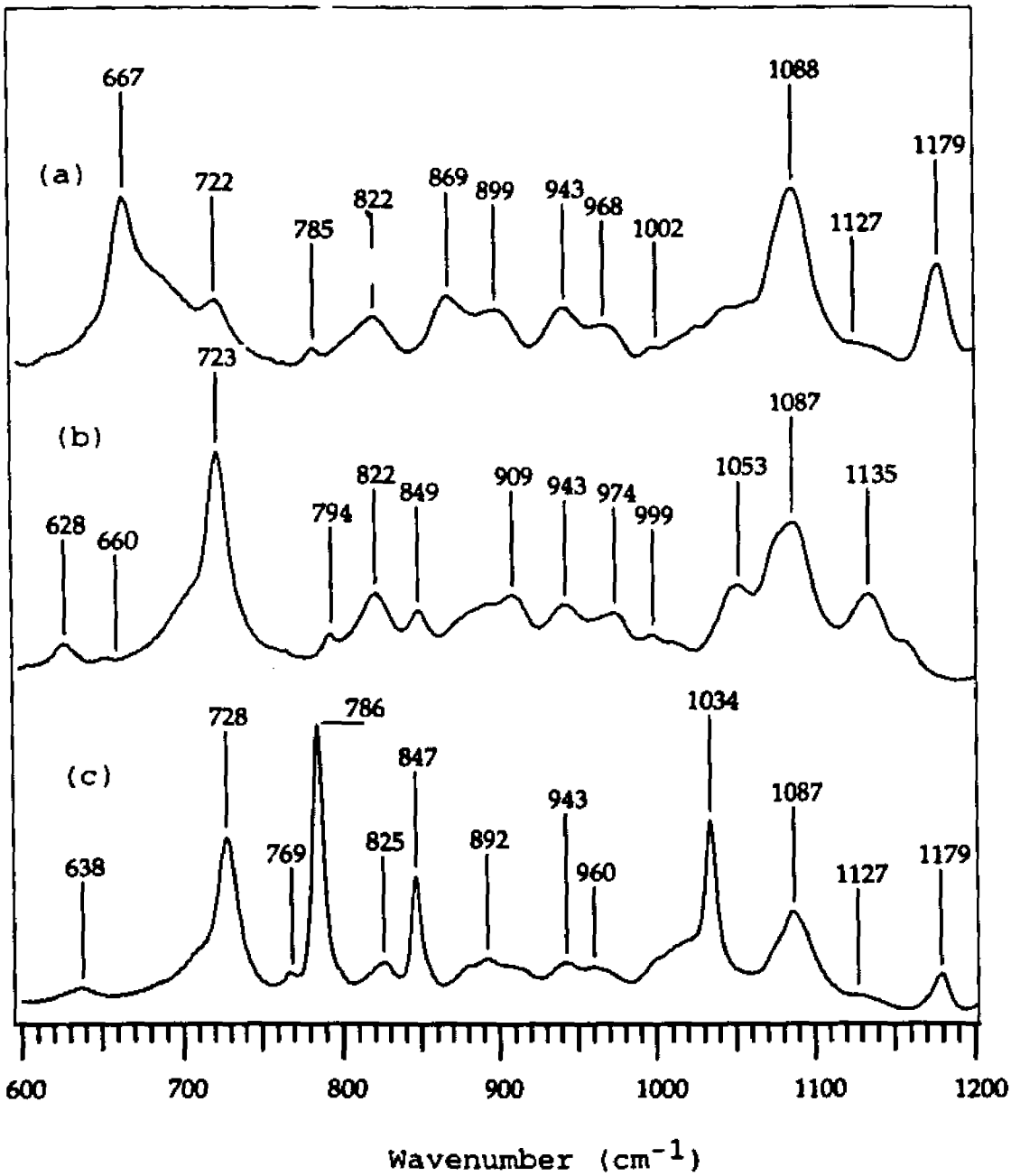

Figure 4.13 Raman spectra of (a) GDP; (b) IDP; (c) ADP at pH 7.5 in solution. Sample concentration: 0.3 M. Laser excitation: 568.2 nm, 150 mW.

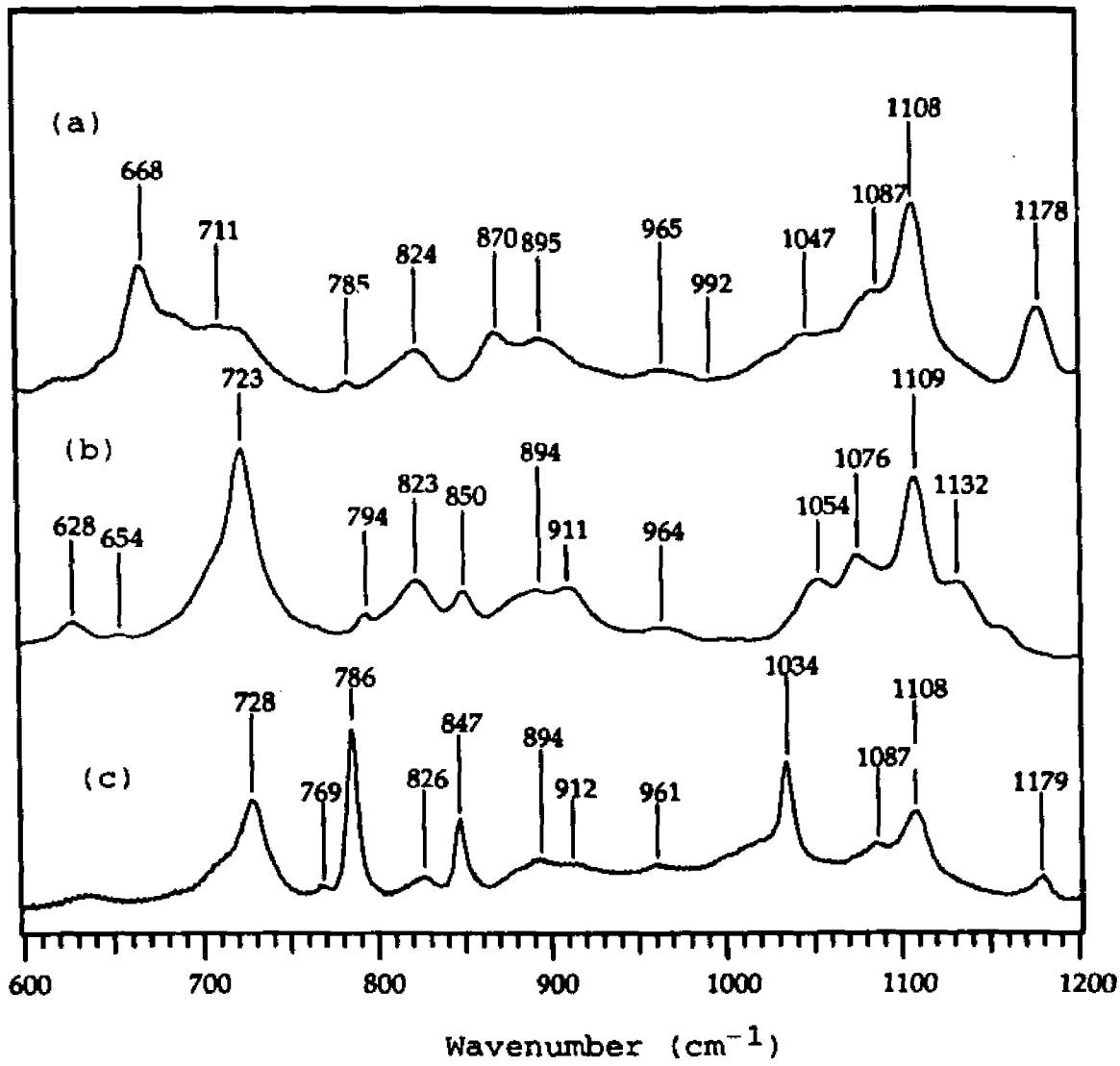

Figure 4.14 Raman spectra of (a) GDP; (b) IDP; (c) ADP at pH 5 in solution. Sample concentration: 0.3 M. Laser excitation: 568.2 nm, 150 mW.

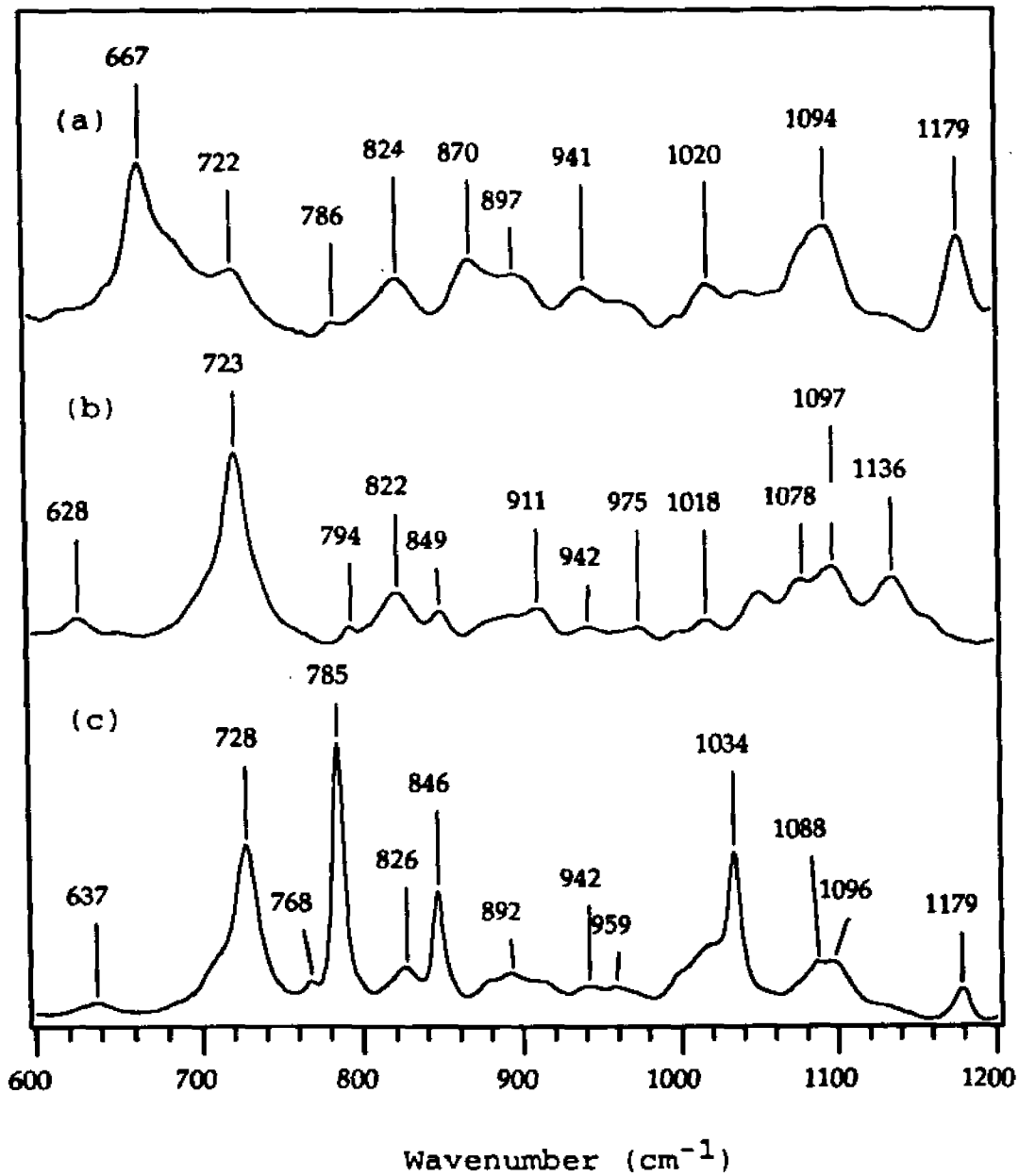

Figure 4.15 Raman spectra of (a) GDP; (b) IDP; (c) ADP with 1:1 $MgCl_2$ at pH 7.5 in solution.

Sample concentration: 15 mM. Laser excitation: 568.2 nm, 150 mW.

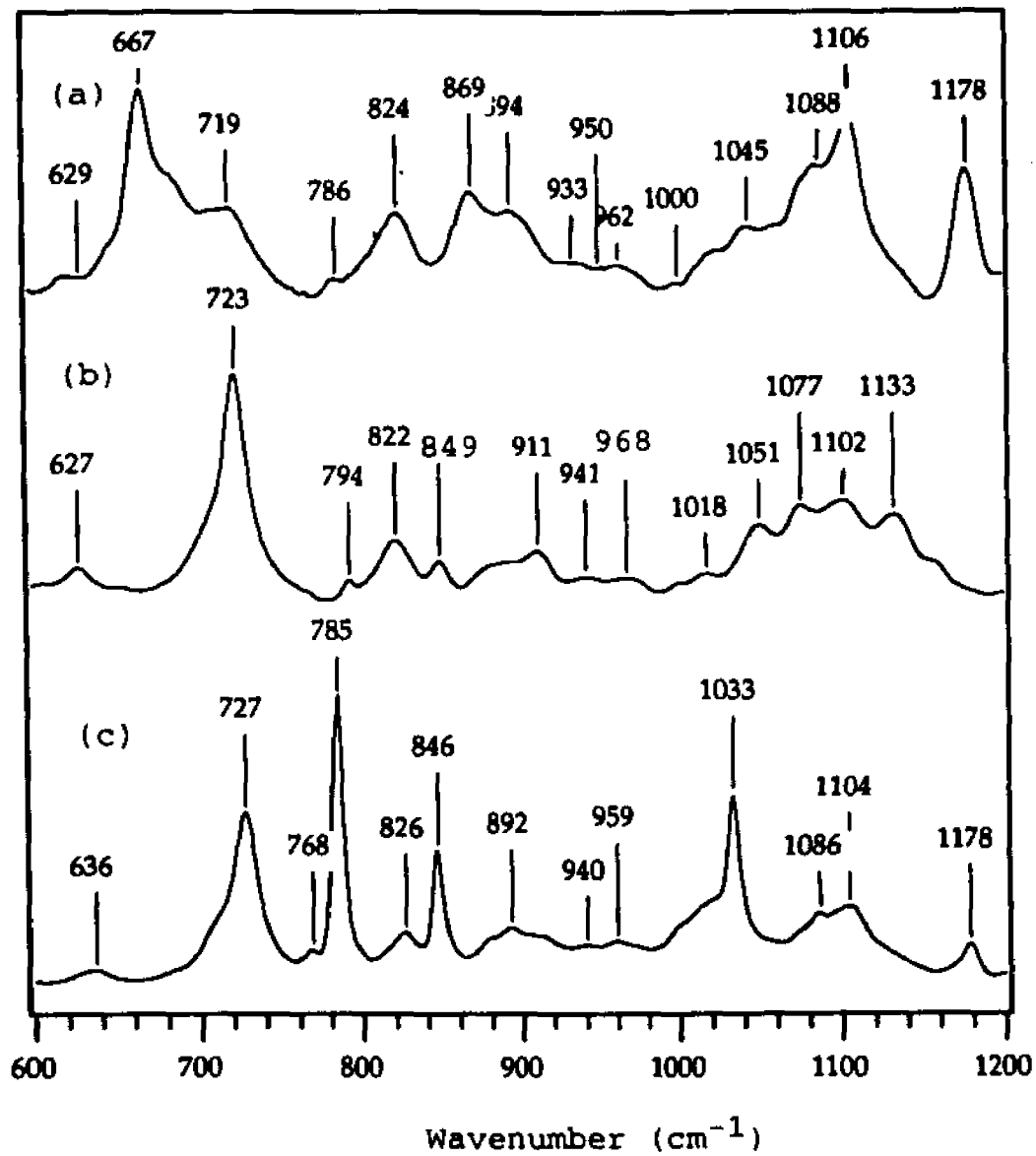

Figure 4.16 Raman spectra of (a) GDP; (b) IDP; (c) ADP with 1:1 MgCl2 at pH 5 in solution.

Sample concentration: 15 mM. Laser excition: 568.2 nm, 150 mW.

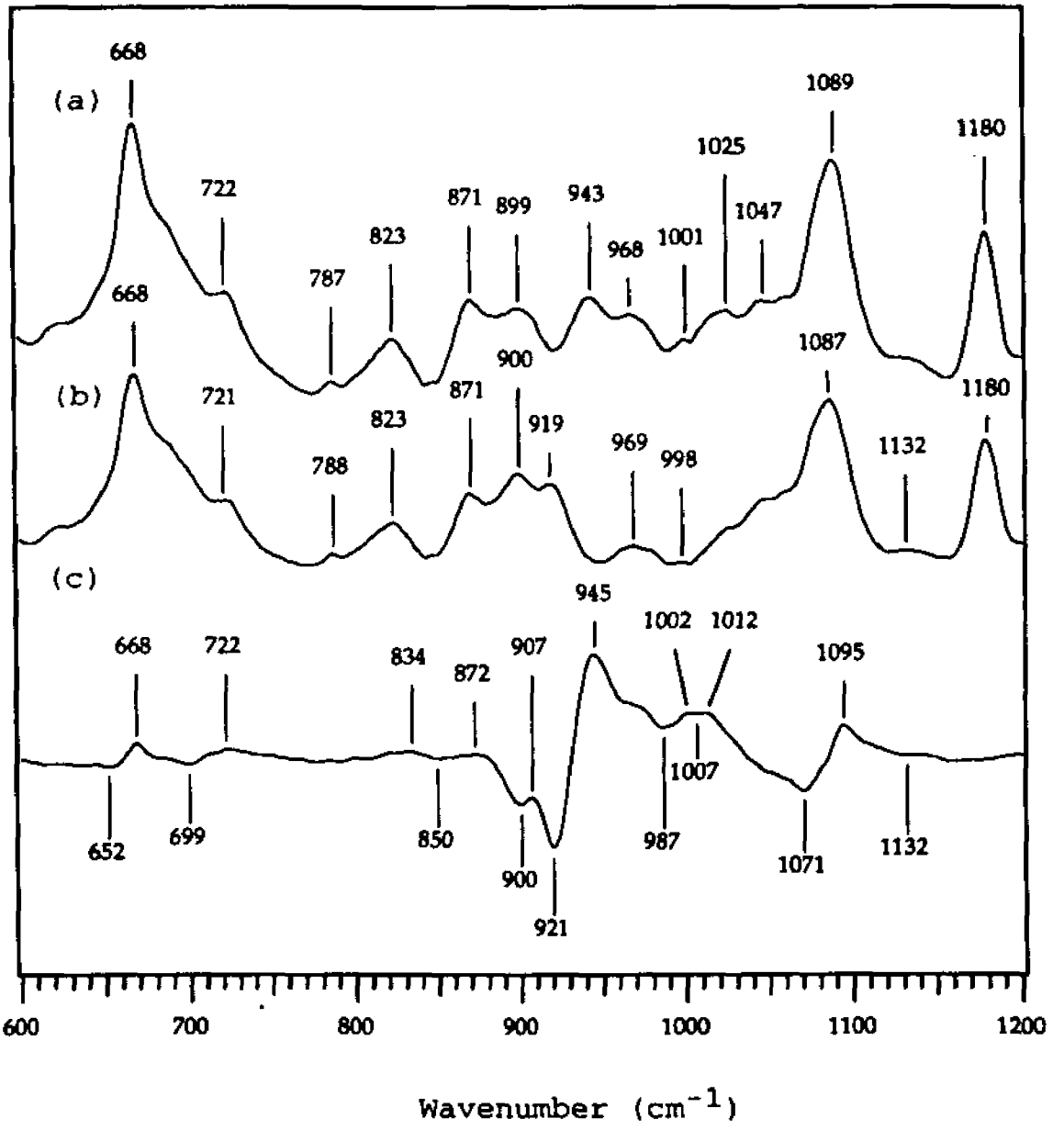

Figure 4.17 Raman spectra of (a) GDP; (b) β-$^{18}O_3$GDP; and (c) GDP minus β-$^{18}O_3$GDP; at pH 7.5 in solution.

Sample concentration: 30 mM. Temperature: 4°C

Laser excitation: 568.2 nm, 150 mW.

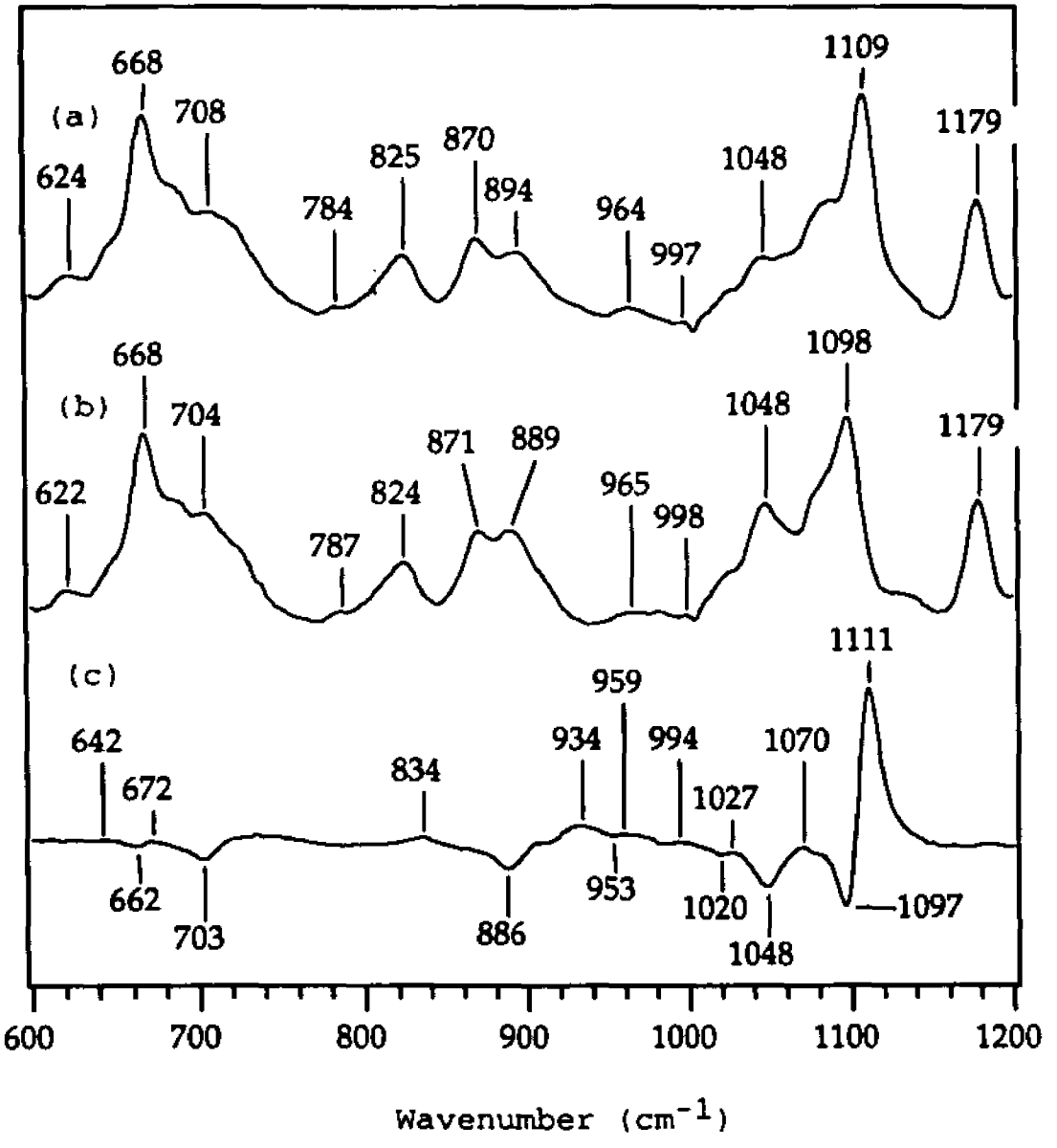

Figure 4.18 Raman spectra of (a) GDP; (b) β-$^{18}O_3$GDP; and (c) GDP minus β-$^{18}O_3$GDP; at pH 5 in solution.

Sample concentration: 30 mM. Temperature: 4°C

Laser excitation: 568.2 nm, 150 mW.

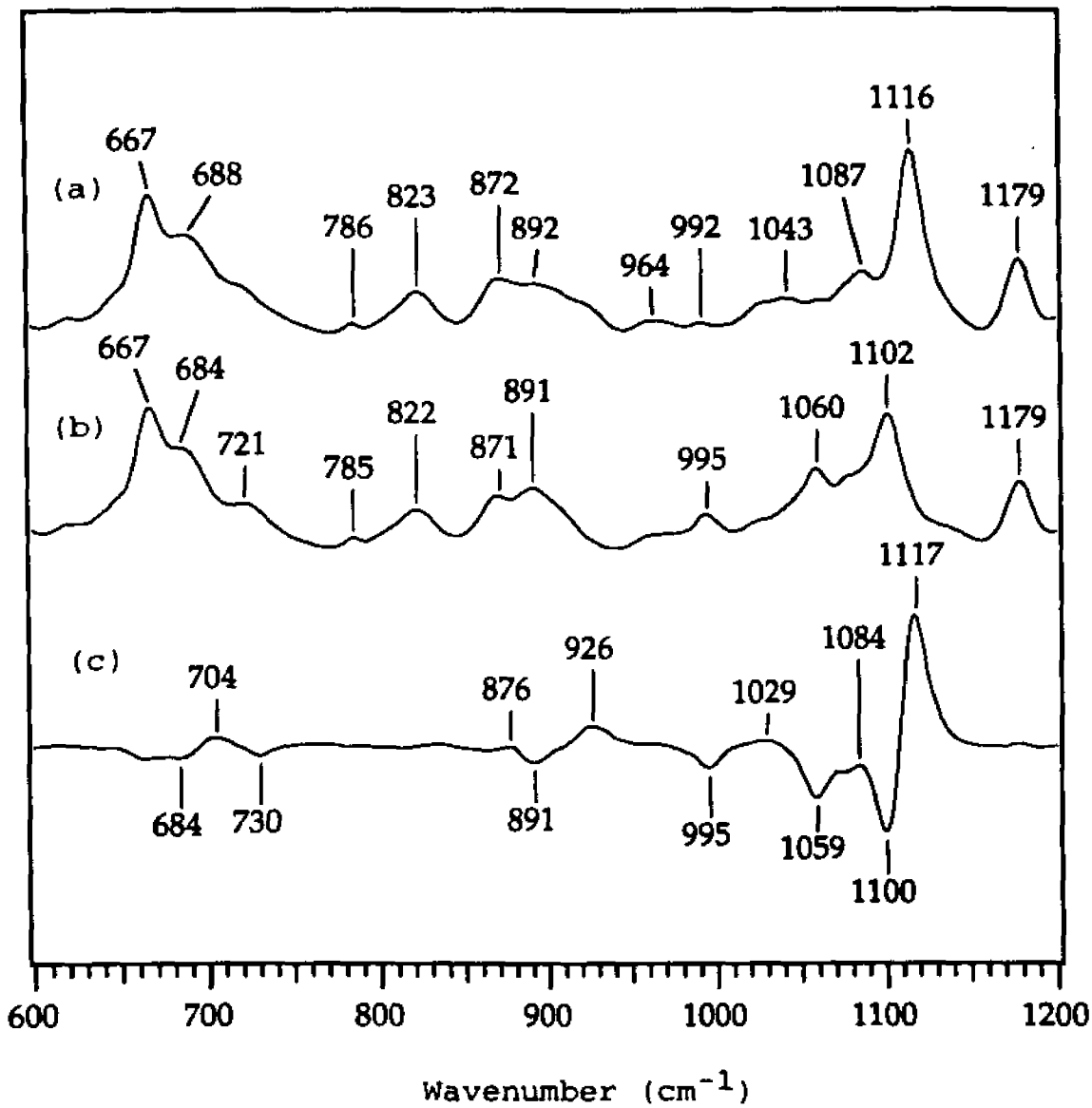

Figure 4.19 Raman spectra of (a) GTP; (b) β-$^{18}O_3$GTP; and (c) GTP minus β-$^{18}O_3$GTP; at pH 7.5 in solution.

Sample concentration: 30 mM. Temperature: 4°C.

Laser excitation: 568.2 nm, 150 mW.

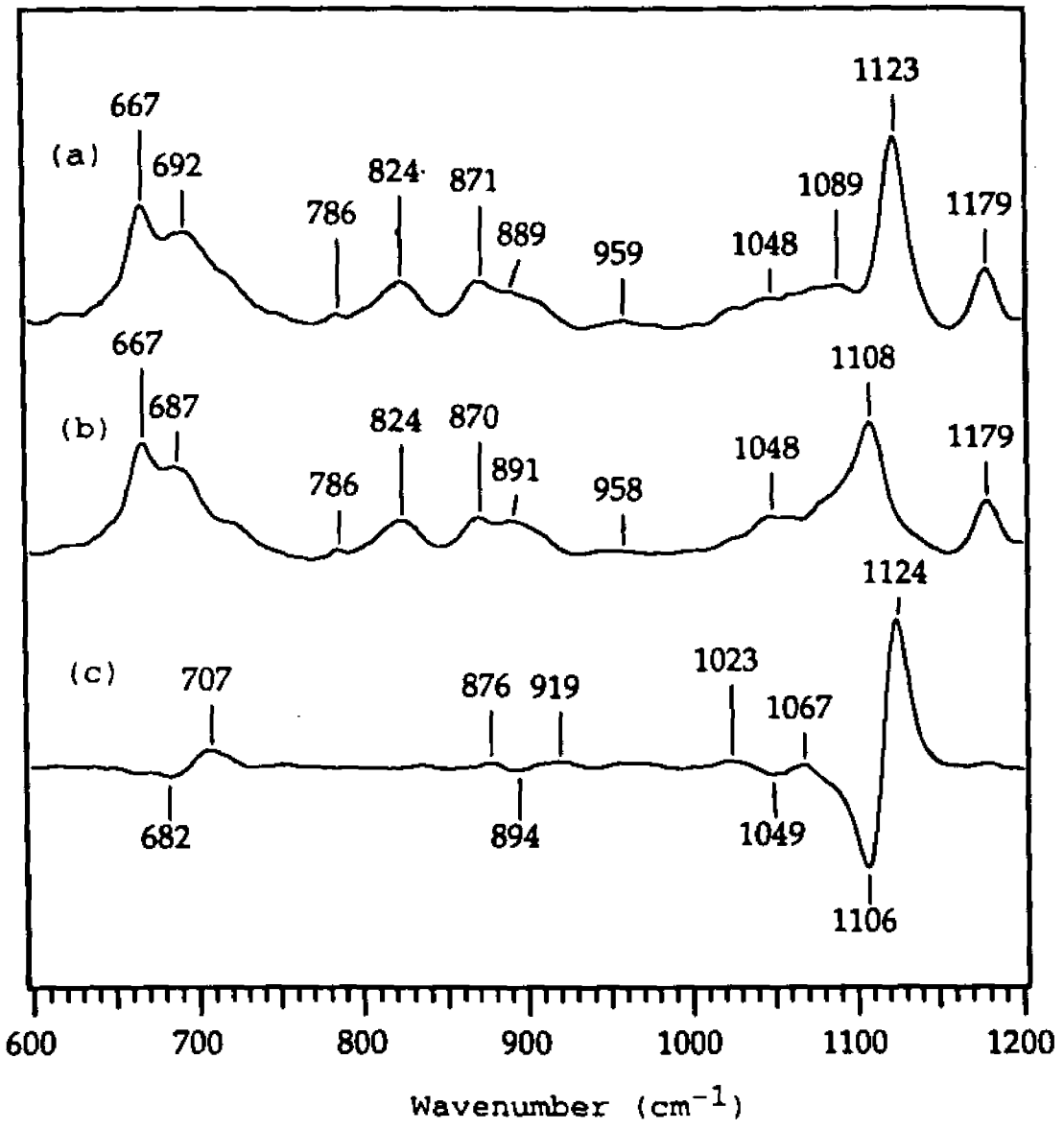

Figure 4.20 Raman spectra of (a) GTP; (b) β-$^{18}O_3$GTP and (c) GTP minus β-$^{18}O_3$GTP; at pH 5 in solution.

Sample concentration: 30 mM. Temperature: 4°C.

Laser excitation: 568.2 nm, 150 mW.

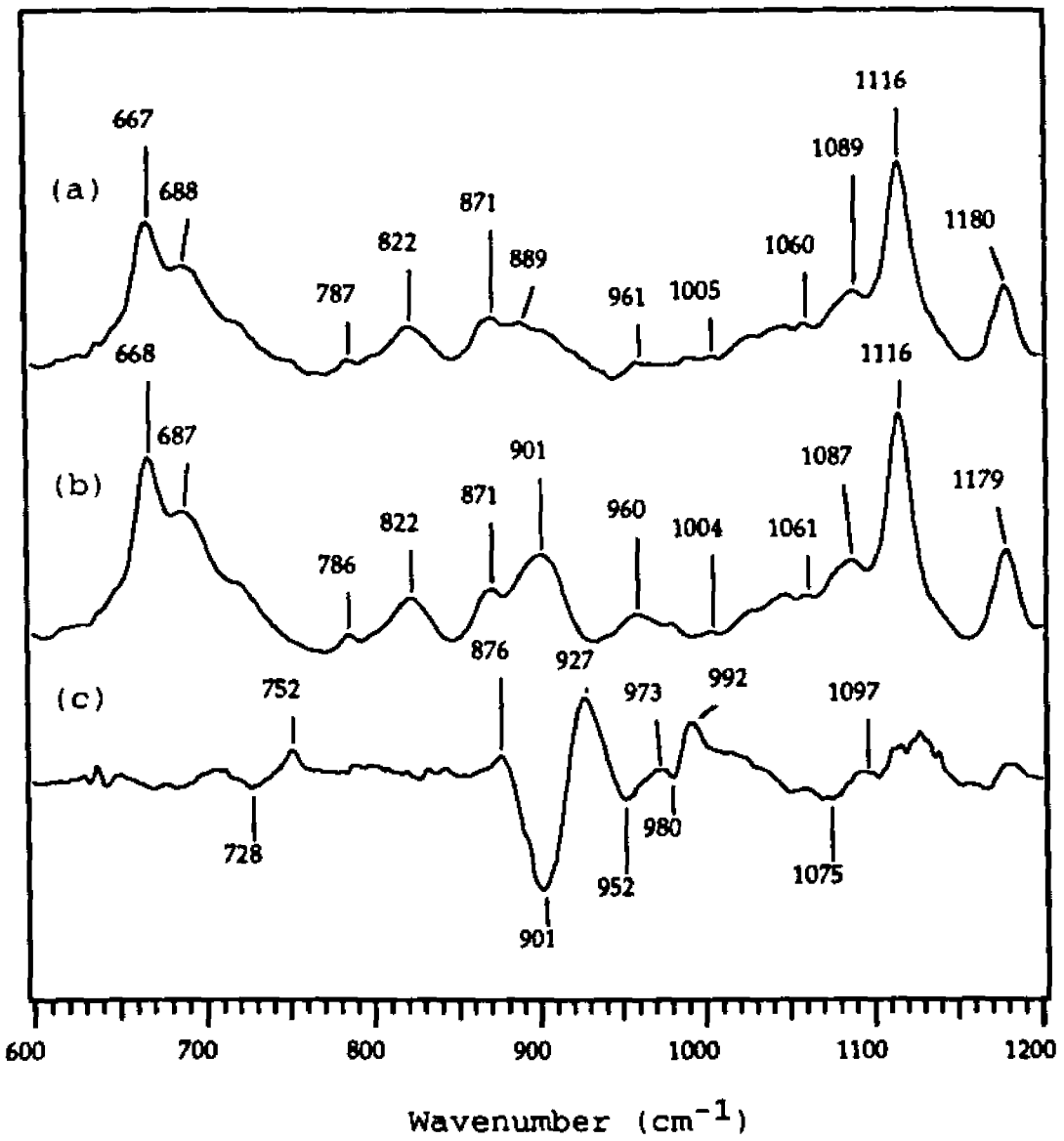

Figure 4.21 Raman spectra of (a) GTP; (b) γ-$^{18}O_3$GTP; and (c) GTP minus γ-$^{18}O_3$GTP; at pH 7.5 in solution.

Sample concentration: 30 mM. Temperature: 4°C.

Laser excitation: 568.2 nm, 150 mW.

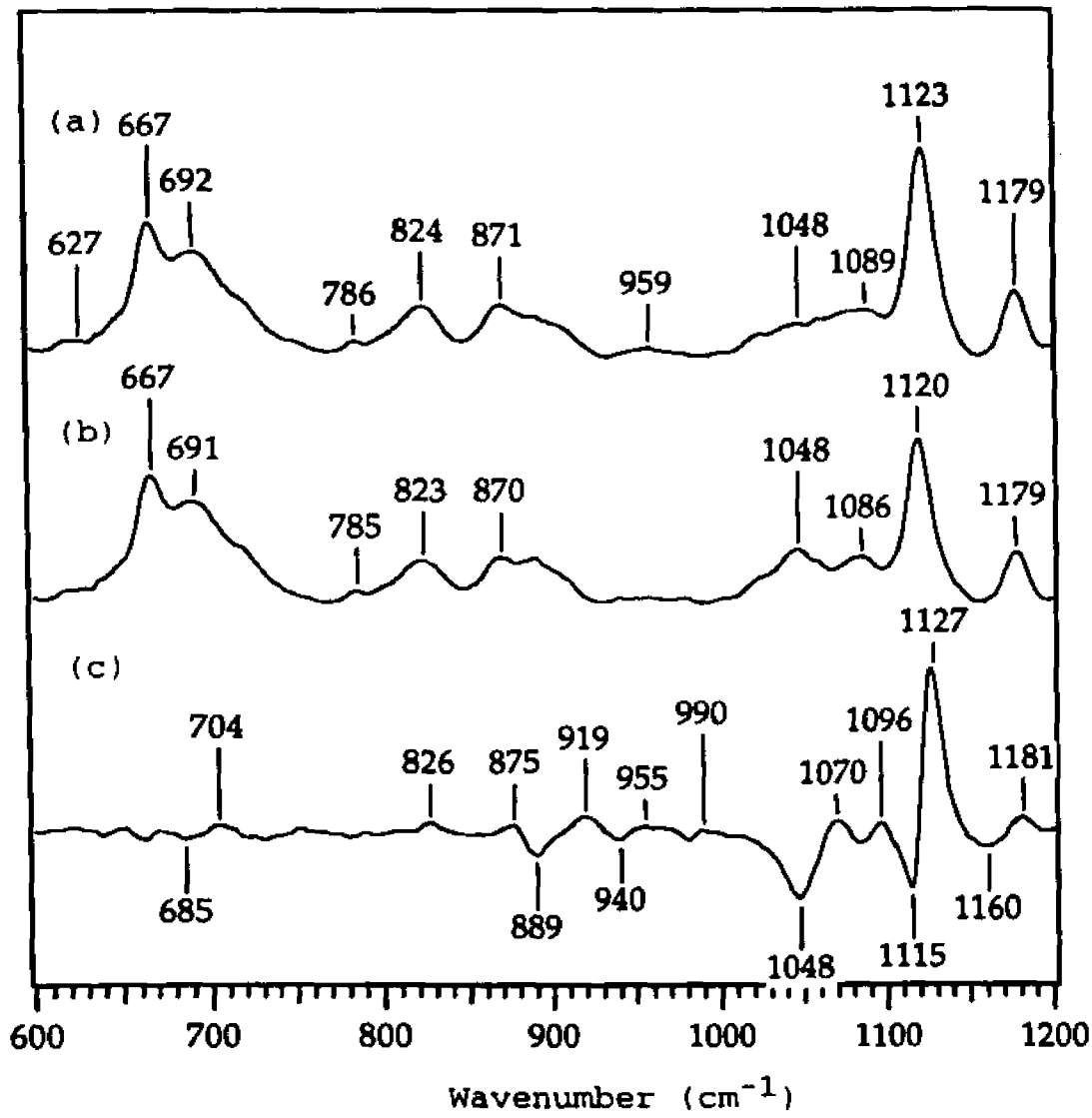

Figure 4.22 Raman spectra of (a) GTP; (b) γ-$^{18}O_3$GTP; and (c) GTP minus γ-$^{18}O_3$GTP; at pH 5 in solution.

Sample concentration: 568.2 nm, 150 mW.

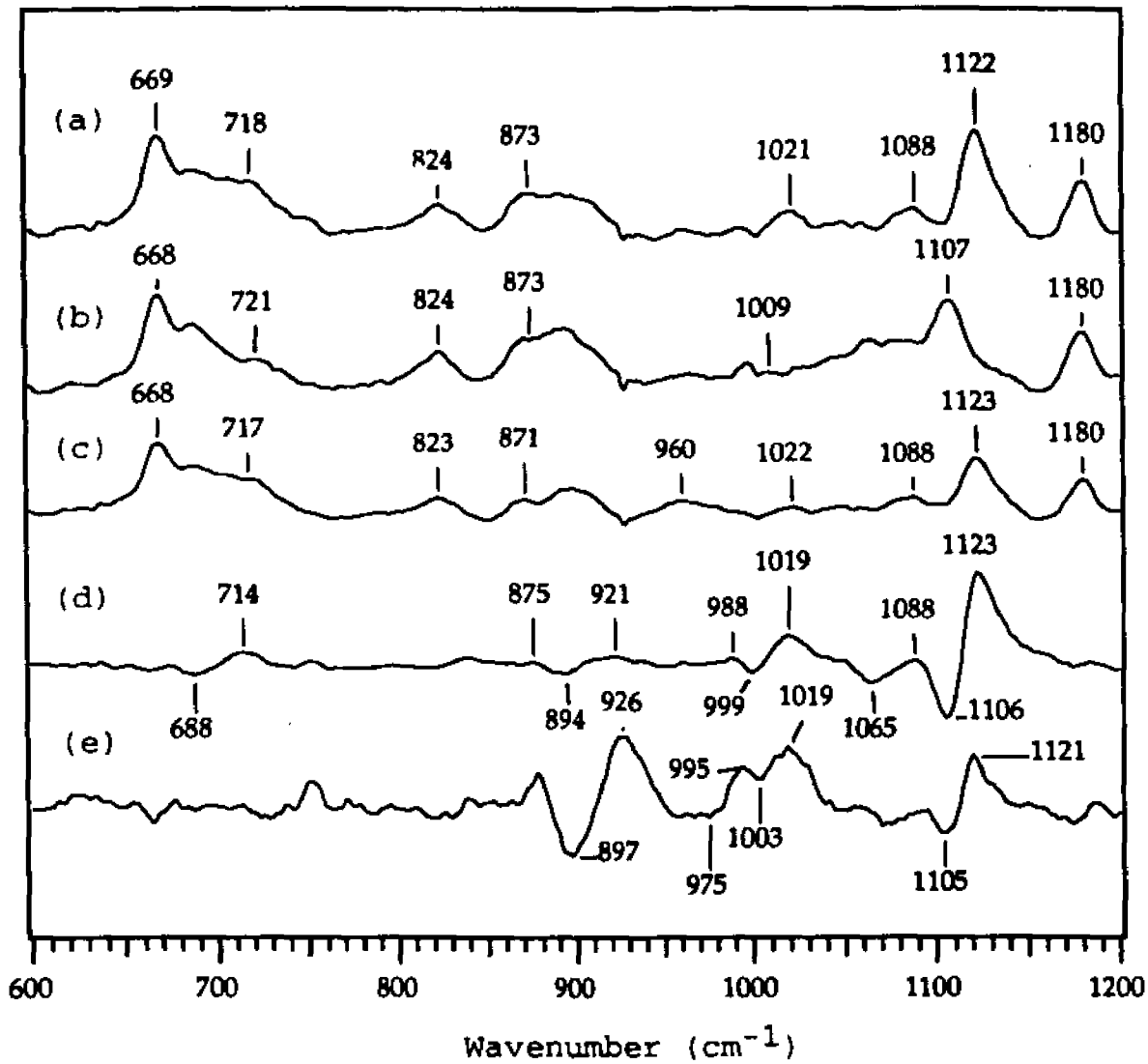

Figure 4.23 Raman spectra of (a) GTP; (b) β-$^{18}O_3$GTP; (c) γ-$^{18}O_3$GTP; (d) GTP minus β-$^{18}O_3$GTP; (e) GTP minus γ-$^{18}O_3$GTP with 1:1 $MgCl_2$ at pH 7.5 in solution. Sample concentration: 15 mM. Temperature: 4°C. Laser excitation: 568.2 nm, 150 mW.

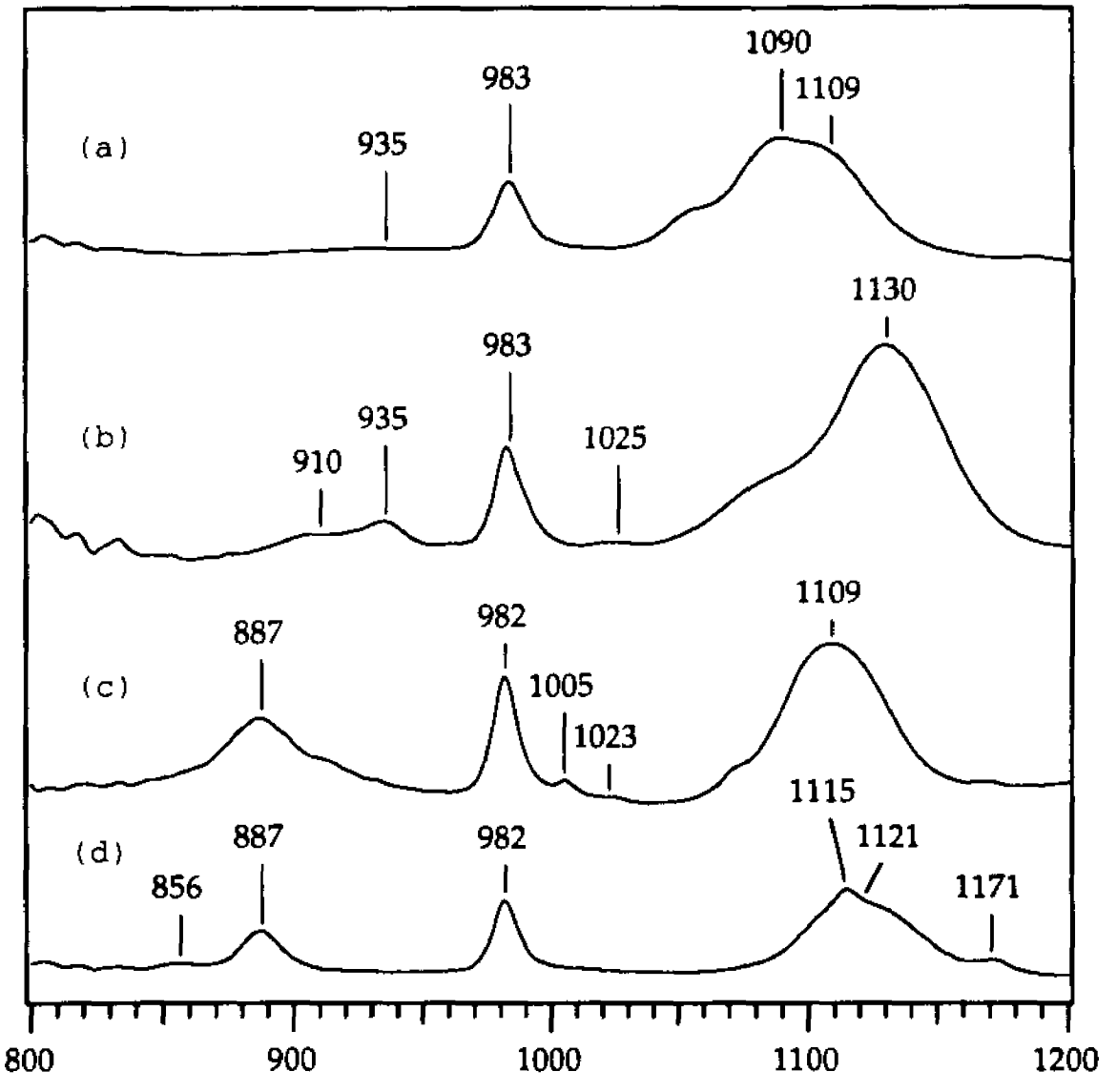

Figure 4.24 FTIR spectra of (a) Methyl phosphate; (b) Actic phosphate; (c) Phenyl phosphate and (d) 4-Nitrophenyl phosphate in their unprotonated state of the $-PO_3^{2-}$ group.

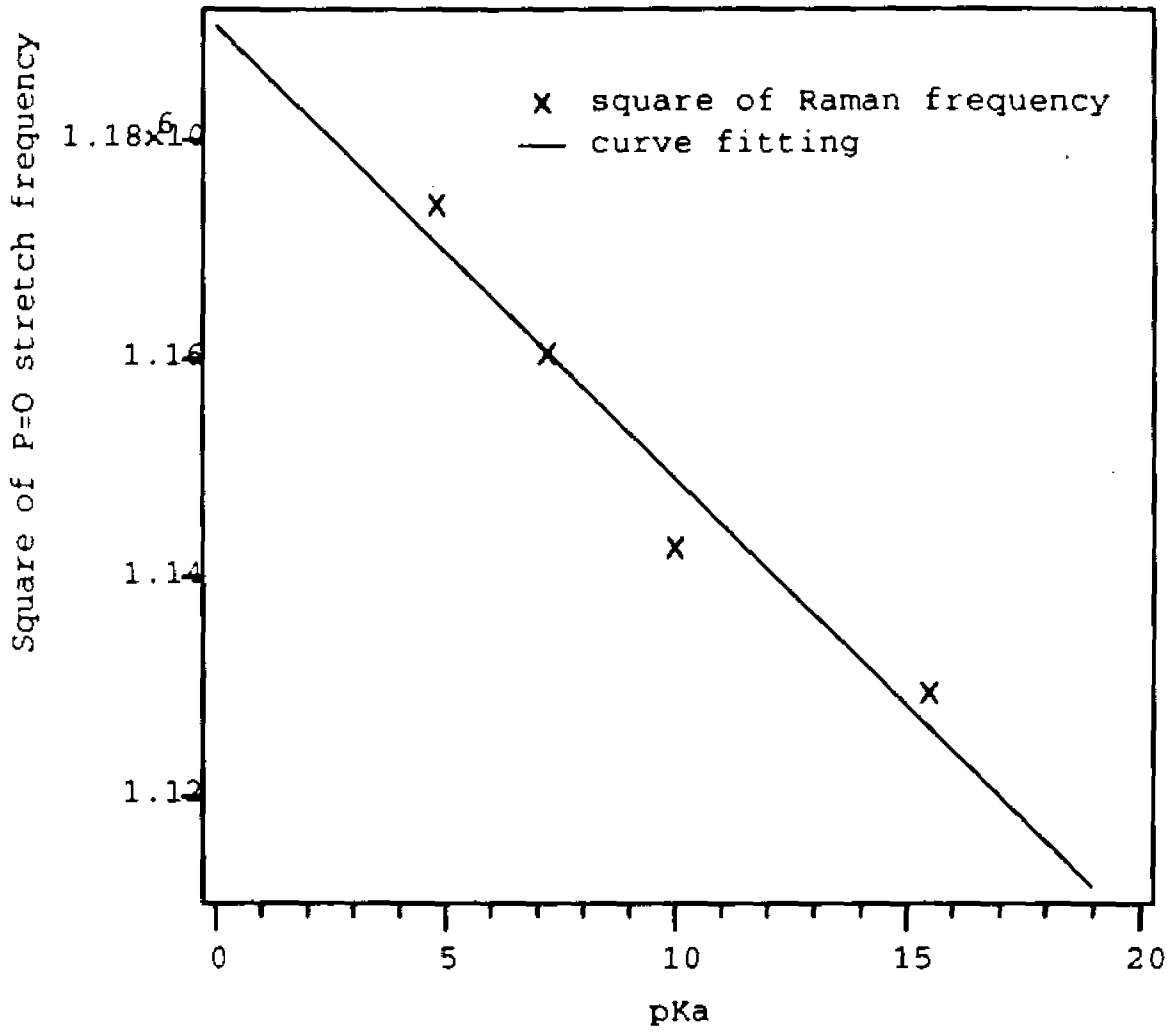

Figure 4.25 Curve fitting of P=O stretching frequencies of methyl phosphate, acetic phosphate, phenyl phosphate and 4-nitrophenyl phosphate vesus the pKa values of their corresponding R-OH compounds.

Chapter 5

NORMAL MODE ANALYSIS OF PHOSPHATE COMPOUNDS

Vibrational spectra can provide detailed information about molecular motions and interactions. To understand these molecular motion and interactions, it is essential to accurately determine the molecular normal modes. Therefore there is increasing interest in obtaining the accurate force fields for biological macromolecules and the small molecular components of which they are made.

There are several methods to perform normal mode calculation, including *ab initio* calculations, semi-empirical calculations and empirical calculations. In general, the *ab initio* and semi-empirical calculations can not be applied to large molecules and they can not reproduce observed frequencies very well. For example, the frequencies calculated by semi-empirical method, MINDO/3, can lead to an error within something like 50%. To fit the observed frequencies, scaling factors for the force fields obtained quantum mechanically are normally used in the *ab initio* and semi-empirical calculations. However, these scaling factors have some degree of uncertainties, and they can not be transferred from one system to another generally. To solve this problem, we use here an empirical method, which treats molecules classical mechanically as coupled harmonic oscillators consisting of

point masses connected by springs with a defined equilibrium geometry. The normal modes are obtained as the solutions of the equations of the motion for the considered system. The theoretical details are discussed in Chapter 2.

The empirical method for the force field calculation of the phosphate compounds is more reliable, and the force field from one phosphate compound can be transferred to the other similar phosphate compound within minimum modifications in general. However, the number of force constants in one force field is very large, so a lot of work and patience are needed to fit the experimental data. In addition, there are a large number of internal coordinates and related force constants than independent data points used for the fitting, it is possible that several different force fields could reproduce the observed vibrational frequencies equally well; therefore, the determination of the normal modes is not unique by the empirical method. In order to reduce this problem, data from isotopic derivatives of the phosphate compounds are used. However, Our goal here is not to obtain an exact force field to fit the experimental data. It is unclear to us whether this is even feasible. Our central goal here is to understand how a normal mode is related with certain force constants in a force field, and how a force field of a molecule responds to external perturbations of the molecule, such as point charges. Specifically, we would like to determine the frequency changes of the vibrational modes

of a phosphate molecule when it interacts with polar or charged groups of another molecule.

The theoretical background of the normal mode analysis is discussed in detail previously in Chapter 2. The program we use to carry out the normal mode analysis is VIB Program with little modifications by our group. The parameters used for constructing the G-Matrix are calculated by program AM1, which minimized the energy of a specific structure. The normal frequencies are calculated using the generalized valence force field. The initial values of the force field are transferred from previous published data (Guan, Y. et al., 1994; Chapman, A. C. et al., 1964, 1965; Taga, K. et al., 1991; Snyder, R. G. et al., 1967). The force constants are then refined in order to fit the calculated frequencies of those phosphate compounds and their isotopic derivatives with those observed in our experiments.

The procedures we use to obtain the force field to fit the observed frequencies and the correlation between the frequencies and force constants are as following:

First, we choose an initial set of force constants to construct a F-Matrix. The frequencies of all vibrational modes are then obtained from the F-Matrix and G-Matrix from program VIB. Next, by changing each force constant by a certain amount (0.4 mdyn/Å for stretching force constant, 0.2 mdyn/Å for bending force constants and 0.1 mdyn/Å for coupling force constants), we get a correlation table of each frequency change corresponding to the change of each force

constant. Then, by comparing the calculated frequencies with observed frequencies, we refine those force constants which are responsible for those frequencies needed to be fit according to the correlation table, and then calculate the frequencies again. Repeating these procedures for several times, we will be able to get a set of force field, which can reproduce the observed frequencies reasonably well.

Force fields for PO_4^{3-}, HPO_4^{2-}, $H_2PO_4^-$, H_3PO_4, dimethyl phosphate and diethyl phosphate were previously developed by other groups (Guan, Y. et al., 1994; Chapman, A. C. et al., 1965; Taga, K. et al., 1991). Here we present the force fields developed to fit the observed frequencies of PO_4^{3-}, HPO_4^{2-}, $H_2PO_4^-$, H_3PO_4, methyl phosphate and their ^{18}O labeled derivatives. Most importantly, we have developed correlation tables which relate the vibrational frequency changes with one or more force constant changes for these phosphate compounds. Such information is very useful to explain the phosphate vibrational mode changes when the phosphate compound binds to protein.

5.1 Generalized Valence Force Field for PO_4^{3-}

Table 5.1 shows the geometry parameters for the construction of G-Matrix of PO_4^{3-}. Figure 5.1 shows the chemical structure of PO_4^{3-} from Chem3D program in Macintosh. Table 5.2 shows the force field obtained from program VIB to fit

the observed frequencies. The calculated frequencies fit the observed frequencies of PO_4^{3-} and $P^{18}O_4^{3-}$ very well with an average least square error of 3.5 cm^{-1} for all the phosphate bands of both PO_4^{3-} and $P^{18}O_4^{3-}$. Table 5.3 illustrates the observed and calculated frequencies and the correlation between each frequency and each force constant in the force field. The first and second column in table 5.3 are observed and calculated frequencies respectively. The third column and after are the changes of frequencies corresponding to the changes of force constants (the stretching force constants are increased by 0.4 mdyn/Å, the bending force constants are increased by 0.2 mdyn/Å and the off diagonal coupling constants are increased by 0.1 mdyn/Å).

As we expect, there are one P=O symmetric stretching band and one three-fold degenerate asymmetric stretching band in the Raman spectrum of PO_4^{3-} because it has a T_d symmetry. The P=O symmetric and asymmetric stretching modes at 937 cm^{-1} and 1010 cm^{-1} shift up by 22 cm^{-1} and 34 cm^{-1} respectively due to the 0.4 mdyn/Å increase of P=O stretching force constant [s2]. They are also largely affected by the P=O/P=O coupling constant [c22] and P=O/O=P=O coupling constant [x21, x22]. The increase of c22 makes the symmetric and asymmetric bands move together by shifting up the symmetric stretching band by 16 cm^{-1} and shifting down the asymmetric band by 8 cm^{-1}. There are also one two-fold degenerate O=P=O bending mode at 416 cm^{-1} and one three-fold degenerate O=P=O bending mode at 554 cm^{-1}. They are all re-

lated with the O=P=O bending force constant [b2] and are all largely affected by the changes of the O=P=O/O=P=O coupling constants [y21, y22]. However, the three-fold degenerate O=P=O bending mode is also affected by the stretching/bending coupling [x21, x22] constant, while the two-fold degenerate O=P=O bending mode is not.

5.2 Generalized Valence Force field for HPO_4^{2-}

Table 5.4 shows the geometry parameters for construction of the G-Matrix of HPO_4^{2-}. Figure 5.2 shows the chemical structure of HPO_4^{2-} from Chem3D program in Macintosh. The force field derived is shown in Table 5.5. Table 5.6 illustrates the observed and calculated frequencies, and the correlation between the frequencies and force constants. The least square error for the calculated frequencies from the force field shown in Table 5.5 is 6.2 cm^{-1}.

The symmetric and degenerate asymmetric stretching modes of P=O double bond at 990 cm^{-1} and 1084 cm^{-1} respectively are directly related with the P=O stretching force constant [s2]. The 0.4 mdyn/Å increase of s2 shifts up these two bands by 19 cm^{-1} and 33 cm^{-1} respectively. They are also related with stretching/stretching, stretching/bending and bending/ bending coupling constants. For example, the increase of the P=O/P=O stretching coupling constants [c22] shift up the P=O symmetric stretching vibration by 9 cm^{-1}

and shift down the P=O asymmetric stretching vibration by 8 cm^{-1}; the changes of P-O/P=O stretching coupling constants [c12] shift up the P-O stretching mode by 7 cm^{-1} and shift down the P=O symmetric stretching mode by 9 cm^{-1}. The stretching/bending coupling constants [x211, x212, x221, x222] and bending/bending coupling constants [y121, y122, y22] have relatively less effects on these stretching modes. The P-O single bond stretching mode at 858 cm^{-1} is mostly related with the P-O stretching force constants [s1]. The changes of s1 cause a upshift of this band by 26 cm^{-1}. It is also affected by stretching/stretching, stretching/bending and bending/bending coupling constants, such as, P-O/P=O stretching coupling constants [c12], which cause a 7 cm^{-1} upshift; P-O/O-P=O coupling constants, which cause a 11 cm^{-1} downshift; and also P-O/O=P=O coupling constants. The lower degenerate bending mode at 393 cm^{-1} is mostly related with O-P=O bending constants [b1]. A 30 cm^{-1} upshift of this band is caused by the increase of b1. The changes of O-P=O/O-P=O coupling constants [y11] shift down this band by 15 cm^{-1}. This band is almost not influenced by the other force constants. The other double degenerate O=P=O bending mode at 533 cm^{-1} is mostly related with O=P=O bending force constants [b2], which cause a 26 cm^{-1} upshift of this band. The other major factor affecting this mode is the O=P=O/O=P=O coupling constants, changes of which cause a 12 cm^{-1} downshift of this band. The O=P=O symmetric bending mode, which is also at 533 cm^{-1}, is related with both b1 and b2, and is

also affected by many other factors, especially the bending/bending coupling constants.

5.3 Generalized Valence Force Field For $H_2PO_4^-$

Table 5.7 shows the geometry parameters used to construct the G-Matrix for $H_2PO_4^-$. Depending on the orientation of OH group, two models of $H_2PO_4^-$ are chosen in the calculation. Model I has C_2 symmetry, with each hydroxyl group trans- to an O of PO_2 forming two planar HOPO group perpendicular to one another. Model II has a planar HOPOH group and C_{2v} symmetry. Because of the geometry differences of these two models, we get different average least square error of the calculated frequencies for them (6 cm^{-1} for model I and 10 cm^{-1} for model II) from the same force field. This implies that the force field is sensitive to the geometry structure, and different force field should be used for different model. However, our goal is to derive a correlation between the frequency of each vibration and the force constant of each chemical bond, and we have found that the correlation for these two models are basically the same. Therefore only the correlation table for model I is presented here (Table 5.9). Table 5.8 shows the force field derived for $H_2PO_4^-$. Figure 5.3 shows the chemical structure of $H_2PO_4^-$ from Chem3D program in Macintosh.

The P=O symmetric and asymmetric vibration modes of the PO_2 group at 1077 cm^{-1} and 1160 cm^{-1} are directly related with the P=O stretching force constants [s2], a 0.4 mdyn/Å change of which causes upshifts of these two modes by 23 cm^{-1} and 31 cm^{-1} respectively. The P-O symmetric and asymmetric stretching modes of the $P-(O-H)_2$ group at 878 cm^{-1} and 943 cm^{-1} are directly related with the P-O stretching force constant [s1] accordingly. These two modes shift up by 27 cm^{-1} and 33 cm^{-1} respectively because of the 0.4 mdyn/Å change of s1. These stretching vibration frequencies are also largely affected by the stretching/stretching coupling constants. For example, the P=O/P=O coupling constant [c22] can cause the P=O symmetric and asymmetric stretching modes moving together or separating apart, and accordingly the P-O/P-O coupling constants [c11] work the same way on P-O symmetric and asymmetric stretching modes. A 0.1 mdyn/Å increase of P-O/P=O coupling constants shift up the P-O symmetric stretching mode by 9 cm^{-1} and shift down the P=O symmetric stretching mode by 12 cm^{-1}. The stretching/bending coupling constants have also some degree of effects on the stretching frequencies, while the bending/bending coupling constants have little or no effect on them. The O-P-O bending mode at 370 cm^{-1} is directly related with the O-P-O bending force constants [b0]. It also largely depends on the value of the O-P-O/O-P=O [y01], O-P-O/O=P=O [y02] and other bending/bending coupling constants. The lower double degenerate O-P=O bending mode at 390 cm^{-1} is mostly related with O-P=O

bending force constant [b1], a 0.2 mdyn/Å increase of which shifts up this mode by 32 cm^{-1}. It is also largely affected by the other bending/bending coupling constants, such as O-P=O/O-P=O [y11] and O-P=O/O=P=O [y12]. The higher double degenerate O=P=O bending band at 515 cm^{-1} is related with both O-P=O bending force constants [b1] and O=P=O bending force constants [b2]. Accordingly it is also affected by the bending/bending coupling constants, such as O-P=O/O-P=O [y11] and O-P=O/O=P=O [y12].

5.4 Generalized Valence Force Field for H_3PO_4

Table 5.10 shows the geometry parameters for the construction of G-Matrix of H_3PO_4. Figure 5.4 shows the chemical structure of H_3PO_4 obtained from program Chem3D in Macintosh. The force field derived is shown in Table 5.11. Table 5.12 shows the observed and calculated frequencies, and the correlation between the frequencies and force constants. The average least square error for the calculated frequencies is 4 cm^{-1} for all the frequencies of H_3PO_4 and $H_3P^{18}O_4$.

The P=O stretching mode at 1177 cm^{-1} is directly associated with P=O stretching force constants [s2]. It is also largely affected by some stretching/stretching, stretching/bending coupling constants, such as P-O/P=O [c12], P=O/O-P-O [x20], P=O/O-P=O [x21] and P=O/P-O-H [x23]. The P-O single bond symmetric and double degenerate asymmetric

modes are directly related with the P-O stretching force constants [s1]. As discussed above in previous sections, the P-O/P-O coupling constants [c11] can change the relative position of symmetric stretching mode to asymmetric stretching mode by either moving them together or separating them apart. The stretching/bending coupling constants, such as P-O/O-P-O [x101, x102], P-O/O-P-O [c111, c112] and P-O/P-O-H [x131, x132], can also have large effects on these modes. The bending force constants and bending/bending coupling constants have little or no effects on all these stretching vibrational modes. The double degenerate O-P-O deformation mode at 370 cm^{-1} is basically related with the O-P-O bending force constants [b0]. It is almost not affected by the other force constants except the O-P-O/P-O-H coupling constants [y031, y032]. The other double degenerate O-P=O bending mode at 499 cm^{-1} is mostly related with the O-P=O bending force constants [b1], but it is somehow also affected by some stretching/bending force constants. The symmetric O-P=O bending mode at 390 cm^{-1} is sensitive to many force constants. It is basically related with the O-P-O [b0], O-P=O [b1] and H-O-P [b3] bending constants, but it is also affected by some stretching/bending, especially some bending/bending coupling constants.

5.5 Generalized Valence Force Field for Methyl Phosphate

Table 5.13 shows the geometry parameters for the construction of G-Matrix of methyl phosphate. Figure 5.4 shows the chemical structure of methyl phosphate obtained from program Chem3D in Macintosh The force field derived is shown in Table 5.14. Table 5.15 illustrates the observed and calculated frequencies, and the correlation between the frequencies and force constants. The least square error from experiment for the calculated frequencies is 5.1 cm^{-1} for all Raman bands list in the table.

As shown in Figure 4.6, the deformation bands in the region between 300 cm^{-1} and 600 cm^{-1}, and the double degenerate asymmetric stretching bands around 1100 cm^{-1} of the PO_3^- group are very broad. It is difficult to fit such broad bands. In general, the $-PO_3^{2-}$ group has a local C_{3v} symmetry, and one symmetric and one double degenerate asymmetric P=O stretching modes are expected in the region of 900 cm^{-1} to 1200 cm^{-1}. In the region between 300 cm^{-1} and 600 cm^{-1}, two double degenerate and one symmetric deformation modes are expected. According to this analysis, we then fit the two broad bands around 398 cm^{-1} and 520 cm^{-1} to five Lorentzian components, and fit the broad band at 1100 cm^{-1} to two Lorentzian components. However, after the curve fitting of these broad bands, the double degenerate asymmetric P=O stretching mode is separated to two bands at 1090 cm^{-1} and 1115 cm^{-1} respectively. During the process of refining the force field, we are not able to fit these two bands by a single P=O stretching force constant for all three P=O bonds

of the $-PO_3^{2-}$ group. According to the geometry structure of methyl phosphate calculated by quantum mechanical method, one P=O double bond is almost in the H-O-P plane. Therefore the oxygen atom in this P=O bond is closer to the carbon atoms and hydrogen atoms than the oxygen atoms in the other two P=O bonds. We then choose different force constant [s21] for this P=O bond from the force constants [s22] for the other two P=O bonds. Same treatment is applied to the bending modes of the $-PO_3^{2-}$ group.

The symmetric and asymmetric P=O stretching vibration modes at 982 cm^{-1}, 1090 cm^{-1} and 1115 cm^{-1} are basically associated with the P=O stretching force constants [s21, s22]. By adjusting the s21 and s22, we can fit the two separated asymmetric frequencies. As discussed above for the case of HPO_4^{2-}, the relative position between the symmetric and asymmetric P=O stretching modes is sensitive to the P=O/P=O coupling constants (c22). The P-O single bond stretching mode at 761 cm^{-1} is mostly related with P-O stretching force constants [s1]. A 0.4 mdyn/Å increase of s1 can shift up this mode by 29 cm^{-1}. The C-O stretching mode at 1055 cm^{-1} is related with c-O stretching force constant, and is almost not affected by the other constants. The deformation modes of $-PO_3^{2-}$ group have similar pattern of correlation as that of HPO_4^{2-} discussed above.

The vibration frequencies of the methyl group are also fitted. Since our major interest is to investigate the phos-

phate group, the correlation for the methyl group, which are also listed in Table 5.15, are not discussed in detail here.

As shown in Table 5.2 and Table 5.14, the P-O stretching force constants for HPO_4^{2-} and $CH_3PO_4^{2-}$ are 4.86 mdyn/Å and 4.26 mdyn/Å, respectively, with a difference about 13.2%. The P=O stretching force constants for HPO_4^{2-} and $CH_3PO_4^{2-}$ are 7.09 mdyn/Å and 6.72 mdyn/Å respectively, with a difference about 5.3%. These force constants of P-O and P=O bonds for HPO_4^{2-} and $CH_3PO_4^{2-}$ are close enough to be transferred between each other, such as from HPO_4^{2-} to $CH_3PO_4^{2-}$, with little modification. In addition, the correlation between the frequencies and the force constants for HPO_4^{2-} and $CH_3PO_4^{2-}$ shown in Table 5.6 and Table 5.15, is similar. Therefore, we can apply these force constants and correlation tables developed from the mono-phosphate compounds to some other similar phosphate compounds with some modifications. For example, we can continue to develop the force fields and correlation between the frequencies and the force constants for di-phosphate and tri-phosphate compounds, by using these force constants and correlation tables developed from the mono-phosphate compounds. More experimental data on di-phosphate and tri-phosphate compounds and their isotopomers will be necessary to carry out these studies.

It is shown in these correlation between the Raman frequencies and the force constants that the frequencies of each chemical functional group mostly depend on the force

constants associate with it. One major advantage of using Raman spectroscopy to study biological system is that Raman frequencies are very sensitive to the hydrogen bondinginteractions, which perturb the electron distributions, and therefore change the force constant of the chemical bond of some chemical functional group. However, the coupling constants between the phosphate vibrational modes can also have large effects on them. The change of Raman frequency sometimes is not caused by the change of force constant or bond order, which is affected by the hydrogen bonding interaction, but is caused by the change of coupling constant or geometry, which is affected also by the environment of certain chemical functional group. This may sometimes make Raman studies complicated.

Atom type	Atom number	Connection	Bond Length	Bond Angle	Dihedral Angle
P	1		0	0	0
O	2	1,	1.55548	0	0
O	3	1, 2,	1.55549	109.474	0
O	4	1, 2, 3,	1.55552	109.472	-119.985
O	5	1, 2, 3,	1.55545	109.468	120.018

Figure 5.1 Structure of PO_4^{3-} from Chem3D.

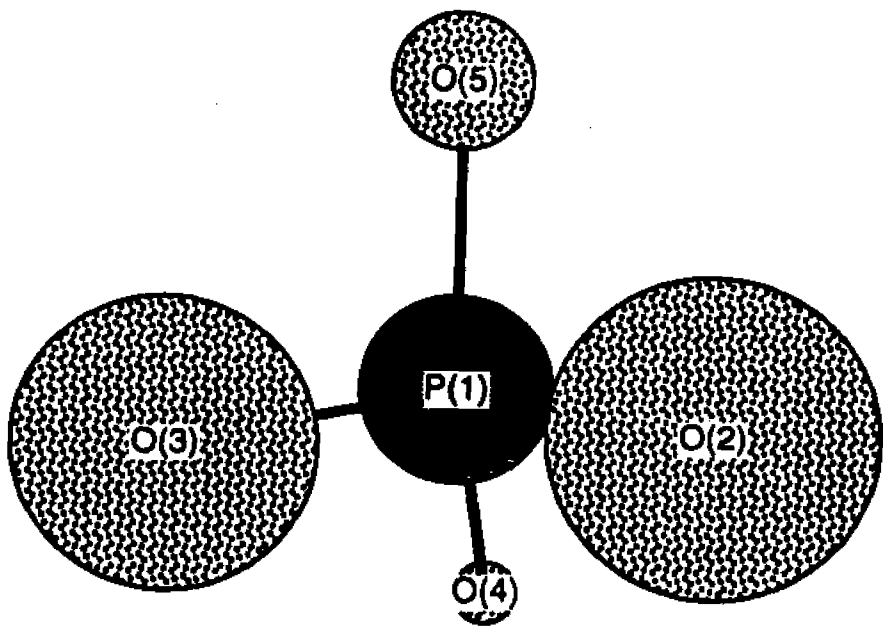

Table 5.1 Geometry parameter used to construct the G matrix for PO_4^{3-}.

Symbol	Description	Force Constant (mdyn/Å)
s2	P=O	5.85
b2	O=P=O	2.3
c22	P=O/P=O	0.84
x22	P=O/O=P=O	0.37
x21	P=O/O=P=O (share P=O)	0.5
y22	O=P=O/O=P=O	0.09
y21	O=P=O/O=P=O (share P=O)	0.53

Table 5.2 General valence force constants obtained from Program VIB for PO_4^{3-}.

f(obs)	f(cal)	Δb2	Δc22	Δs2	Δx21	Δx22	Δy21	Δy22
416	418	31	0	0	0	0	-31	16
416	418	31	0	0	0	0	-31	16
554	557	20	-1	4	8	-8	0	-10
554	557	20	-1	4	8	-8	0	-10
554	557	20	-1	4	8	-8	0	-10
937	942	0	16	22	0	0	0	0
1010	1006	10	-8	34	-18	18	0	-5
1010	1006	10	-8	34	-18	18	0	-4
1010	1006	10	-8	34	-18	18	0	-4
f(obs) (18O)	f(cal) (18O)	Δb2	Δc22	Δs2	Δx21	Δx22	Δy21	Δy22
398	394	29	0	0	0	0	-29	15
398	394	29	0	0	0	0	-29	15
534	529	19	-1	4	9	-9	0	-9
534	529	19	-1	4	9	-9	0	-9
534	529	19	-1	4	9	-9	0	-9
886	888	0	16	22	0	0	0	0
978	981	10	-8	32	-18	18	0	-5
978	981	10	-8	32	-18	18	0	-5
978	981	10	-8	32	-18	18	0	-5

Table 5.3 Correlation table between Raman frequencies and force constants for PO_4^{3-}.

The first column is the observed Raman frequencies; the second column is the calculated Raman frequencies from Program VIB; the third column and after are the changes of frequencies corresponding to the change of each force constant. The symbles for force constants are described as following:

b2: O=P=O bending force constant; s2: P=O stretching force constant; c22: P=O and P=O coupling constant; x21: P=O and O=P=O coupling constant (one shared bond); x22: P=O and O=P=O coupling constant (no shared bond); y21: O=P=O and O=P=O coupling constant (one shared bond); y22: O=P=O and O=P=O coupling constant (no shared bond).

Atom Type	Atom Number	Connection	Bond Length	Bond Angle	Dihedral Angle
P	1		0	0	0
O	2		1.50898	0	0
O	3	1, 2,	1.70232	104.613	0
O	4	1, 2, 3	1.50898	115.655	-114.486
O	5	1, 2, 3	1.51513	115.756	105.434
H	6	3, 1, 2	0.94763	107.439	118.986

Table 5.4 Geometry parameter used to construct the G matrix for HPO_4^{2-}.

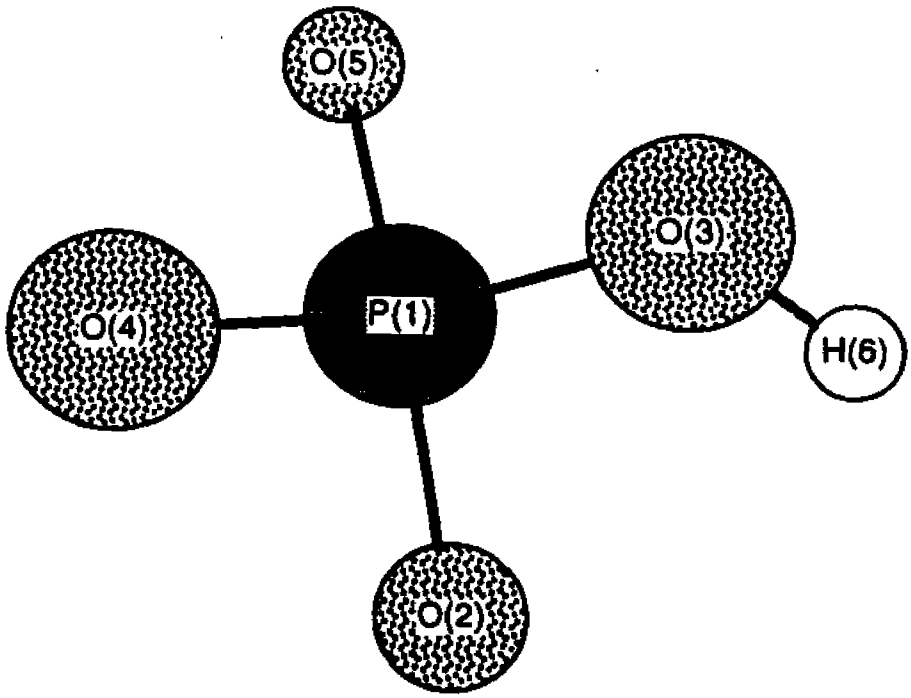

Figure 5.2 Structure of HPO_4^{2-} from Chem3D.

Symbol	Description	Force Constant (mdyn/Å)
s1	P-O	4.86
s2	P=O	7.09
s3	O-H	8
b1	O-P=O	1.6
b2	O=P=O	1.85
b3	H-O-P	1
c12	P-O/P=O	0.35
c22	P=O/P=O	0.67
x11	P-O/O-P=O	0.25
x13	P-O/H-O-P	0.2
x211	P=O/O-P=O (share P=O)	0.6
x212	P=O/O-P=O	0.05
x221	P=O/O=P=O (shareP=O)	0.3
x222	P=O/O=P=O	0.1
x23	P=O/H-O-P	-0.14
x33	O-H/H-O-P	0.2
y11	O-P=O/O-P=O	0.3
y121	O-P=O/O=P=O (share P=O)	-0.06
y13	P-O/H-O-P	-0.02
y22	O=P=O/O=P=O	0.2

Table 5.5 General valence force constants obtained from Program VIB for HPO_4^{2-}.

f(obs)	f(cal)	Δb1	Δb2	Δb3	Δc12	Δc13	Δc22	Δc23
393	385	30	0	0	0	0	0	0
393	401	30	1	0	0	0	0	0
533	523	10	12	0	-1	0	0	0
533	536	3	27	0	0	0	0	0
533	538	2	26	0	0	0	0	0
858	864	3	1	1	7	1	1	1
990	993	3	1	2	-9	0	9	-1
1084	1085	1	5	1	0	0	-8	0
1084	1085	2	5	0	0	0	-8	0
f(obs) (18O)	f(cal) (18O)	Δb1	Δb2	Δb3	Δc12	Δc13	Δc22	Δc23
377	365	28	0	0	0	0	0	0
377	379	28	1	0	0	0	0	0
513	499	10	12	0	-1	0	1	0
513	509	3	25	0	0	0	0	0
513	511	2	24	0	0	0	0	0
833	829	2	1	0	9	0	2	0
950	952	3	1	2	-11	0	9	-1
1053	1052	2	6	2	0	0	-8	0
1053	1053	2	6	0	0	0	-8	0

Table 5.6 Correlation table between Raman frequencies and force constants for HPO_4^{2-}.

The first column is the observed Raman frequencies; the second column is the calculated Raman frequencies from Program VIB; the third column and after are the changes of frequencies corresponding to the change of each force constant. The symbols for force constants are described as following:

Table 5.6

Δs1	Δs2	Δs3	Δx11	Δx12	Δx13	Δx211	Δx212	Δx221	Δx222	Δx23
0	0	0	0	0	0	-1	1	0	0	0
0	0	0	0	0	0	-1	1	0	0	0
2	1	0	6	-4	0	-1	-3	2	0	0
0	0	0	2	0	0	0	0	3	-2	0
0	1	0	0	0	0	1	-1	3	-3	0
26	3	0	-11	7	2	-3	-5	3	1	1
7	19	0	-5	3	-3	5	9	-7	-3	9
1	33	0	0	0	-1	-5	5	-9	9	0
0	34	0	0	0	0	-5	5	-9	9	0
Δs1	Δs2	Δs3	Δx11	Δx12	Δx13	Δx211	Δx212	Δx221	Δx222	Δx23
0	0	0	0	0	0	-1	1	0	0	0
0	0	0	0	0	0	-2	2	0	0	0
2	1	0	5	-3	0	-1	-3	3	1	0
0	1	0	2	-1	0	0	-1	3	-2	0
0	0	0	0	0	0	0	0	4	-4	0
22	5	0	-9	6	2	-2	-5	3	2	2
9	17	0	-7	5	-3	5	11	-7	-3	7
1	32	0	0	0	0	-4	4	-9	9	0
0	33	0	0	0	0	-6	6	-9	9	0

(Table 5.6 continues) b1: O-P=O bending force constant; b2: O=P=P bending force constant; b3: H-O-P bending force constant; c12: P-O and P=O coupling constant; c13: P-O and H-O coupling constant; c22: P=O and P=O coupling constant; c23: P=O and H-O stretching coupling; s1: P-O single bond stretching force constant; s2 P=O double bond stretching force constant; s3: O-H stretching force constant; x11: P-O and O-P=O coupling constant; x12: P-O and O=P=O coupling constant; x13: P-O and H-O-P coupling constant; x211: P=O and O-P=O coupling constant (one shared bond); x212: P=O and O-P=O coupling constant (no shared bond);

Δx31	Δx32	Δx33	Δy11	Δy121	Δy122	Δy13	Δy22	Δy23
0	0	0	-15	-2	2	0	0	0
0	0	0	-15	-5	5	0	0	0
0	0	0	10	-12	-9	0	2	0
0	0	0	2	3	-4	0	-12	0
0	0	0	0	4	-7	0	-13	0
-1	1	0	3	-3	-1	-2	1	1
0	0	0	3	-3	-1	4	1	-3
0	0	0	0	2	-2	0	-2	0
0	0	0	-1	3	-3	0	-2	0
Δx31	Δx32	Δx33	Δy11	Δy121	Δy122	Δy13	Δy22	Δy23
0	0	0	-14	-2	2	0	0	0
0	0	0	-14	-5	5	0	0	0
1	-1	0	9	-10	-7	0	0	0
0	0	0	3	2	-4	0	-11	0
0	0	0	-1	4	-7	0	-12	0
0	0	0	2	-4	-2	-2	1	1
0	0	0	3	-5	-3	4	1	-3
0	0	0	0	2	-2	0	-2	0
0	0	0	-1	3	-3	0	-3	0

(Table 5.6 continues) x221: P=O and O=P=O coupling constant (one shared bond); x222: P=O and O=P=O coupling constant (no shared bond); x23: P=O and H-O-P coupling constant; x31: H-O and O-P=O coupling constant; x32: H-O and O=P=O coupling constant; x33: H-O and H-O-P coupling constant; y11: O-P=O and O-P=O coupling constant; y121: O-P=O and O=P=O coupling constant (one shared bond); y122: O-P=O and O=P=O coupling constant (no shared bond); y13: O-P=O and H-O-P coupling constant; y22: O=P=O and O=P=O coupling constant; y23: O=P=O and H-O-P coupling constant.

Atom type	Atom number	Connection	Bond Length	Bond Angle	Dihedral Angle
P	1				
O	2		1.47764	0	0
O	3	1, 2,	1.63634	110.17	0
O	4	1, 2, 3,	1.63635	103.074	-103.885
O	5	1, 2, 3,	1.47764	128.332	126.707
H	6	3, 1, 2,	0.94966	111.478	154.824
H	7	4, 1, 2,	0.94966	111.475	15.037

Table 5.7 Geometry parameter used to construct the G matrix for $H_2PO_4^-$.

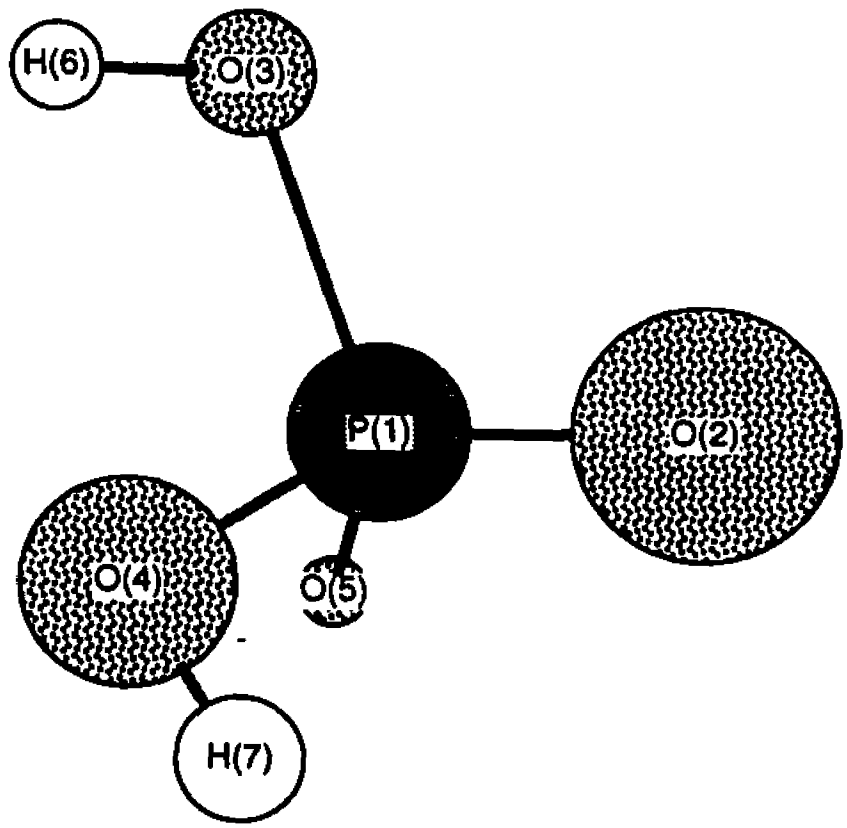

Figure 5.3 Structure of $H_2PO_4^-$ from Chem3D.

Symbol	Description	Force Constant (mdyn/Å)
s1	P-O	5.68
s2	P=O	8.16
s3	O-H	8
b0	O-P-O	1.8
b1	O-P=O	1.5
b2	O=P=O	1.4
b3	H-O-P	1
c11	P-O/P-O	-0.05
c12	P-O/P=O	0.5
c22	P=O/P=O	1.02
x10	P-O/O-P-O	0.2
x111	P-O/O-P=O (share P-O)	0.4
x131	P-O/H-O-P (share P-O)	0.2
x20	P=O/O-P-O	0.1
x211	P=O/O-P=O (share P=O)	0.4
x22	P=O/O=P=O	0.4
x30	O-H/O-P-O	0.1
x331	O-H/H-O-P (share O-H)	0.2
y01	O-P-O/O-P=O	0.2
y03	O-P-O/H-O-P	0.2
y1111	O-P=O/O-P=O (share P-O)	0.05
y1112	O-P=O/O-P=O (share P=O)	0.25
y112	O-P=O/O-P=O	0.1
y12	O-P=O/O=P=O	0.2
y131	O-P=O/H-O-P (share P-O)	-0.02

Table 5.8 General valence force constants obtained from Program VIB for $H_2PO_4^-$.

f(obs)	f(cal)	Δb0	Δb1	Δb2	Δb3	Δc11	Δc12
370	372	16	9	6	1	1	0
390	393	0	33	0	0	0	0
390	400	0	31	0	0	0	0
515	510	0	22	6	0	0	0
515	514	7	13	15	0	0	-1
878	882	1	1	3	1	7	9
943	939	0	4	0	0	-8	0
1077	1078	1	0	2	1	1	-12
1160	1156	0	4	0	6	0	0
f(obs)(18O)	f(cal)(18O)	Δb0	Δb1	Δb2	Δb3	Δc11	Δc12
350	351	15	8	6	2	0	0
370	377	0	31	0	0	0	0
370	378	0	29	0	0	0	0
496	488	1	19	7	0	0	0
496	490	6	13	12	1	1	0
838	845	2	0	2	0	6	10
918	908	0	4	0	0	-8	0
1039	1034	1	1	3	1	1	-12
1131	1122	0	5	0	5	0	0

Table 5.9 Correlation table between Raman frequencies and force constants for $H_2PO_4^-$.

The first column is the observed Raman frequencies; the second column is the calculated Raman frequencies from Program VIB; the third column and after are the changes of frequencies corresponding to the change of each force constant. The symbols for force constants are described as following:

Δc131	Δc132	Δc22	Δc23	Δc33	Δs1	Δs2	Δs3	Δx10
-1	-1	1	1	0	1	1	1	1
0	0	0	0	0	0	0	0	0
0	0	0	0	0	0	0	0	0
0	0	0	0	0	0	0	0	0
0	0	0	0	0	1	0	0	2
1	1	1	1	0	27	1	0	-7
0	0	0	0	0	33	1	0	0
0	0	6	0	0	4	23	0	-2
0	0	-8	0	0	1	31	0	0
Δc131	Δc132	Δc22	Δc23	Δc33	Δs1	Δs2	Δs3	Δx10
0	0	0	0	0	0	0	0	2
0	0	0	0	0	0	0	0	0
0	0	0	0	0	0	0	0	0
0	0	0	0	0	0	0	0	0
0	0	0	0	0	1	0	0	3
0	0	0	0	0	25	2	0	-6
0	0	0	0	0	32	0	0	0
0	0	5	-1	0	5	21	0	-3
0	0	-8	0	0	1	30	0	0

(Table 5.9 continues) b0: O-P-O binding force constant; b1: O-P=O bending force constant; b2: O=P=O bending force constant; b3: H-O-P bending force constant; c11: P-O and P-O coupling constant; c12: P-O and P=O coupling constant; c131: P-O and H-O coupling constant (one shared atom); c132: P-O and H-O coupling constant (no shared atom); c22: P=O and P=O coupling constant; c23: P=O and H-O stretching coupling; c33: H-O and H-O coupling constant;

Δx111	Δx112	Δx12	Δx131	Δx132	Δx20	Δx211	Δx212	Δx22
-1	-1	1	-1	-1	5	1	1	-1
0	0	0	0	0	0	0	0	0
0	0	0	0	0	0	0	0	0
0	0	0	0	0	1	2	-2	0
2	2	-4	0	0	4	-1	-1	2
-3	-3	9	4	4	4	-1	-1	1
-12	12	0	2	-2	0	0	0	0
-1	-1	3	1	1	-21	3	3	-7
0	0	0	-2	2	0	-12	12	0
Δx111	Δx112	Δx12	Δx131	Δx132	Δx20	Δx211	Δx212	Δx22
-1	-1	1	0	0	5	0	0	0
0	0	0	0	0	0	0	0	0
0	0	0	0	0	0	0	0	0
0	0	0	0	0	3	2	-2	0
2	2	-5	-1	-1	2	-1	-1	2
-2	-2	8	3	3	4	0	0	2
-12	12	0	1	-1	0	0	0	0
-1	-1	4	1	1	-22	3	3	-8
0	0	0	-2	2	0	-12	12	0

(Table 5.9 continues) s1: P-O single bond stretching force constant; s2 P=O double bond stretching force constant; s3: O-H stretching force constant; x10: P-O and O-P-O coupling constant; x111: P-O and O-P=O coupling constant (one shared bond); x112 P-O and O-P=O coupling constant (no shared bond); x12: P-O and O=P=O coupling constant; x131: P-O and H-O-P coupling constant (one shared bond); x132: P-O and H-O-P coupling constant (no shared bond); x20: P=O and O-P-O coupling constant;

Δx23	Δx30	Δx311	Δx312	Δx32	Δx331	Δx332	Δy01	Δy02
1	-1	1	1	-1	1	1	-23	10
0	0	0	0	0	0	0	0	0
0	0	0	0	0	0	0	0	0
0	0	0	0	0	0	0	1	-2
0	0	0	0	0	0	0	9	-10
1	-1	0	0	1	1	1	1	-1
0	0	0	0	0	0	0	0	0
-5	0	0	0	0	0	0	1	-2
0	0	0	0	0	0	0	0	0
Δx23	Δx30	Δx311	Δx312	Δx32	Δx331	Δx332	Δy01	Δy02
0	0	0	0	0	0	0	-22	9
0	0	0	0	0	0	0	0	0
0	0	0	0	0	0	0	0	0
0	0	0	0	0	0	0	2	-3
1	0	0	0	0	0	0	7	-8
2	0	0	0	0	0	0	2	-2
0	0	0	0	0	0	0	0	0
-5	0	0	0	0	0	0	1	-2
0	0	0	0	0	0	0	0	0

(Table 5.9 continues) x211: P=O and O-P=O coupling constant (one shared bond); x212: P=O and O-P=O coupling constant (no shared bond); x22: P=O and O=P=O coupling constant; x23: P=O and H-O-P coupling constant; x30: H-O and O-P-O coupling constant; x311: H-O and O-P=O coupling constant (one shared bond); x312: H-O and O-P=O coupling constant (no shared bond); x32: H-O and O=P=O coupling constant; x331: H-O and H-O-P coupling constant (one shared bond); x332: H-O and H-O-P coupling constant (no shared bond); y01: O-P-O and O-P=O coupling constant;

Δy03	Δy1111	Δy1112	Δy112	Δy12	Δy131	Δy132	Δy23	Δy33
-8	4	4	5	-14	5	5	-5	1
0	7	-16	-7	0	3	-3	0	0
0	-6	-15	6	0	0	0	-1	0
0	-10	12	-11	-4	0	0	0	0
-2	-2	4	-3	-13	-2	-2	5	0
-1	1	1	1	-1	-1	-1	3	1
0	2	-2	-2	0	-1	1	0	0
-1	0	0	0	-1	-1	-1	1	0
0	-2	2	-2	0	1	-1	0	-3
Δy03	Δy1111	Δy1112	Δy112	Δy12	Δy131	Δy132	Δy23	Δy33
-7	4	4	4	-13	6	6	-4	1
0	2	-16	-2	0	3	-3	0	0
0	0	-14	0	0	0	0	0	0
0	-9	10	-9	-5	0	0	0	0
-3	-4	5	-4	-11	-2	-2	4	1
-2	0	0	0	-2	0	0	2	0
0	2	-2	-2	0	0	0	0	0
-1	0	0	0	-2	-1	-1	1	1
0	-2	2	-2	0	0	0	0	-2

(Table 5.9 continues) y02: O-P-O and O=P=O coupling constant; y03: O-P-O and H-O-P coupling constant; y1111: O-P=O and O-P=O coupling constant (one shared P-O single bond); y1112: O-P=O and O-P=O coupling constant (one shared P=O double bond); y112: O-P=O and O-P=O coupling constant (no shared bond); y12: O-P=O and O=P=O coupling constant; y131: O-P=O and H-O-P coupling constant (one shared bond); y132: O-P=O and H-O-P coupling constant (no shared bond); y23: O=P=O and H-O-P coupling constant; y33: H-O-P and H-O-P coupling constant.

Atom type	Atom number	Connection	Bond Length	Bond Angle	Dihedral Angle
P	1				
O	2		1.44486	0	0
O	3	1, 2,	1.59234	119.062	0
O	4	1, 2, 3,	1.59242	119.03	-119.986
O	5	1, 2 ,3,	1.59237	119.011	120.054
H	6	3, 1, 2,	0.95341	118.319	-110.688
H	7	4, 1, 2,	0.95332	118.353	-110.291
H	8	5, 1, 2,	0.95334	118.346	-110.535

Table 5.10 Geometry parameter used to construct the G matrix for H_3PO_4.

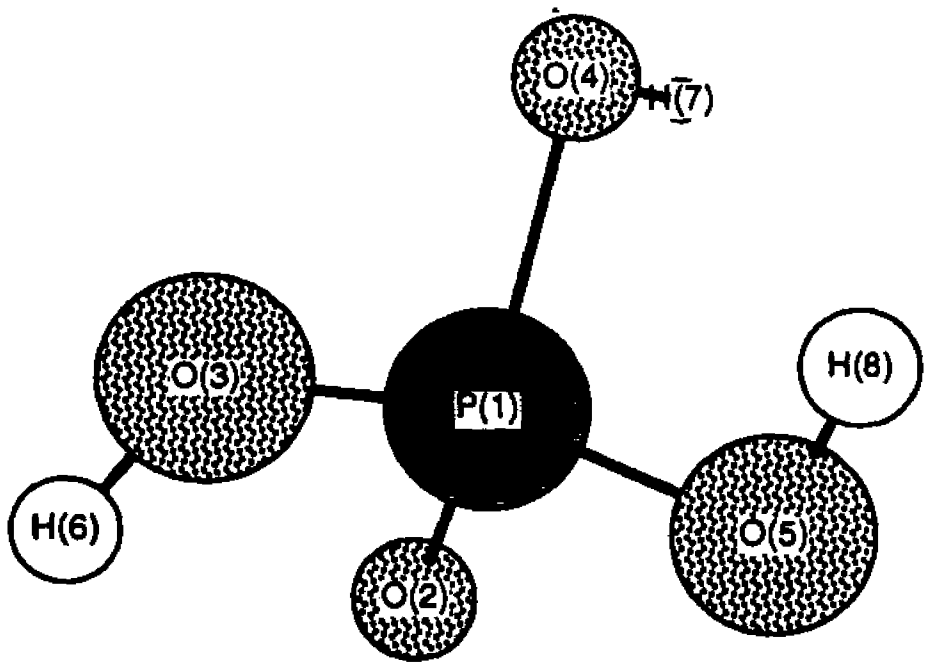

Figure 5.4 Structure of H_3PO_4 from Chem3D.

Symbol	Description	Force Constant (mdyn/Å)
s1	P-O	5.98
s2	P=O	9.18
s3	O-H	8
b0	O-P-O	1.585
b1	O-P=O	1.88
b3	H-O-P	1
c11	P-O/P-O	-0.13
c12	P-O/P=O	0.65
c131	P-O/H-O-P (share P-O)	0.2
x101	P-O/O-P-O	0.2
x111	P-O/O-P=O	0.4
x131	P-O/H-O-P	0.2
x20	P=O/O-P-O	-0.1
x21	P=O/O-P=O	0.7
x301	O-H/O-P=O	0.1
x331	O-H/H-O-P (share O-H)	0.2
y00	O-P-O/O-P-O	0.2
y011	O-P-O/O-P=O	0.2
y031	O-P-O/H-O-P (share P-O)	0.325
y032	O-P-O/H-O-P	0.2
y11	O-P=O/O-P=O	0.3
y131	O-P=O/H-O-P (share P-O)	-0.02

Table 5.11 General valence force constants obtained from Program VIB for H_3PO_4.

f(obs)	f(cal)	Δs1	Δs2	Δs3	Δb0	Δb1	Δb3	Δc11
370	370	0	0	0	26	0	0	0
370	370	0	0	0	26	0	0	0
390	389	4	0	0	23	14	28	2
499	499	1	0	0	0	29	0	-1
499	499	1	0	0	0	29	0	0
890	891	23	1	0	3	2	0	11
1010	1010	28	0	0	2	4	9	-7
1010	1010	28	0	0	1	5	9	-7
1177	1178	5	27	0	3	1	3	2
f(obs)(18O)	f(cal)(18O)	Δs1	Δs2	Δs3	Δb0	Δb1	Δb3	Δc11
350	352	0	0	0	25	0	1	0
350	352	0	0	0	25	0	1	0
370	369	4	0	0	22	13	27	2
483	473	1	0	0	0	28	0	-1
483	474	1	0	0	0	27	0	-1
849	848	21	1	0	3	1	0	11
979	985	27	0	0	2	6	7	-6
979	985	27	0	0	2	5	7	-7
1143	1139	6	25	0	4	2	3	2

Table 5.12 Correlation table between Raman frequencies and force constants for H_3PO_4.

The first column is the observed Raman frequencies; the second column is the calculated Raman frequencies from Program VIB; the third column and after are the changes of frequencies corresponding to the change of each force constant. The symbols for force constants are described as following:

Δc12	Δc131	Δc132	Δc23	Δc33	Δx101	Δx102	Δx111	Δx112	Δ131
0	0	0	0	0	2	-2	0	0	0
0	0	0	0	0	2	-2	0	0	0
1	0	0	0	0	14	7	-5	-11	-7
0	0	0	0	0	0	0	5	-5	0
0	0	0	0	0	0	0	4	-4	0
4	0	1	0	0	-11	-5	4	9	1
0	0	0	0	0	-4	4	-8	8	10
0	0	0	0	0	-4	4	-8	8	10
-10	0	0	0	0	-5	-3	2	4	3
Δc12	Δc131	Δc132	Δc23	Δc33	Δx101	Δx102	Δx111	Δx112	Δx131
0	0	0	0	0	2	-2	0	0	0
0	0	0	0	0	2	-2	0	0	0
1	0	-1	0	0	13	7	-5	-11	-7
0	0	0	0	0	0	0	5	-5	1
0	0	0	0	0	0	0	5	-5	0
5	1	1	0	0	-11	-5	4	8	1
0	0	0	0	0	-4	4	-8	8	8
0	0	0	0	0	-4	4	-8	8	8
-10	0	0	0	0	-6	-3	2	4	3

(Table 5.12 continues) s1: P-O single bond stretching force constant; s2 P=O double bond stretching force constant; s3: O-H stretching force constant; b0: O-P-O binding force constant; b1: O-P=O bending force constant; b3: H-O-P bending force constant; c11: P-O and P-O coupling constant; c12: P-O and P=O coupling constant; c131: P-O and H-O coupling constant (one shared atom); c132: P-O and H-O coupling constant (no shared atom); c23: P=O and H-O stretching coupling; c33: H-O and H-O coupling constant; x101: P-O and O-P-O coupling constant (one shared bond); x102: P-O and O-P-O coupling constant (no shared bond); x111: P-O and O-P=O coupling constant (one shared bond); x112 P-O and O-P=O coupling constant (no shared bond);

Δx132	Δx20	Δx21	Δx23	Δx301	Δx302	Δx311	Δx312	Δx331	Δx332
0	0	0	0	0	0	0	0	0	0
0	0	0	0	0	0	0	0	0	0
-15	2	-2	-2	-1	0	0	1	0	1
0	0	0	0	0	0	0	0	0	0
0	0	0	0	0	0	0	0	0	0
2	-2	1	1	0	0	0	0	0	0
-10	0	0	0	0	0	0	0	0	0
-10	0	0	0	0	0	0	0	0	0
5	10	-8	-10	0	0	0	0	0	0
Δx132	Δx20	Δx21	Δx23	Δx301	Δx302	Δx311	Δx312	Δx331	Δx332
0	0	0	0	0	0	0	0	0	0
0	0	0	0	0	0	0	0	0	0
-14	2	-1	-2	-1	-1	1	1	1	1
-1	0	0	0	0	0	0	0	0	0
0	0	0	0	0	0	0	0	0	0
1	-3	1	1	-1	0	0	1	0	0
-8	0	0	0	0	0	0	0	0	0
-8	0	0	0	0	0	0	0	0	0
5	11	-8	-10	0	0		0	0	0

(Table 5.12 continues) x131: P-O and H-O-P coupling constant (one shared bond); x132: P-O and H-O-P coupling constant (no shared bond); x20: P=O and O-P-O coupling constant; x21: P=O and O-P=O coupling constant; x23: P=O and H-O-P coupli g constant; x301: H-O and O-P-O coupling constant (one shared atom); x302: H-O and O-P-O coupling constant (no shared atom); x311: H-O and O-P=O coupling constant (one shared bond); x312: H-O and O-P=O coupling constant (no shared bond); x331: H-O and H-O-P coupling constant (one shared bond); x332: H-O and H-O-P coupling constant (no shared bond);

Δy00	Δy011	Δy012	Δy031	Δy032	Δy11	Δy131	Δy132	Δy33
-14	-1	0	-10	3	0	0	3	0
-14	0	0	-3	3	0	0	0	0
23	-37	-19	-44	-26	0	20	38	28
0	-1	1	0	0	0	1	-1	0
0	-1	1	0	0	0	1	-1	0
3	-4	-2	-1	-1	0	1	1	0
0	2	-2	-4	4	0	-6	6	-4
-1	2	-2	-3	3	0	-6	6	-4
3	-4	-2	-5	-3	0	2	5	3
Δy00	Δy011	Δy012	Δy031	Δy032	Δy11	Δ131	Δy132	Δy33
-12	-1	0	-10	2	0	0	3	0
-13	0	0	-2	2	0	0	0	0
21	-34	-17	-41	-24	0	19	35	27
0	0	0	0	0	0	0	0	0
0	0	0	0	0	0	1	-1	0
3	-4	-2	-1	-1	0	1	1	0
0	2	-2	-3	3	0	-6	6	-4
-1	3	-3	-3	3	0	-6	6	-4
4	-5	-2	-5	-3	0	2	5	3

(Table 5.12 continues) y00: O-P-O and O-P-O coupling constant; y011: O-P-O and O-P=O coupling constant (one shared bond); y012: O-P-O and O-P=O coupling constant (no shared bond); y031: O-P-O and H-O-P coupling constant (one shared bond); y032: O-P-O and H-O-P coupling constant (no shared bond); y11: O-P=O and O-P=O coupling constant; y131: O-P=O and H-O-P coupling constant (one shared bond); y132: O-P=O and H-O-P coupling constant (no shared bond); y33: H-O-P and H-O-P coupling constant.

Atom type	Atom number	Connection	Bond Length	Bond Angle	Dihedral Angle
P	1				
O	2		1.50434	0	0
O	3	1, 2,	1.50708	116.544	0
O	4	1, 2, 3,	1.50706	116.547	-140.678
O	5	1, 2, 3,	1.74322	102.109	109.657
C	6	5, 1, 2,	1.36437	113.711	180.055
H	7	6, 5, 1,	1.13347	110.977	121.657
H	8	6, 5, 1,	1.12274	112.019	0.016
H	9	6, 5, 1,	1.13349	110.978	-121.626

Table 5.13 Geometry parameters used to cinstruct the G Matrix for Methyl phosphate.

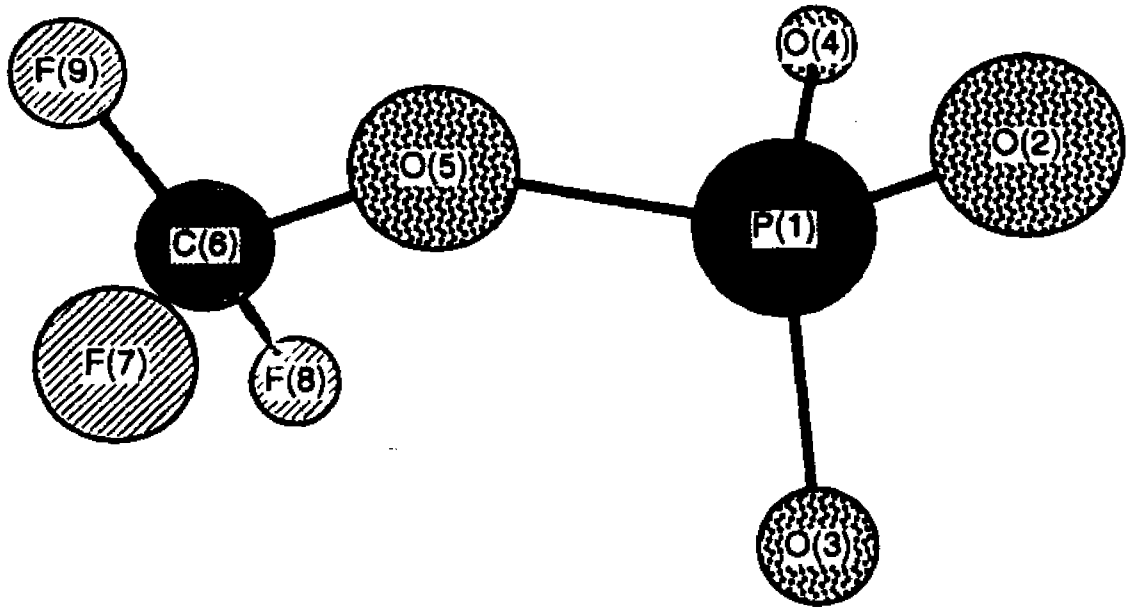

Figure 5.5 Structure of Methyl phosphate from Chem3D.

Symbol	Description	Force Constant (mdyn/Å)
s1	P-O	4.26
s21	P=O (in C-O-P plane)	7
s22	P=O (out of C-O-P plane)	6.58
s3	C-O	4.94
s41	C-H (in C-O-P plane)	4.6
s42	C-H (out of C-O-P plane)	4.86
b11	O-P=O (in C-O-P plane)	1.74
b12	O-P=O (out of C-O-P plane)	1.74
b21	O=P=O (normal to C-O-P)	1.8
b22	O=P=O	2.14
b3	C-O-P	0.7
b41	H-C-H (normal to C-O-P)	0.59
b42	H-C-H	0.59
b51	H-C-O (in C-O-P plane)	0.98
b52	H-C-O (out of C-O-P plane)	1.05
c12	P-O/P=O	0.5
c13	P-O/C-O	0.2
c22	P=O/P=O	0.85
c34	C-O/C-H	0.5
c44	C-H/C-H	0.02
x11	P-O/O-P=O	0.4
x13	P-O/C-O-P	0.2
x21	P=O/O-P=O	0.4
x22	P=O/O=P=O	0.4
x33	C-O/C-O-P	0.2
x35	C-O/H-C-O	0.4
x44	C-H/H-C-H	0.09
x45	C-H/H-C-O	0.3

y11	O-P=O/O-P=O	0.3
y12	O-P=O/O=P=O	0.06
y13	O-P=O/C-O-P	-0.015
y22	O=P=O/O=P=O	0.2
y35	C-O-P/H-C-O	0.1
y44	H-C-H/H-C-H	0.045
y45	H-C-H/H-C-O	0.05
y55	H-C-O/H-C-O	0.05

Table 5.14 General valence force constants obtained from Program VIB for Methyl phosphate.

MP(obs)	MP(cal)	Δs1	Δs21	Δs22	Δs3	Δs41	Δs42	Δb11	Δb12
215	215	0	0	0	0	0	0	1	1
387	386	0	0	0	1	0	0	15	4
402	403	0	0	0	0	0	0	0	27
516	508	1	0	1	0	0	0	1	7
540	549	1	1	1	0	0	0	0	4
566	566	0	0	3	0	0	0	0	0
761	762	29	0	0	2	0	0	3	2
982	982	1	4	18	0	0	0	1	1
1055	1055	3	2	0	37	0	1	1	1
1090	1090	0	0	32	0	0	0	0	3
1115	1119	1	22	8	2	0	0	1	1
1160	1160	0	0	0	0	0	0	0	1
1188	1187	2	0	0	0	0	0	0	0
1450	1451	1	0	0	0	0	0	0	0
1464	1465	0	0	0	0	0	0	0	0
1464	1495	0	0	0	4	2	4	0	0
2915	2918	0	0	0	0	101	20	0	0
2997	3001	0	0	0	0	24	99	0	0
3021	3020	0	0	0	0	0	124	0	0
MOP(obs)	MOP(cal)	Δs1	Δs21	Δs22	Δs3	Δs41	Δs42	Δb11	Δb12
382	382	0	0	0	1	0	0	15	4
398	395	0	0	1	0	0	0	0	26
509	501	2	0	0	0	0	0	2	8
532	546	1	1	1	0	0	0	0	3
557	566	0	0	3	0	0	0	0	0
743	746	28	0	0	2	0	0	4	2
981	982	2	4	18	0	0	0	0	1
1025	1025	3	1	0	37	1	1	1	1
1090	1090	0	0	32	0	0	0	0	2
1112	1117	1	23	8	1	0	0	1	1
1158	1157	0	0	0	0	0	0	0	0
1188	1180	1	0	0	0	0	0	0	0
MPO(obs)	MPO(cal)	Δs1	Δs21	Δs22	Δs3	Δs41	Δs42	Δb11	Δb12
377	374	0	0	0	1	0	0	14	3
391	391	0	0	0	0	0	0	0	26
497	488	0	0	0	0	0	0	2	6
518	526	1	2	0	0	0	0	0	6
551	536	0	0	3	0	0	0	0	0
756	758	28	0	1	2	0	0	3	1
945	934	2	4	16	0	0	0	1	1
1052	1051	3	5	5	29	0	0	0	0
1067	1063	0	0	28	2	0	0	0	3
1095	1094	1	18	7	7	0	0	2	2
1160	1160	0	0	0	0	0	0	0	0
1188	1187	2	0	0	1	0	0	0	0

Δb21	Δb22	Δb3	Δb41	Δb42	Δb51	Δb52	Δc12	Δc13	Δc14	Δc22	Δc23	Δc24
0	0	24	1	0	0	1	0	0	0	0	0	0
0	1	6	0	0	0	0	0	0	0	0	0	0
0	1	0	0	0	0	0	0	0	0	0	0	0
13	0	3	0	0	0	1	-1	0	0	0	0	0
8	11	3	1	0	0	1	-1	0	0	-1	0	0
0	26	0	0	0	0	0	0	0	0	-1	0	0
1	1	3	1	0	1	1	2	3	-1	0	1	0
1	0	0	0	0	0	0	-5	-1	0	11	2	0
0	0	1	0	1	2	0	1	-5	1	-1	-2	1
0	7	0	1	0	0	1	0	0	0	-8	0	0
3	3	1	9	0	0	2	-1	-1	1	-7	1	-1
0	0	0	67	10	62	75	0	0	0	0	0	0
0	0	4	12	47	0	19	0	0	0	0	0	0
0	0	0	77	80	24	27	0	0	0	0	0	0
0	0	0	159	21	0	48	0	0	0	0	0	0
0	0	0	88	48	33	61	0	0	0	0	0	0
0	0	0	3	0	0	3	0	0	0	0	0	0
0	0	0	0	2	2	0	0	0	0	0	0	0
0	0	0	1	0	0	1	0	0	0	0	0	0
Δb21	Δb22	Δb3	Δb41	Δb42	Δb51	Δb52	Δc12	Δc13	Δc14	Δc22	Δc23	Δc24
0	1	7	0	0	0	0	0	0	0	0	0	0
0	1	0	1	0	0	1	0	0	0	-1	0	0
11	0	4	0	0	0	0	0	0	0	0	0	0
10	11	3	0	0	0	1	-1	0	0	-1	0	0
0	26	0	0	0	0	0	0	0	0	-1	0	0
0	2	2	0	0	0	1	2	4	-1	0	0	0
0	0	0	0	0	0	0	-6	0	0	10	3	-1
0	0	1	0	1	1	0	1	-5	1	0	-3	1
0	7	0	0	0	0	1	0	0	0	-8	0	0
3	3	1	9	1	1	3	-1	-1	1	-7	1	-1
0	0	0	65	13	64	71	0	0	0	0	0	0
0	0	4	11	42	0	23	0	0	0	0	0	0
Δb21	Δb22	Δb3	Δb41	Δb42	Δb51	Δb52	Δc12	Δc13	Δc14	Δc22	Δc23	Δc24
0	1	7	0	0	0	0	0	0	0	0	0	0
0	0	0	0	0	0	0	0	0	0	0	0	0
15	0	2	0	0	0	0	0	0	0	0	0	0
5	11	5	0	0	0	0	-1	0	0	0	0	0
0	24	0	0	0	0	0	0	0	0	-1	0	0
1	1	3	1	0	1	1	3	3	-1	1	1	-1
0	0	0	0	0	0	0	-6	0	0	10	0	0
0	0	0	0	0	2	0	0	-5	2	-2	-1	0
0	7	0	1	0	0	1	0	0	0	-7	0	0
3	2	2	0	0	0	0	0	-1	0	-6	1	0
0	0	0	74	11	62	76	0	0	0	0	0	0
0	0	4	12	46	0	19	0	-1	0	0	0	0

Δc34	Δc44	Δx11	Δx12	Δx13	Δx14	Δx15	Δx21	Δx22	Δx23	Δx24	Δx25	Δx31
0	0	1	0	1	1	-1	0	0	0	0	0	0
0	0	0	0	1	0	0	0	0	0	0	0	1
0	0	0	0	0	0	0	0	0	0	0	0	0
0	0	3	-3	-1	-1	1	-5	3	1	1	-1	1
0	0	1	-1	-1	-1	1	-1	1	1	1	-1	0
0	0	0	0	0	0	0	0	0	0	0	0	0
-1	0	-15	10	-7	-2	2	-2	1	-1	-1	1	-3
0	0	-1	1	0	0	0	11	-7	0	1	0	1
-5	1	-1	0	1	0	0	0	0	1	0	0	1
0	0	0	0	0	0	0	0	0	0	0	0	0
-1	0	-1	0	1	1	-1	1	0	-1	-1	1	1
0	0	0	0	0	0	0	0	0	0	0	0	0
0	0	0	0	-2	-3	2	0	0	0	0	0	0
0	0	0	0	0	1	-1	0	0	0	0	0	0
0	0	0	0	0	0	0	0	0	0	0	0	0
4	3	0	0	0	2	-1	0	0	0	0	0	0
-4	29	0	0	0	0	0	0	0	0	0	0	0
-2	-2	0	0	0	0	0	0	0	0	0	0	0
0	-31	0	0	0	0	0	0	0	0	0	0	0
Δc34	Δc44	Δx11	Δx12	Δx13	Δx14	Δx15	Δx21	Δx22	Δx23	Δx24	Δx25	Δx31
0	0	1	0	1	0	0	0	0	0	0	0	1
0	0	0	0	0	0	0	0	0	0	0	0	0
0	0	5	-4	-2	0	0	-4	3	2	0	0	0
0	0	1	-1	-1	-1	1	-1	1	1	0	0	0
0	0	0	0	0	0	0	0	0	0	0	0	0
0	0	-16	10	-6	-1	1	-2	2	-1	0	0	-4
0	0	-2	1	0	0	0	11	-8	0	1	-1	2
-5	1	0	0	1	1	-1	0	0	1	1	0	1
0	0	0	0	0	0	0	0	0	0	0	0	0
-1	0	-1	1	1	1	-1	1	-1	-1	-1	1	1
0	0	0	0	0	0	0	0	0	0	0	0	0
0	0	0	0	-2	-2	2	0	0	0	-1	0	0
Δc34	Δc44	Δx11	Δx12	Δx13	Δx14	Δx15	Δx21	Δx22	Δx23	Δx24	Δx25	Δx31
0	0	1	0	1	0	0	0	0	0	0	0	1
0	0	0	0	0	0	0	0	0	0	0	0	0
0	0	3	-2	0	0	0	-4	2	1	0	0	0
0	0	2	-1	-1	0	0	-3	2	1	0	0	0
0	0	0	0	0	0	0	0	0	0	0	0	0
-1	0	-13	9	-7	-2	2	-3	2	-1	-1	1	-3
0	0	-2	2	0	0	0	13	-9	1	1	0	0
-4	0	0	0	0	0	0	0	0	0	0	0	1
0	0	0	0	0	0	0	0	0	0	0	0	0
-1	0	0	0	1	0	0	0	0	0	0	0	1
0	0	0	0	0	0	0	0	0	0	0	0	0
0	0	0	0	-2	-3	2	0	0	0	0	0	0

Table 5.15

Δx32	Δx33	Δx34	Δx35	Δx41	Δx42	Δx43	Δx44	Δx45	Δy11	Δy12	Δy13	Δy14
0	-1	0	0	1	0	1	1	-1	-1	-1	3	1
0	2	0	0	0	0	0	0	0	-9	-1	3	0
0	0	0	0	0	0	0	0	0	-13	0	0	0
-1	-1	0	0	-1	1	0	0	0	9	-17	-8	-2
0	0	0	0	0	0	0	0	0	3	-6	-6	-1
0	0	0	0	0	0	0	0	0	0	0	0	0
3	-2	-1	1	1	-1	1	0	0	5	-10	7	2
-1	0	0	0	0	0	0	0	0	1	-3	0	0
-1	-4	-2	1	0	0	1	0	0	-1	0	0	0
0	0	0	0	0	0	0	0	0	-1	0	0	0
-1	-1	-1	1	-1	0	1	0	-1	-1	0	-1	-1
0	0	0	0	0	0	0	0	0	0	0	0	0
0	1	1	-1	0	0	0	0	0	0	0	0	0
0	0	0	0	0	0	0	1	-1	0	0	0	0
0	0	0	0	0	0	0	0	0	0	0	0	0
0	0	23	-21	0	0	-1	54	-51	0	0	0	0
0	0	1	-1	0	0	3	-30	29	0	0	0	0
0	0	0	0	0	0	-4	-13	11	0	0	0	0
0	0	0	0	0	0	0	0	0	0	0	0	0
Δx32	Δx33	Δx34	Δx35	Δx41	Δx42	Δx43	Δx44	Δx45	Δy11	Δy12	Δy13	Δy14
0	1	0	0	0	0	0	0	0	-9	-1	3	1
0	0	0	0	0	0	0	0	0	-13	0	0	0
0	0	0	0	0	0	0	0	0	9	-18	-10	-2
0	0	0	0	0	0	0	0	0	1	-4	-4	-1
0	0	0	0	0	0	0	0	0	0	0	0	0
2	-2	0	0	1	0	0	0	0	6	-12	8	2
0	0	0	0	0	0	0	0	0	2	-3	0	0
-1	-3	-1	1	0	0	1	1	-1	-1	0	0	0
0	0	0	0	0	0	0	0	0	-1	0	0	0
-1	-1	-1	1	-1	0	1	0	-1	-1	-1	-1	-1
0	0	0	0	0	0	0	0	0	0	0	0	0
0	1	1	-1	0	0	0	0	0	0	0	0	1
Δx32	Δx33	Δx34	Δx35	Δx41	Δx42	Δx43	Δx44	Δx45	Δy11	Δy12	Δy13	Δy14
-1	2	0	0	0	0	0	0	0	-8	-1	4	1
0	0	0	0	0	0	0	0	0	-13	0	0	0
0	0	0	0	0	0	0	0	0	7	-14	-6	-1
0	0	0	0	0	0	0	0	0	4	-10	-8	-2
0	0	0	0	0	0	0	0	0	0	0	0	0
3	-1	-1	1	1	-1	1	1	-1	4	-9	7	2
0	0	0	0	0	0	0	0	0	2	-3	0	0
0	-2	-1	1	0	0	0	0	0	0	0	0	0
0	0	0	0	0	0	0	0	0	-1	0	0	0
0	-3	0	0	0	0	1	0	0	-2	0	0	0
0	0	0	0	0	0	0	0	0	0	0	0	0
0	1	1	-1	0	0	1	1	-1	0	0	1	1

Δy15	Δy22	Δy23	Δy24	Δy25	Δy34	Δy35	Δy44	Δy45	Δy55
-1	0	-2	-1	1	5	-4	1	-1	1
0	0	-2	0	0	1	-1	0	0	0
0	0	0	0	0	0	0	0	0	0
2	0	5	1	-1	1	-1	0	0	0
1	-8	4	1	-1	1	-1	0	-1	0
0	-12	0	0	0	0	0	0	0	0
-2	3	-5	-2	2	1	-1	0	-1	-1
0	1	0	0	0	0	0	0	0	0
0	0	0	0	0	0	0	0	0	-1
0	-3	0	0	0	0	0	0	0	-1
1	-3	1	0	0	1	-1	0	0	0
0	0	0	0	0	0	0	-35	0	-39
0	0	0	0	0	5	-4	-29	-7	-38
0	0	0	0	0	-1	1	-29	-126	-2
0	0	0	0	0	0	0	-79	-13	-10
0	0	0	0	0	-6	5	39	-183	66
0	0	0	0	0	-1	1	2	-8	2
0	0	0	0	0	1	-1	0	-3	0
0	0	0	0	0	0	0	-1	0	-1
Δy15	Δy22	Δy23	Δy24	Δy25	Δy34	Δy35	Δy44	Δy45	Δy55
-1	0	-2	0	0	2	-2	0	0	0
0	-1	0	0	0	0	0	-1	0	-1
2	1	6	1	-1	0	0	0	0	0
1	-9	3	1	-1	1	-1	0	0	0
0	-12	0	0	0	0	0	0	0	0
-2	2	-4	-1	1	1	-1	0	0	0
0	0	0	0	0	0	0	0	0	0
0	0	0	0	0	1	-1	0	0	-1
0	-3	0	0	0	0	0	0	0	0
1	-3	1	0	0	1	-1	-1	0	-1
0	0	0	0	0	0	0	-35	0	-39
0	0	0	0	0	5	-4	-28	-7	-39
Δy15	Δy22	Δy23	Δy24	Δy25	Δy34	Δy35	Δy44	Δy45	Δy55
-1	0	-2	0	0	2	-2	0	0	0
0	0	0	0	0	0	0	0	0	0
1	-3	4	1	-1	0	0	0	0	0
2	-4	5	1	-1	1	-1	0	0	0
0	-12	0	0	0	0	0	0	0	0
-2	2	-5	-1	1	1	-1	0	-1	-1
0	1	0	0	0	0	0	0	0	0
0	0	0	0	0	0	0	0	0	0
0	-3	0	0	0	0	0	0	0	0
0	-3	0	0	0	0	0	0	0	0
0	0	0	0	0	0	0	-35	0	-39
-1	0	-1	-1	1	5	-4	-29	-7	-39

Table 5.15 Correlation table between Raman frequencies and force constants for MP, MOP and MPO.

The first column is the observed Raman frequencies; the second column is the calculated Raman frequencies from Program VIB; the third column and after are the changes of frequencies corresponding to the change of each force constant. The symbols for force constants are described as following:

s1: P-O single bond stretching force constant; s21: P=O double bond stretching force constant (in the plane of C-O-P); s22: P=O double bond stretching force constant (out of the plane of C-O-P); s3: C-O stretching force constant; s41: C-H stretching force constant (in the plane of C-O-P); s42: C-H stretching force constant (out of the plane of C-O-P); b11: O-P=O bending force constant (in the plane of C-O-P); b12: O-P=O bending force constant (out of the plane of C-O-P); b21: O=P=O bending force constant (perpendicular to the plane of C-O-P); b22: O=P=O bending force constant (not perpendicular to the plane of C-O-P); b3: C-O-P bending force constant; b41: H-C-H bending force constant (perpendicular to the plane of C-O-P); b42: H-C-H bending force constant (not perpendicular to the plane of C-O-P); b51: H-C-O bending force constant (in the plane of C-O-P); b52: H-C-O bending force constant (out of the plane of C-O-P); c12: P-O and P=O coupling constant; c13: P-O and C-O coupling constant; c14: P-O and C-H coupling constant; c22: P=O and P=O coupling constant; c23: P=O and C-O coupling constant; c24: P=O and C-

H coupling constant; c34: C-O and C-H coupling constant; c44: C-H and C-H coupling constant; x11: P-O and O-P=O coupling constant; x12: P-O and O=P=O coupling constant; x13: P-O and C-O-P coupling constant; x14: P-O and H-C-H coupling constant; x15: P-O and H-C-O coupling constant; x21: P=O and O-P=O coupling constant; x22: P=O and O=P=O coupling constant; x23: P=O and C-O-P coupling constant; x24: P=O and H-C-H coupling constant; x25: P=O and H-C-O coupling constant; x31: C-O and O-P=O coupling constant; x32: C-O and O=P=O coupling constant; x33: C-O and C-O-P coupling constant; x34: C-O and H-C-H coupling constant; x35: C-O and H-C-O coupling constant; x41: C-H and O-P=O coupling constant; x42: C-H and O=P=O coupling constant; x43: C-H and C-O-P coupling constant; x44: C-H and H-C-H coupling constant; x45: C-H and H-C-O coupling constant; y11: O-P=O and O-P=O coupling constant; y12: O-P=O and O=P=O coupling constant; y13: O-P=O and C-O-P coupling constant; y14: O-P=O and H-C-H coupling constant; y15: O-P=O and H-C-O coupling constant; y22: O=P=O and O=P=O coupling constant; y23 O=P=O and C-O-P coupling constant; y24: O=P=O and H-C-H coupling constant; y25: O=P=O and H-C-O coupling constant; y34: C-O-P and H-C-H coupling constant; y35: C-O-P and H-C-P coupling constant; y44: H-C-H and H-C-H coupling constant; y45: H-C-H and H-C-O coupling constant; y55: H-C-O and H-C-O coupling constant.

Chapter 6

INTERACTIONS BETWEEN *ras*-p21 PROTEINS AND GUANINE NUCLEOTIDES AT PHOSPHATE MOIETY

The phosphate motif of guanine nucleotide plays a very important role both in binding and in GTP hydrolysis. It has been found that the removal of the second phosphate of the nucleotide seems to induce a structural rearrangement, and therefore, reduces its affinity to *ras*-p21 proteins by a factor of more than 10^6 (John, J. et al., 1990). Phosphate groups of GDP and GTP are negatively charged under physical pH. As it is generally believed that phosphotransferases require at least one divalent cation complexed directly to phosphoryl group oxygen atoms for catalytic activity, the GTPase activity of p21 is absolutely dependent on the presence of Mg^{2+}, underscoring the importance of this cofactor (Wittinghofer, F. et al, 1991).

Figure 6.1 shows the protein-nucleotide interactions of p21 GppNHp from X-ray studies (Pai, E. F. et al., 1989). The phosphate binding site is anchored in a pocket formed by Loop1, Loop2 and Loop4, and is characterized by a number of interactions(de Vos, A. M. et al., 1988). Each of the eight phosphate oxygen atoms of GppNHp has at least two hydrogen bond donors or the Mg^{2+} ion close enough for an interaction. The hydrogen bond donors include the main chain-NH groups of

residues 13 to 18, 35, and 60, the hydroxyl groups of Ser17 and Thr35, and the phenolic hydroxyl of Tyr32 from a neighboring p21, which contacts the γ-phosphate. The ϵ-amino group of Lys16 interacts with the β- and γ-phosphate oxygen atoms, but it is closer to the latter. The main chain nitrogen atoms of residues 13 to 18 point toward the phosphate groups, thereby creating a strong electrostatic field. As shown in Figure 6.1, the three dimensional p21-GppNHp complexed with Mg^{2+} is coordinated to one oxygen of each the β- and γ-phosphates, as well as to the side chain hydroxyl groups of Ser17 and Thr35, both of which are highly conserved in all GNB proteins (Pai, E. et al., 1989).

In the p21•GDP complex state, there are several differences at the active site when compared with the GTP state. Lys16 still interacts with the backbone carbonyl group of residues 10 and 11, but not with the β-phosphate. The coordination of Mg^{2+} is similar to that seen for p21-GppNHp, but there are only one interaction with the nucleotide (β-phosphate group).

Here we present the data from our Raman spectroscopic studies on the interactions between *ras*-p21 proteins and GDP or GTP. As discussed previously (Chapter 2), the Raman difference signal from the phosphate group is very weak and is on the same order as that from protein conformational changes; therefore, isotopic editing, which modifies the

oxygen atoms of β- or γ-phosphate by ^{18}O, is used. We use Raman difference spectroscopy to study the protein-nucleotide interactions in order to get rid of the overwhelming protein background signals. Raman spectra of both labeled and unlabeled protein-nucleotide complex are taken, and thus the difference spectrum between protein bound labeled and unlabeled nucleotides are obtained. The bands with derivative-like features, containing both positive peaks and negative peaks due to the shifts caused by the chemical modification and isotopic labeling, dominant the difference spectra.

As described previously by our group (Manor, D. et al., 1990; Weng, G. Thesis), The zero-crossings are of importance in a difference spectrum. Assuming that a particular band can be described by a Lorentzian intensity profile centered at ν_u (for unlabeled) and that the band shifts by $\Delta\nu$ to ν_l (for labeled) upon labeling without change in intensity or band width, then the intensity profile for the unlabeled band is

$$I_u = \frac{A}{(\nu - \nu_u)^2 + \frac{1}{4}\Gamma^2} \qquad \ldots(6.1)$$

while the profile for the labeled band is

$$I_l = \frac{A}{(\nu - \nu_l)^2 + \frac{1}{4}\Gamma^2} \qquad \ldots(6.2)$$

where Γ is the band width and A is an intensity scaling constant. It can be easily calculated that the difference be-

tween I_u and I_l goes to zero at the average frequency position, $(\nu_u + \nu_l)/2$, regardless of the band width and frequency shift. Thus, we use the zero-crossing positions of the derivative-like bands to determine the positions of the Raman bands both in solution and in protein. By comparing the Raman bands in the difference Raman spectra in solution and in protein, we can get the information of the hydrogen bondinginteractions between protein and nucleotide at certain molecular group. Both wild type p21 and mutant p21 proteins, such as p21(G12V), p21(G12D) and p21(G12P) are studied here.

6.1 Difference Spectra between GDP and β-$^{18}O_3$-GDP in Solution, Wild Type p21 and Mutant p21 Proteins.

Figure 6.2 shows the difference spectra between GDP and β-$^{18}O_3$-GDP in solution, wild type p21, mutant p21(G12V) and mutant p21(G12P) at pH 7.5. Because of the importance of Mg^{2+} in the binding and GTP hydrolysis inside p21 proteins, we have 1:1 Mg^{2+} in both solution and protein spectra during our Raman studies.

The major derivative-like band in the solution difference spectrum (Fig 6.2a) has a positive peak at 946 cm^{-1} and a negative peak at 921 cm^{-1} with a zero-crossing position at 933 cm^{-1}. This band is assigned to the symmetric P=O

stretching vibration of the β-PO_3^{2-} group of GDP. This band splits to two bands in the difference spectra in proteins (Fig 6.2b, 6.2c, 6.2d). This may be due to the inhomogeneous interactions on the three oxygen atoms of the β-PO_3^{2-} group inside proteins. X-ray study shows that the three oxygen atoms of $P_\beta O_3^{2-}$ group do not equally interact with the protein. One oxygen atom directly interact with Lys16 residue and the other two oxygen atoms interact with Mg^{2+} and a water molecule respectively (Wittinghofer, F. 1993). These two split bands in proteins have positive peaks at 919 cm^{-1}, 893 cm^{-1} and negative peaks at 904 cm^{-1} and 886 cm^{-1} respectively. The large downshifts of these bands in protein spectra compared with those in solution spectrum are due to the hydrogen bondinginteraction between the oxygen atoms of the β-PO_3^{2-} group of GDP with proteins. As shown in Figure 6.1, several residues, such as Lys16, Ser17, Asp57 and Gly15 are involved in direct or indirect interactions with the oxygen atoms of the β-PO_3^{2-} group. Even though there is 1:1 Mg^{2+} in both solution and protein spectra, the conformation of GDP may be different in proteins with that in solution, and therefore Mg^{2+} may interact with the β-phosphate in different ways.

The other derivative-like band in solution spectrum, which has a positive peak at 1101 cm^{-1} and a negative peak at 1080 cm^{-1} respectively, is assigned to the symmetric stretching vibration of the α-PO^{2-} group. This band has no

significant changes compared with those in protein spectra. This may imply that the hydrogen bondingenvironment around the α-PO^{2-} group of GDP in proteins is similar to that in solution even though X-ray studies show that several residues, such as Ala18 and Ser17, may be close enough to form some interactions.

Comparing the spectrum in wild type p21 with those in mutant p21 proteins, no significant differences are found.

6.2 Difference Spectra between GTP, β-$^{18}O_3$-GTP and γ-$^{18}O_3$-GTP in Solution, Wild Type p21 and Mutant p21 Proteins.

Figure 6.3 shows the difference spectra between GTP and γ-$^{18}O_3$-GTP in solution, wild type p21, mutant p21(G12V) and mutant p21(G12D) at pH 7.5 respectively. The large derivative-like band in solution spectrum (Fig 6.3a), which has a positive peak at 926 cm^{-1} and a negative peak at 897 cm^{-1} respectively, is assigned to the symmetric stretching vibration of the γ-PO_3^{2-} group of GTP as discussed in Chapter 4. This band shifts down more than 30 cm^{-1} to 885 cm^{-1} and 875 cm^{-1} respectively in protein spectra (Fig 6.3b, 6.3c and 6.3d). This shows the strong hydrogen bondinginteraction between the oxygen atoms of γ-phosphate of GTP and proteins. This result is consistent with that obtained from X-ray studies, which show that several residues, such as Lys16,

Tyr32, Gly60 and Thr35, are involved in direct or indirect interactions with the oxygen atoms of γ-phosphate of GTP. The other derivative-like band with a positive peak at 1121 cm^{-1} and a negative peak at 1105 cm^{-1}, which is assigned to the in-phase symmetric stretching vibration of α-PO^{2-} and β-PO^{2-} group of GTP, has no significant changes in protein spectra from solution.

Figure 6.4 shows the difference spectra between GTP and β-$^{18}O_3$-GTP in solution, wild type p21, mutant p21(G12V) and mutant p21(G12D) respectively. The large derivative-like band has a positive peak at 1123 cm^{-1} and a negative peak at 1111 cm^{-1} in the solution spectrum (Fig 6.4a). This band is assigned to the in-phase symmetric stretching mode of α-PO^{-} and β-PO^{2-} group of GTP. This band has no significant changes in protein spectra (Fig 6.4b, 6.4c and 6.4d). This result is consistent with that obtained above from γ-^{18}O-GTP spectra. This may suggest that the hydrogen bonding environment around the α- and β-phosphate of GTP in p21 proteins is similar with that in solution.

The other derivative-like band with a positive peak at 714 cm^{-1} and a negative peak at 688 cm^{-1} in solution spectrum, which is assigned to the stretching vibration of the P_β-O-P_γ linkage, shifts up to 737 cm^{-1} and 714 cm^{-1} respectively. The upshift of this band may be due to the decrease of the bond order of the P=O double bond of the -PO_3^{2-} group.

The bond order of the P-O single bond between O_β and P, must be increased if the bond order of the P=O double bond is decreased, because the total bond order of the P-O single bond and the three P=O double bonds of the $-PO_3^{2-}$ group is believed to be conserved and close to 5.

We did not find any significant differences between the wild type p21 and the mutant p21 proteins. This may due to the fact that the difference of the intrinsic GTPase activity is not large enough to produce a change observed in Raman spectra. Osterheld has studied ATP hydrolysis rate in solution at varies temperature and pH (Osterheld, R. K. 1972). Using the correlation between ATP hydrolysis rate and temperature, the ATP hydrolysis rate at 37°C is estimated to be about 3.3×10^{-6} min^{-1} at pH 7. It has been reported that the intrinsic GTPase activity at pH 7.6 for wild type p21, mutant p21(G12V) and mutant p21(G12D) are $0.028/min^{-1}$, $0.0038/min^{-1}$ and $0.001/min^{-1}$, respectively (Franken, S. M. et al., 1993; John, J. et al., 1989). If the GTP has similar hydrolysis rate as that of ATP in solution under the same condition, the GTP hydrolysis rate in wild type p21 mutant p21(G12) and mutant p21(G12D) are about 8.5×10^3, 1.2×10^3 and 3×10^2 times higher, respectively, than that in solution. we may correlate the 8.5×10^3 times difference of GTPase activity between wild type p21 and solution to the 35 cm^{-1} frequency shift in the observed Raman difference spectra. Moreover, the intrinsic GTPase activity of wild type

p21 is higher than that of mutant p21 proteins by the factor of 10. Therefore, the 10 times difference of GTPase activity between wild type p21 and mutant p21 proteins unlikely produces any significant differences observed in Raman spectra.

Further studies can be carried out with the presence of GAP (GTPase Activating Protein). The presence of GAP may increase the GTPase activity of wild type p21 by approximately 10^5 fold and has no effect on mutant p21 proteins (John, J. et al., 1990; Rensland, H. et al., 1991). We expect to see some differences in our Raman spectra between wild type p21 and mutant p21 proteins due to the 10^5 to 10^6 fold difference of GTPase activity. However, GTP will be hydrolyzed too fast by wild type p21 in the presence of GAP to be observed in the experiment. In order to overcome this problem, it will be necessary to use ^{18}O labeled non-hydrolyzed GTP analogues, such as ^{18}O-GppNHp.

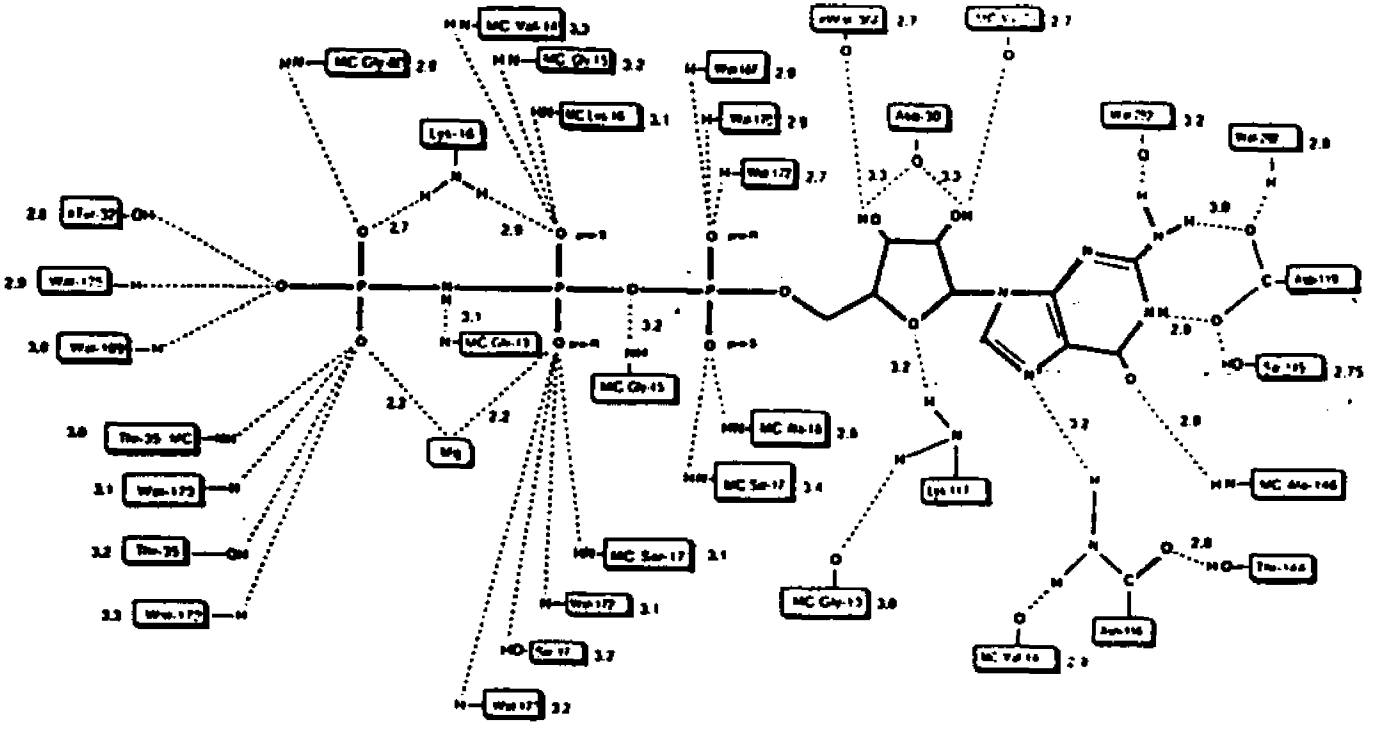

Figure 6.1 Scheme for the interactions between GppNHp and p21 or water molecule. All dashed lines correspond to hydrogen bonding interactions (below 3.4 Å) between appropriate partners. (Wittinghofer, F. et al., 1991)

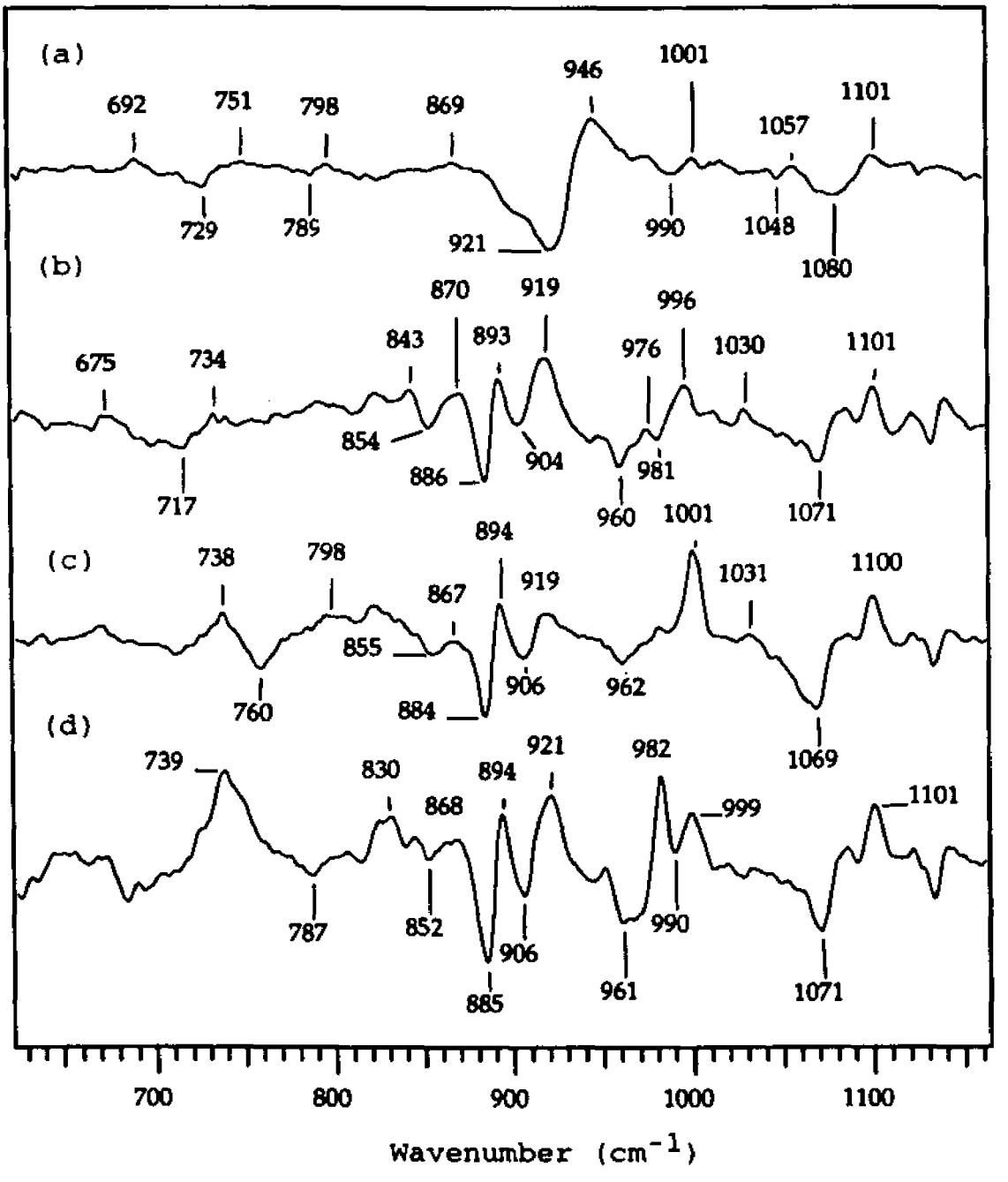

Figure 6.2 Raman spectra of GDP minus β-$^{18}O_3$GDP with 1:1 $MgCl_2$ in (a) solution; (b) wild type p21; (c) mutant p21(G12V); (d) mutant p21(G12P) at pH 7.5; 4°C. Laser excitation: 568.2 nm, 150 mW.

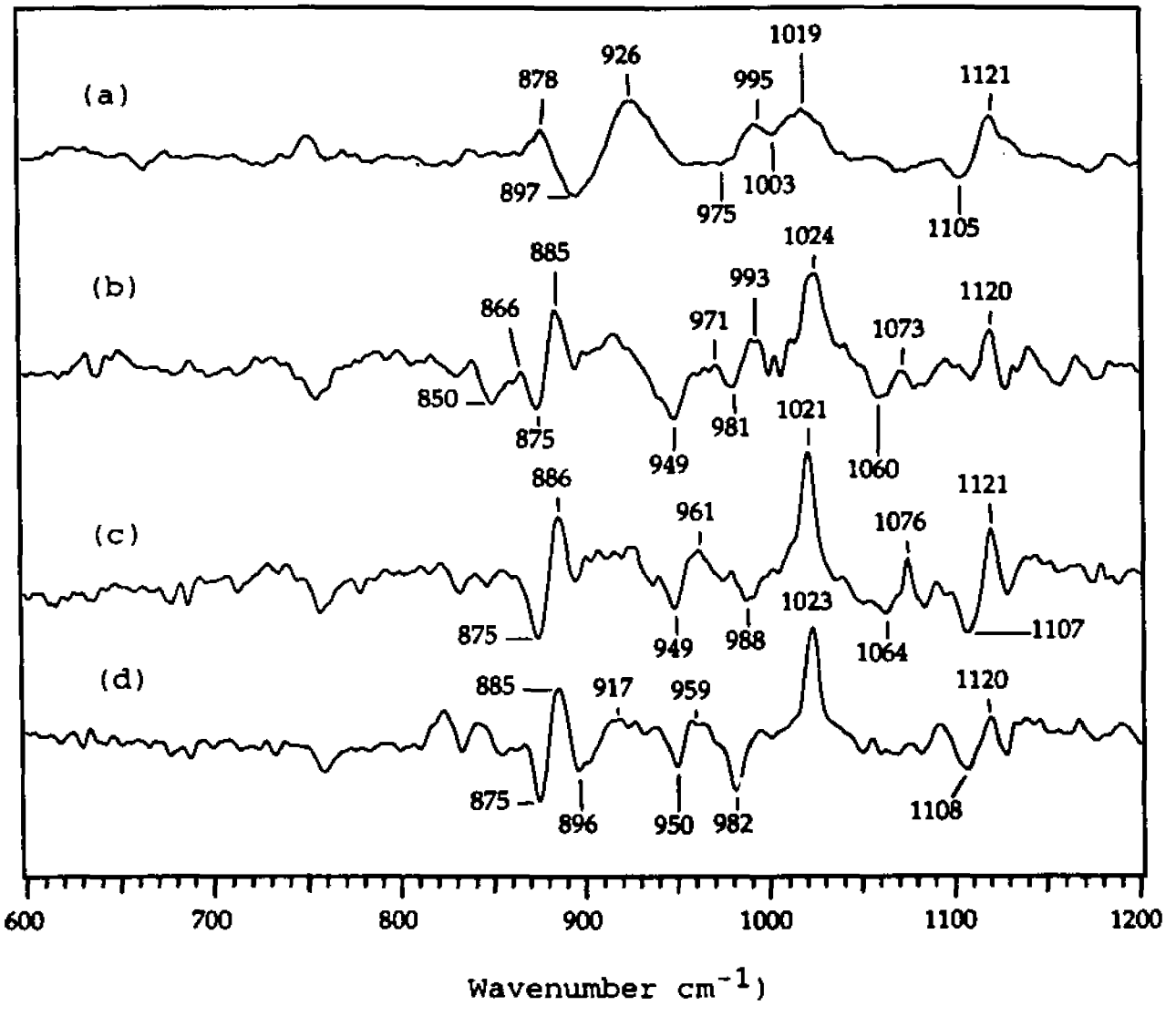

Figure 6.3 Raman spectra of GTP minus γ-$^{18}O_3$GTP at pH 7.5 with 1:1 $MgCl_2$ in (a) solution; (b) wild type p21; (c) mutant p21(G12V) and (d) mutant p21(G12D).Sample concentration for proteins: 4mM; Temperature: 4°C. 568.2 nm; 150 mW.

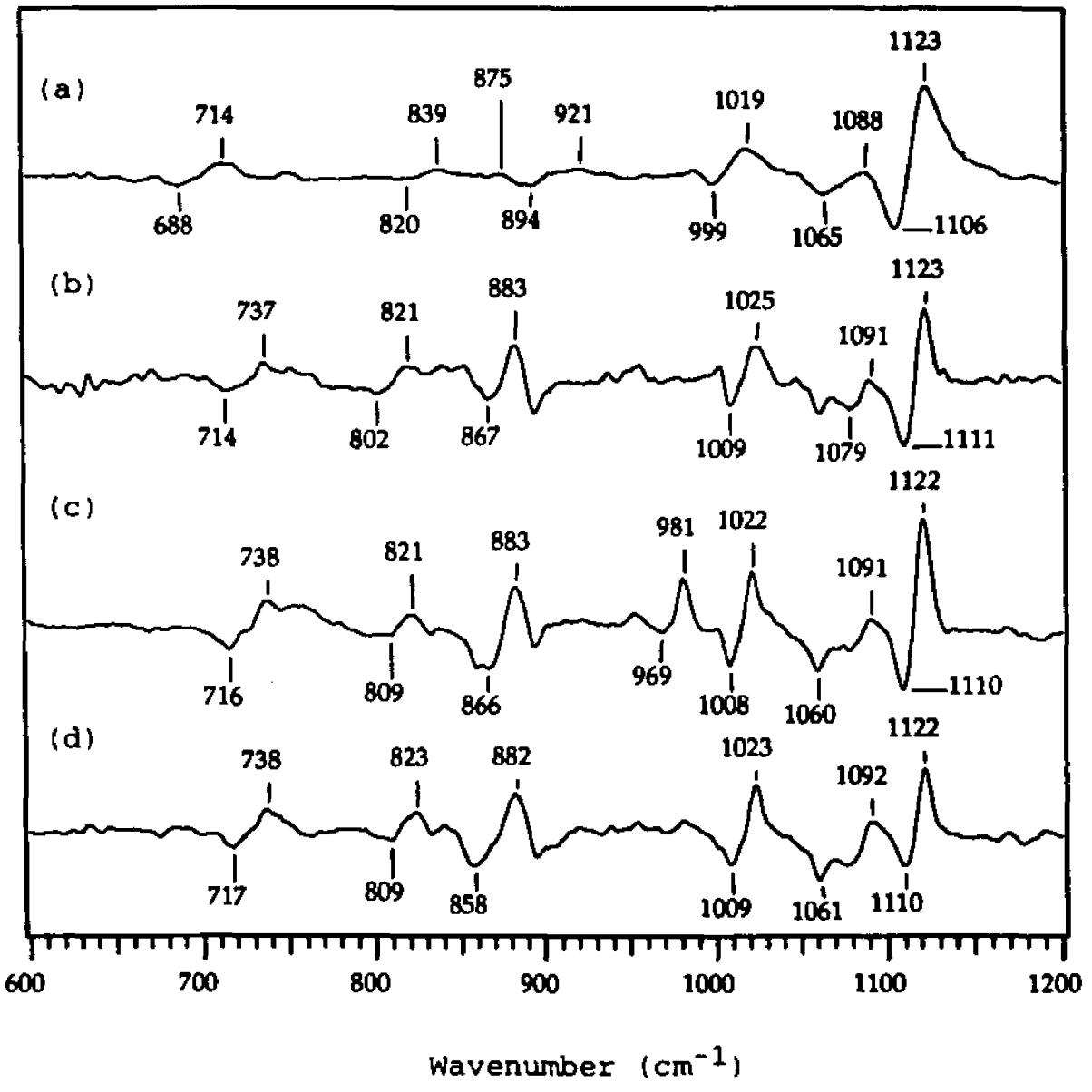

Figure 6.4 Raman spectra of GTP minus β-$^{18}O_3$GTP at pH 7.5 with 1:1 $MgCl_2$ at 4°C in (a) solution; (b) wild type p21; (c) mutant p21(G12V) and (d) mutant p21(G12D). Sample concentration: 4mM. 568.2 nm,150 mW.

Chapter 7

MECHANISM OF GTP HYDROLYSIS

Phosphoryl transfer reactions of phosphomonoesters, like adenosine triphosphate and guanine triphosphate, have been intensively studied by many groups because of their importance in biological system (Ramirez, F. 1980, 1981; Feder, J. 1976; Lipman, F. ,1948; Deng, H. et al., 1993; Ray, W. et al., 1993). As discussed previously, ATP is an energy transfer agent in biological system, and G proteins play an important role in signal transduction, which is tightly controlled by the nature of guanine nucleotides. Therefore, it is very important to understand, at atomic level, the hydrolysis mechanism of phosphates and polyphosphates.

In general, there are two main mechanisms for nucleophilic substitution at phosphorous - associative and dissociative reactions. The associative reaction is an addition-elimination mechanism which involves an pentacovalent intermidiate as shown in Figure 7.1a. The dissociative reaction is an elimination-addition mechanism which involves an metaphosphate anion intermediate as shown in Figure 7.1b. The stereochemical course of a large number of enzymatic phosphoryl transfer reactions has been studied (Eckstein, F. 1982; Floss, H. G. 1984). Most of the enzymatic phosphoryl transfer reactions fall into the category of associative

mechanism involving an pentacovalent intermidiate. The dissociative mechanism involving an metaphosphate intermidiate is rarely encountered although evidence for this process has been obtained on several occasions (Ramirez, F. 1981; Cullis, P. 1986; Westheimer, F. 1981).

Here we present our studies on the mechanism of GTP hydrolysis in *ras*-p21 proteins as well as in solution by Raman spectroscopy.

7.1 Mechanism of GTP Hydrolysis in Solution

The mechanism of non-enzymatic phosphoryl transfer from ATP in solution has been studied by many groups (Ramirez, F. 1981; Jencks, W. P. 1971; Lowenstein, J. M. 1958, 1960,1961; Friess, S. L. 1952). As a summary of these studies, the hydrolysis of the acid $ATPH_4$ and the hydrolysis of the monoanion $ATPH_3^-$ occur by an addition-elimination mechanism *via* a phosphorane intermediate, while the tetra-anion and the trianion, having a terminal P^1 group of the type XPO_3^{2-} and XPO_3H^- respectively, undergo hydrolytic cleavage at that group by an elimination-addition mechanism *via* the metaphosphate ion intermediate. It is not clear whether $ATPH_2^{2-}$ reacts *via* metaphosphate or *via* phosphorane intermediates. It is probable that both mechanisms are competitive in this species.

Since the adenine ring is far from and has no interaction with the phosphate moiety, it is reasonable that guanosine triphosphate has the same hydrolysis mechanism in solution as in adenosine triphosphate. Under biological pH, GTP has a tetra-anion phosphate group with a terminal P^{γ} group of the type $-PO_3^{2-}$. Therefore, the hydrolysis of GTP in solution under biological pH occur by an elimination-addition mechanism *via* the metaphosphate ion intermediate, or so called the dissociative mechanism.

7.2 Mechanism of GTP Hydrolysis in *ras*-p21 Proteins

Studies on the mechanism of GTP hydrolysis in *ras*-p21 proteins have been carried out extensively. In earlier works on *ras*-p21, it was suggested that the side chain of Gln61, together with the backbone carbonyl of Thr35, activates a water molecule by hydrogen-bond formation; and that Gln61, with the assistant of Glu63, abstracts a proton (Pai, et al., 1990; Krengel et al., 1990). Prive et al have suggested that Gln61 stabilize the transition state (Prive, G.G. et al., 1992). Schweins et al proposed that the γ-phosphate group itself is the acceptor of the proton from the water molecule (Schweins, T. et al., 1994). Sondek et al suggested that water attack on the γ-phosphate in a concerted mechanism while a proton is being abstracted by the glutamine

side chain, which in turn protonates an oxygen of the γ-phosphate, effectively shutting the proton from the water to this oxygen (Sondek, J. et al., 1994). Feuerstein et al proposed in their earlier studies on EF-Tu and *ras*-p21 that the mechanism of GTP hydrolysis in protein is a single step, in-line transfer, without a phosphoenzyme or other phosphorylated intermediate (Feuerstein, J. et al., 1989). Even though these opinions do not agree on what happens to the proton of the attacking water molecule, all these studies strongly support that GTP hydrolysis is an in-line attack of water in an associative mechanism (Goody, R. S., 1994).

In our Raman spectroscopic studies (data are shown in the previous chapter), we found that the symmetric stretching frequency of P=O double bond of the terminal $-PO_3^{2-}$ group has a large downshift in protein compared with that in solution. This suggests that the P=O bond order in protein is decreased rather than increased. As we know, the empirical rule for general phosphate compounds is that the total bond order of the terminal $-PO_3^{2-}$ group is believed to be conserved and close to 5, which means that the total bond order of the O_β-P_γ single bond and the three P_γ=O_γ double bonds is equal to 5 (Deng, H. et al., 1993; Ray, W. et al., 1993). Since the bond orders of the three P_γ=O_γ double decrease, the O_β-P_γ single bond order must be increased. If *ras*-p21 stays on the pathway from ground state to transition state during

our measurement, which is most likely the case, it is not likely to form a metaphosphate intermediate because of the stronger O_{β}-P_{γ} bond in protein. In the other word, in the metaphosphate intermediate state, the P_{γ}=O_{γ} double bond order should be increased rather than decreased. Therefore, the hydrolysis of GTP in *ras*-p21 proteins takes place by the associative mechanism *via* a pentacovalent intermidiate. This conclusion is consistent with the results obtained by X-ray and NMR studies.

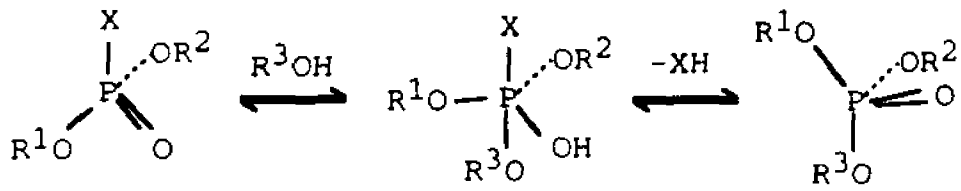

Figure 7.1a The associative reaction of phosphoryl transfer is an addition-elimination mechanism which involves an pentacovalent intermediate.

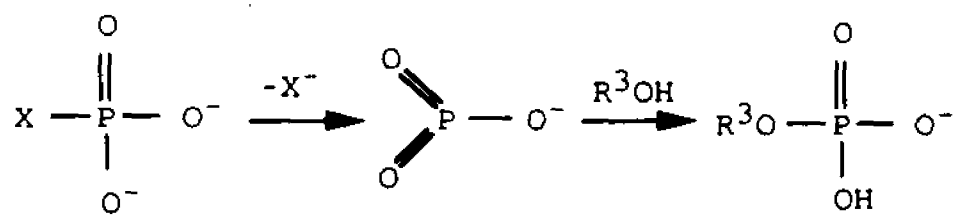

Figure 7.1b The dissociative reaction of phosphoryl transfer is an elimination-addition mechanism which involves an metaphosphate anion intermediate.

Chapter 8

INTERACTIONS BETWEEN *ras*-p21 PROTEINS AND GUANINE NUCLEOTIDES AT GUANINE RING MOIETY

8.1 Difference Spectra of GDP, 8D-GDP, IDP and 6-^{18}O-GDP in Wild Type and Mutant *ras*-p21 Proteins.

As shown in Figure 6.1, the hydrogen bonding interactions between protein and guanine ring at the 6-carbonyl group and the 2-amino group are very important for the binding base. Our group has previously studied these protein-nucleotide interactions at guanine base of EF-Tu and wild type p21 with isotopic labeling and nucleotide analogues chemically modified at selected positions. Here we summarize some previous results, as well as present some new results for mutant p21(G12V), intended to compare the protein-nucleotide interactions at guanine ring moiety between wild type and mutant p21.

Figure 8.1 shows the Raman spectra of GDP, 6-^{18}O-GDP, 8D-GDP and IDP in solution. The strongest GDP band at 1487 cm^{-1}, which is assigned primarily to N7=C8 stretching mode coupled with 8-C-H deformation mode of the ring, shifts down to 1466 cm^{-1} in 8D-GDP due to the deuterium labeling at 8 position, as well as shifts down to 1472 cm^{-1} in IDP due to the influence of the lack of 2-amino group in IDP. The band

at 1576 cm^{-1} in GDP, which is assigned to C4=C5 stretching mode of guanine ring, shifts down to 1555 cm^{-1} in IDP. These data show that the local modes are influenced by the delocalized purine breathing motions. The 6-carbonyl (C=O) stretching mode at 1685 cm^{-1}, which appears at 1691 cm^{-1} in IDP, shifts down to somewhere around 1664 cm^{-1} in 6-^{18}O-GDP upon the ^{18}O labeling. The band at 1180 cm^{-1} in GDP, which is absent in IDP and is assigned to external C-N stretching mode at 2-amino group, shifts up to 1185 cm^{-1} in 8D-GDP. The band at 1646 cm^{-1} in GDP, which is absent in IDP, is assigned to NH_2 scissors mode. These modes are believed to be sensitive to the hydrogen bonding environment.

Figure 8.2 shows the difference Raman spectra between GDP and 6-^{18}O-GDP in solution, wild type p21 and mutant p21(G12V). The 6-carbonyl (C=O) stretching mode has a positive peak at 1694 cm^{-1} and a negative peak at 1661 cm^{-1} in the difference spectrum in solution (Fig 8.2a). This band shifts down to 1675 cm^{-1} and 1656 cm^{-1} respectively when GDP is bound in protein. The zero-crossing position at 1673 cm^{-1} in solution shifts down to 1663 cm^{-1} in protein. The 10 cm^{-1} down shift of C=O stretching band indicates the strong hydrogen bonding interactions between the protein and the guanine base at 6-carbonyl group. This result is consistent with the result from X-ray and kinetic studies. X-ray studies (Figure 6.1) show the distance between O6 of guanine ring and the amide nitrogen of Ala 146 is 2.9 Å, which is close enough to form hydrogen bonding. It has been observed

that 6h-GDP, where the oxygen atom at position 6 of guanine base has been removed, binds with 25 fold lower affinity than GDP (Pai, E. et al., 1989). This proves the importance of the strong hydrogen bonding between 6-keto group and protein.

The shift of Raman band is very sensitive to hydrogen bonding environment and is a good handle to study the protein-ligand interaction problems. For example, the frequency of an isolated keton C=O stretching is quantitatively related to hydrogen bound interaction energy formed with nearby hydrogen bond donors to a good approximation. Every 2 cm^{-1} shift in the C=O stretching mode implies one kcal/mol in interaction enthalpy, and a distance change of the keton bond of less than 0.01 A (Joesten, M. et al., 1974; Thijs, R. et al., 1984).

Figure 8.3 shows the difference spectra between GDP and IDP in solution, wild type p21 and mutant p21(G12V). A pronounced spectral shift is observed in the ring mode assigned to the C4=C5 stretching motion. The derivative-like band, with a positive peak at 1577 cm^{-1} and a negative peak at 1555 cm^{-1} in solution spectrum (Figure 8.3a), shifts to 1568 cm^{-1} and 1547 cm^{-1} respectively when bound to protein (Figures 8.4b, 8.4c). The zero-crossing position of this band at 1566 cm^{-1} in solution shifts down 11 cm^{-1} to 1155 cm^{-1} in proteins due to the hydrogen bonding environment change.

The difference spectra between GDP and 8D-GDP in solution, wild type p21 and mutant p21(G12V) are shown in Figure 8.5. The band with a positive peak at 1173 cm^{-1} and a negative peak at 1190 cm^{-1}, which is believed to be sensitive to the hydrogen bonding environment around 2-NH_2 group, shifts down to 1166 cm^{-1} and 1180 cm^{-1} respectively in proteins. The zero-crossing position at 1181 cm^{-1} in solution shifts down 8 cm^{-1} to 1173 cm^{-1} in protein due to the binding of protein. This indicates the hydrogen bonding interactions between the 2-NH_2 group of the guanine ring and proteins. This result is consistent with the result from X-ray and NMR studies, which suggest that the hydrogen of 2-NH_2 group on guanine ring is about 3.0 A away from the carboxylate group of residue Asp 116, which is close enough to form hydrogen bonding(Pai, E. et al., 1989; Wittinghofer, F., et al., 1977). The largest band, which has a positive peak at 1487 cm^{-1} and a negative peak at 1465 cm^{-1}, does not change upon the binding to the protein. This band is assigned to the N7=C8 stretching mode coupled with 8-H deformation mode. This data suggest that the guanine ring do not interact with the protein through the N7 position differently than it interacts with water in solution. This conclusion is supported by the fact that modification of the 8 position with bulky groups as in 8-Br-GDP has almost no influence on the binding affinity to p21(Wittinghofer, F., et al., 1977).

Tsuboi and his colleagues (Nishimura, Y., et al., 1986) have determined the Raman spectra of a number of guanosine salts and have compared their Raman spectra with the guanosine conformations determined by X-ray diffraction analysis. Their studies showed that the Raman bands in 1300-1400 cm^{-1} region, which arise from ring motions and contain also substantial motions from the bonded ribose group, as well as the bands in the 600-700 cm^{-1} region are quite sensitive to the torsional angle about the glycosidic bond and the pucker state of the ribose ring. In GDP solution spectrum (Figure 8.1a), the pattern of the guanosine conformation is C2' *endo-enti*. Compared with the GDP spectrum in solution, the spectra in proteins have the same patterns as that in solution. This suggests that the binding of the protein do not affect the conformation of the nucleotide, and the guanosine remain the C2' *endo-enti* conformation in protein.

As discussed in Chapter 2, the isotopic labeling does not change the chemical properties of the nucleotide, and does not cause any protein changes in the difference spectra; however, the analogue of the nucleotides, such as IDP, may cause some protein changes in difference spectra due to different chemical properties. The magnitude of bands caused by protein changes may count in about 1% of the largest protein peak. So we are normally able to pick and assign those larger peaks safely.

Spectrum of GDP in wild type p21 is compared with that in mutant p21(G12V) in Figures 8.1, 8.2, 8.3 and 8.4, and no significant differences are found. This suggests that there are essentially no differences between wild type p21 and mutant p21(G12V) when they bind to the guanine nucleotide at the guanine ring moiety. This conclusion is quite within expectation, and is consistent with the results from X-ray studies (Wittinghofer, F., et al, 1991; de Vos, A. et al., 1988; Tong, L., 1989; Brandt-Rauf, P. W. et al., 1989;).

8.2 Difference Spectra between *ras*-p21•GDP Complex and Nucleotide Free *ras*-p21 in Both Wild Type and Mutant Proteins.

As discussed in Chapter 2, we can use the approach by taking difference spectra between protein-nucleotide complex and apo-protein to study the interactions between proteins and nucleotide at guanine ring moiety. This method is particularly useful when isotopically labeled nucleotides are difficult and expensive to achieve, and also when the signal from nucleotide is bigger enough to overcome the signal from the protein conformational changes due to the binding of the nucleotides. It also gives more information than isotopic labeling method, in which the unrelated information with the labeled part is lost due to the subtraction.

The details of getting nucleotide-free p21 are describe in Chapter 2. Spectra of p21•GDP complex and nucleotide-free

p21 are taken at the same time, and the difference spectrum between them is thus obtained. The difference spectrum is then compared with the spectrum of GDP in solution, yielding the information of the hydrogen bonding interactions between p21 proteins and nucleotides.

Figure 8.5 shows the GDP spectra in solution, wild type p21 and mutant p21(G12V). The overall pattern of the spectra of GDP in proteins remain the same as that in solution. These major bands are bigger than those from protein changes, and are clearly seen in the spectra in proteins. The band at 1681 cm^{-1} in solution, which is assigned to C=O stretching mode, shifts down to 1675 cm^{-1} in proteins. The C4=C5 stretching mode at 1576 cm^{-1} in solution shifts down 9 cm^{-1} to 1567 cm^{-1} in proteins. The external C-N stretching mode at 1180 cm^{-1} shifts down to 1172 cm^{-1}, and the band at 1487 cm^{-1}, which is assigned to N7=C8 stretching mode coupled with 8-H deformation mode, remains in the same position in proteins. The details about these changes due to the protein binding are discussed in the previous section. It is clearly seen that the Raman bands in proteins are sharper than those in solutions. This suggests that GDP is more constrained and has less freedom in protein than in solution.

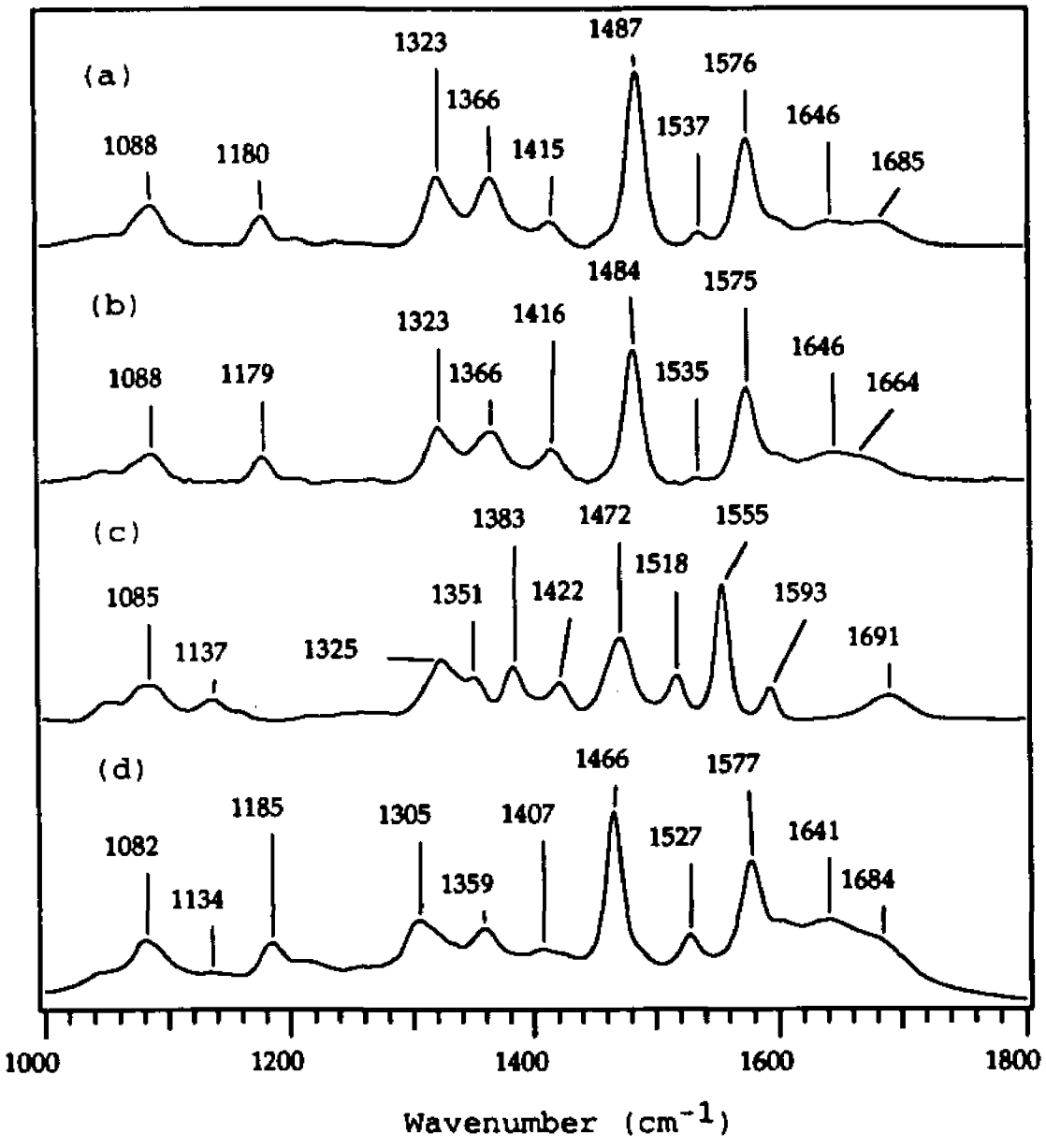

Figure 8.1 Raman spectra of (a) GDP; (b) 6-^{18}OGDP; (c) IDP; (d) 8D-GDP in solution at pH 7.5. Sample concentration: 0.1 M. Laser excitation: 568.2 nm, 150 mW. 4°C.

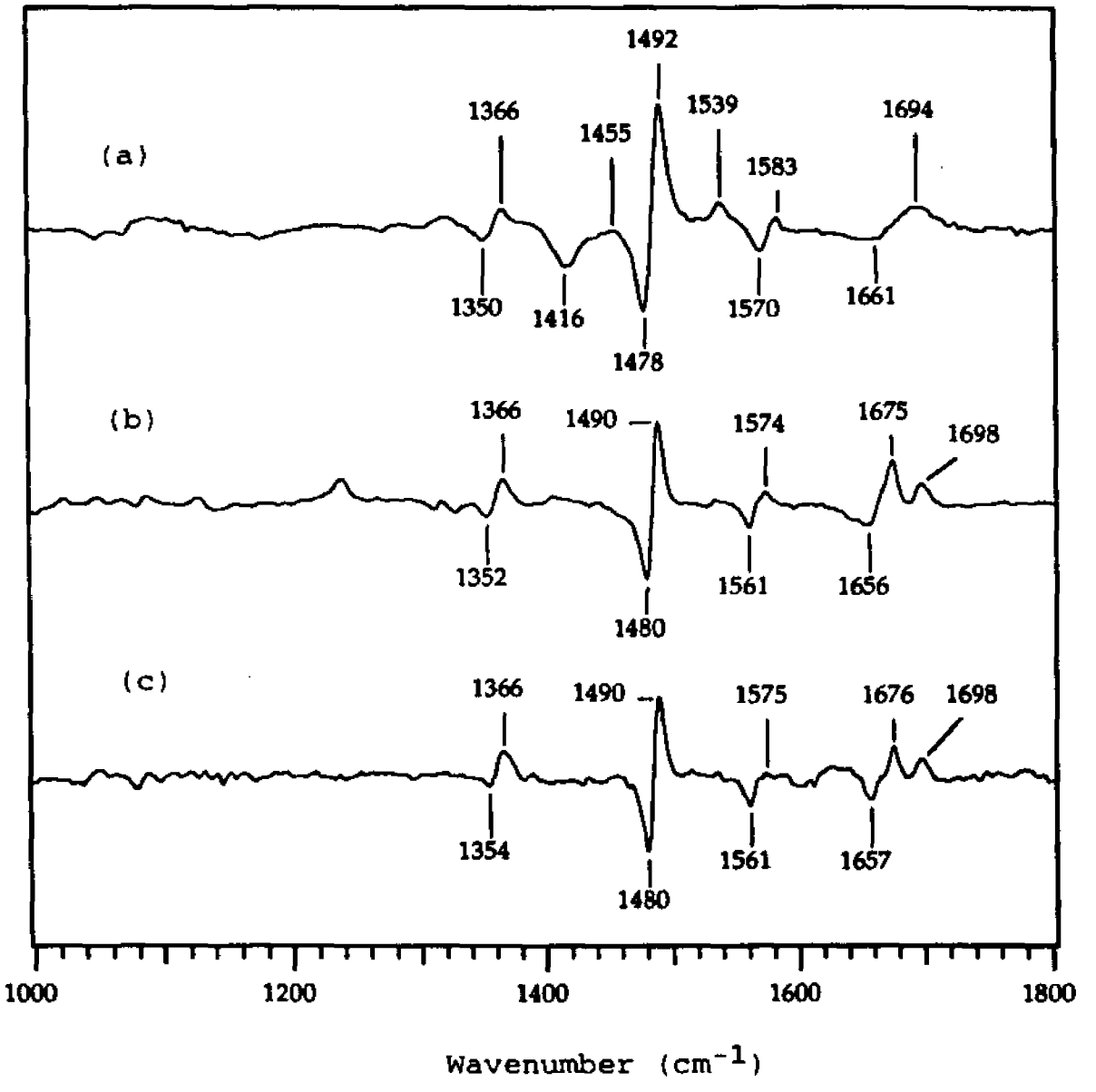

Figure 8.2 Raman spectra of GDP minus 6-^{18}OGDP at pH7.5 in (a) solution; (b) wild type p21 and (c) mutant p21(G12V). Protein sample concentration: 4 mM, at 4^{o}C. Laser excitation: 568.2 nm, 150 mW.

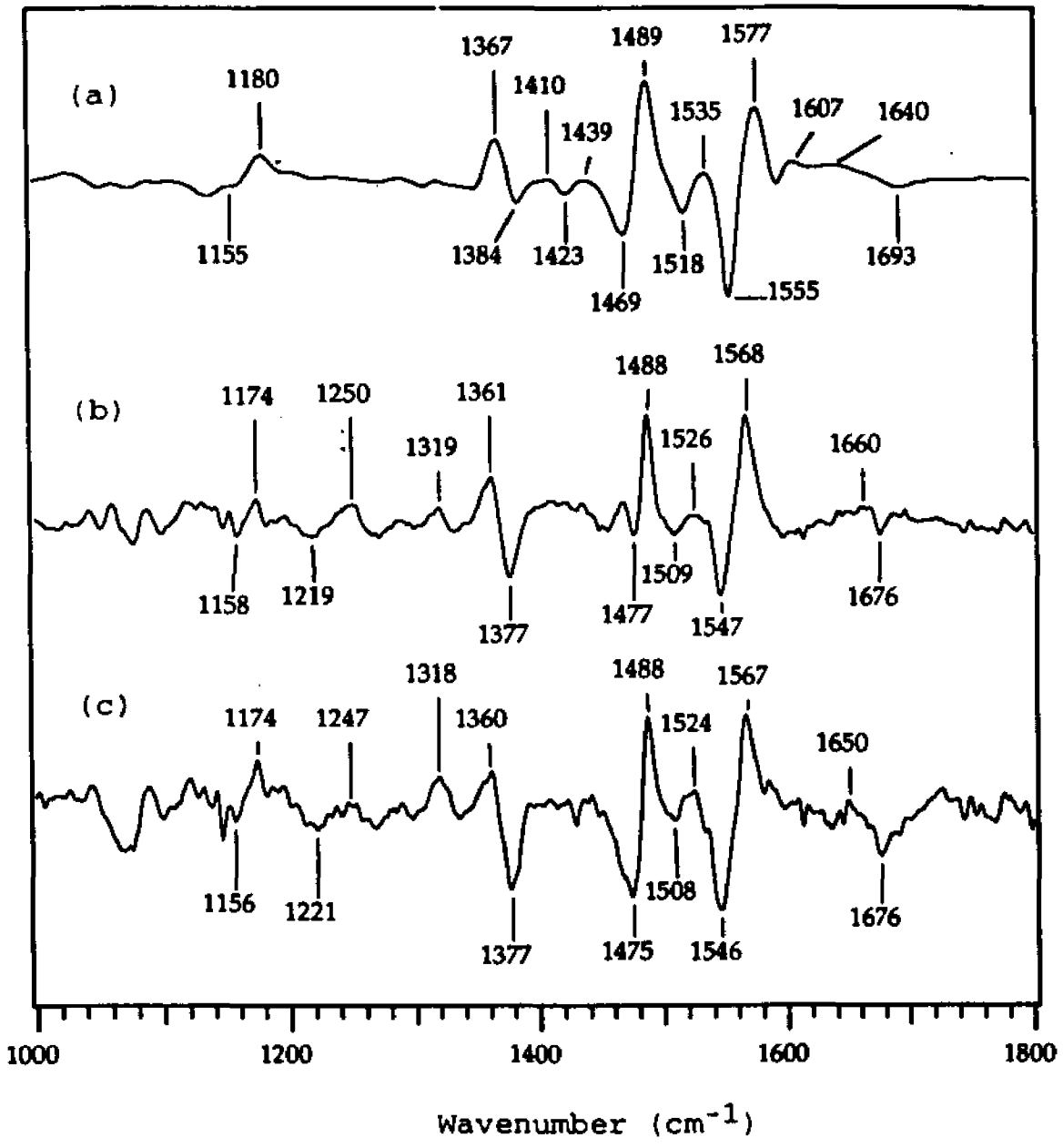

Figure 8.3 Raman spectra of GDP minus IDP at pH 7.5 in (a) solution; (b) wild type p21 and (c) mutant p21(G12V). Protein sample concentration: 4mM, at 4°C. Laser excitation: 568.2 nm, 150 mW.

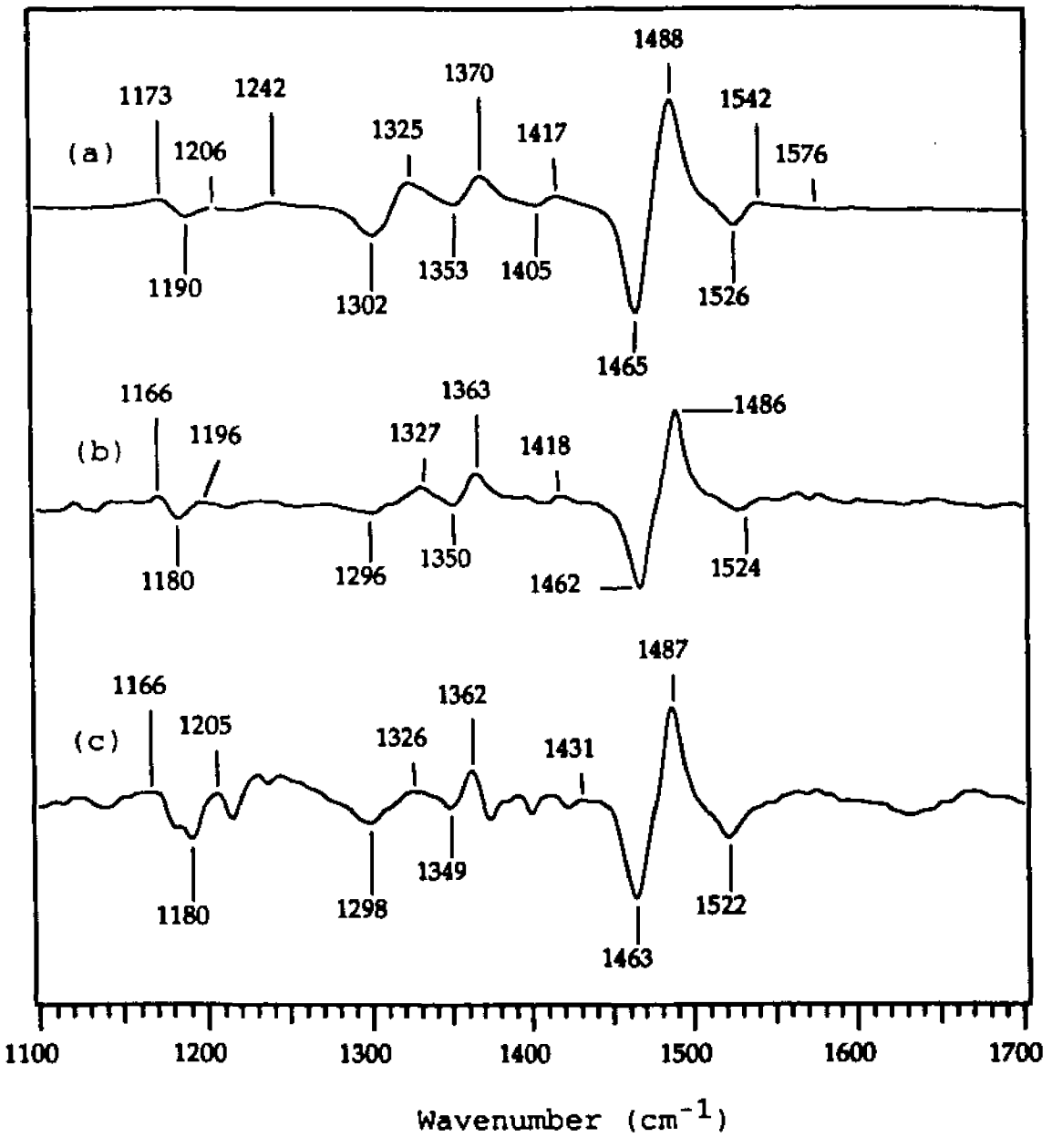

Figure 8.4 Raman spectra of GDP minus 8D-GDP at pH 7.5 in (a) solution; (b) wild type p21 and (c) mutant p21(G12V). Protein samples: 4 mM, at 4°C. Laser excitation: 514.5 nm, 150 mW.

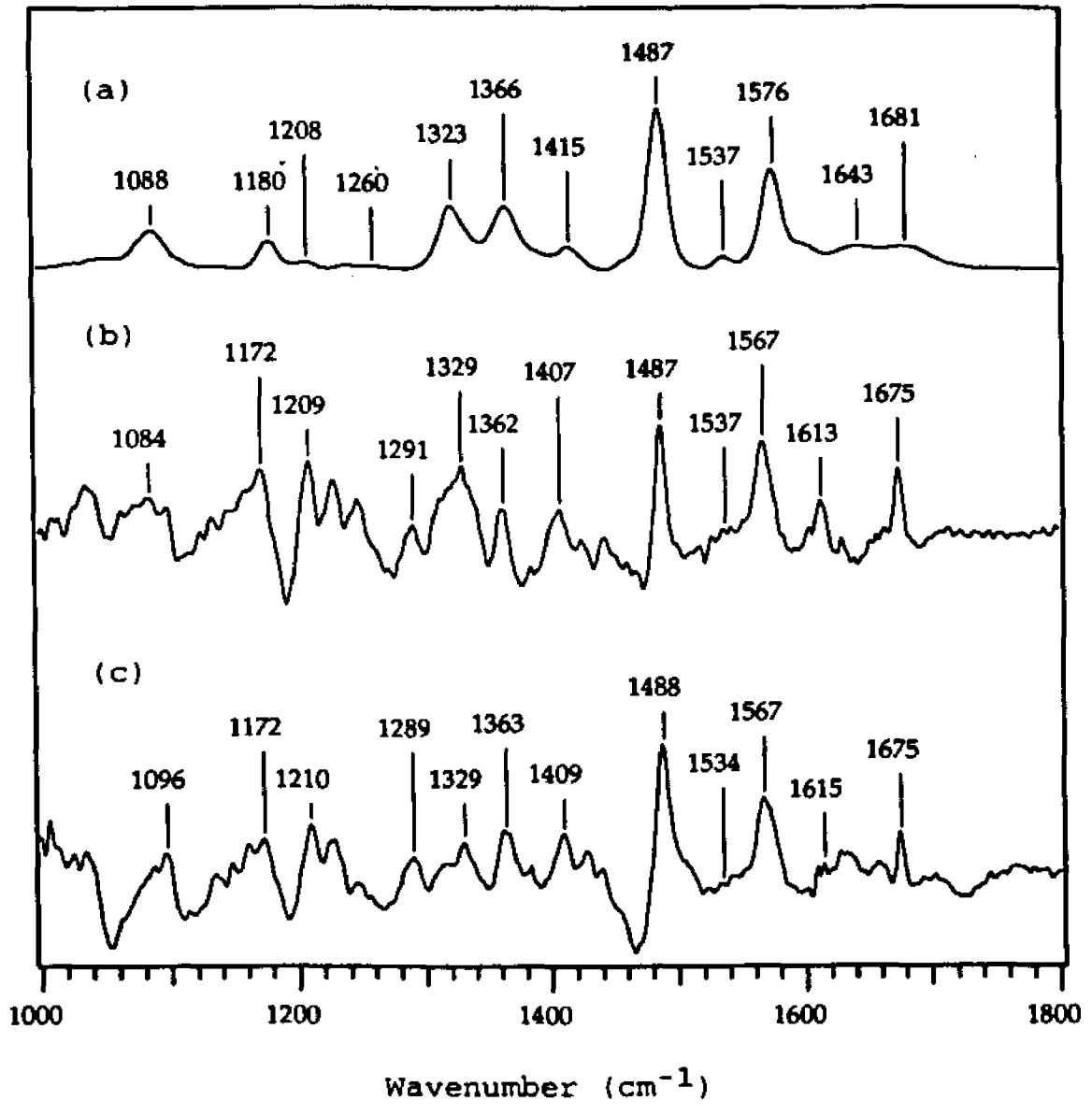

Figure 8.5 Raman spectra of GDP at pH 7.5 in (a) solution; (b) wild type p21 and (c) mutant p21(G12V). Protein samples: 3 mM, at 4 ^{o}C. Laser excitation: 568.2 nm, 150 mW.

REFERENCES

Adari, H., D. R. Lowy, B. M. Willumsen, C. J. Der and F. McCormick. 1988. Guanosine Triphosphatase Activating Protein (GAP) Interacts With the p21 ras Effector Binding Domain. *Science* 240: 518-521.

Barbacid, M. 1987. *ras* Genes. *Ann. Rev. Biochem.* 56: 779-827.

Bellamy, L. J. 1980. The Infrared Spectra of Complex Molecules: Advances in Infrared Group Frequencies (2 ed.). London: Chapman and Hall.

Berni, R., M. Stoppini, M. C. Zapponi, M. L. Meloni, H. L. Monaco and G. Zanotti. 1990. The Bovine Retinol Binding Protein. *Eur. J. Biochem.* 192: 507-513.

Bosch, L. ;., B. Kraal and A. Parmeggiani. 1989. The Guanine-Nucleotide Binding Proteins. Plenum Press.

Bourne, H. R., D. A. Sanders and F. McCormick. 1990. The GTPase Superfamily: a Conserved Switch for Diverse Cell Functions. *Nature* 348: 125-131.

Bourne, H. R., D. A. Sanders and F. McCormick. 1991. The GTPase Superfamily: Conserved Structure and Molecular Mechanism. *Nature* 349: 117-127.

Bourne, N. and A. Williams. 1984. Effective Charge on Oxygen in Phosphoryl ($-PO_3^{2-}$) Group Transfer from an Oxygen Donor. *J. Org. Chem.* 49:(7) 1200-1204.

Brandt-Rauf, P. W., M. R. Pincus, R. P. Carty, J. Lubowsky, A. Avitable, H. Kung and J. Maizel. 1989. Conformational Effects of Amino Acid Substitutions at Positions 10, 12, and 13 in the p21 Protein. *J. Prot. Chem.* 8:(1) 79-86.

Brown, E. B. and W. L. Peticolas. 1975. Conformational Geometry and Vibrational Frequencies of Nucleic Acid Chains. *Biopolymers* 14: 1259-1271.

Callender, R. (1991). Raman Spectroscopic Studies of Ligand Bound to Protein Active Sites: Enzymes and G-Proteins. In R. E. Hester & R. B. Girling (Ed.), Spectroscopy of Biological Molecules, (pp. 227-230). Cambridge: The Royal Society of Chemistry.

Callender, R. and H. Deng. 1994. Non-Resonance Raman Difference Spectroscopy: A General Probe Of Protein Structure, Ligand Binding,

Enzymatic Catalysis and the Structures Of Other Ras-Like ... Ann. Rev. Biophys. Biomol. Struct. 23: 215-245.

Callender, R., H. Deng, D. Sloan, J. Burgner and T. K. Yue (1989). Raman Difference Spectroscopy and the Energetics of Enzymatic Catalysis. In Proccedings of International Society for Optical Engineering, 1057 (pp. 154-160). Los Angeles: International Society for Optical Engineering.

Carey, P. R. 1982. Biochemical Applications of Raman and Resonance Raman Spectroscopy. New York: Academic Press.

Chapman, A. C. 1965. Spectra of Phosphorus Compounds - II. Spectrochim. Acta 21: 633 - 640.

Chapman, A. C. and L. E. Thirlwell. 1964. Spectra of Phosphorus Compounds - I. *Spectrochim. Acta* 20: 937-947.

Chen, D., K. T. Yue, C. Martin, K. W. Rhee, D. Sloan and R. Callender. 1987. Classical Raman Spectroscopic Studies of NADH and NAD+ Bound to Liver Alcohol Dehydrogenase by Difference Techniques. *Biochemistry* 26: 4776-4784.

Chen, Y. C. (1995) The Mechanism of Action of Dihydrofolate Reductase Revealed by Nonresonance Raman Difference Spectroscopy. Ph.D diss. The City University of New York.

Colthup, N. B., L. H. Daly and S. E. Wiberley. 1990. Introduction to Infrared and Raman Spectroscopy (3rd ed.). San Diego: Academic Press.

de Vos, A. M., L. Tong, M. V. Milburn, P. M. Matias, J. Jancarik, S. Noguchi, S. Nishimura, K. Miura, E. Ohtsuka and S.-H. Kim. 1988. Three-Dimensional Structure of an Oncogene Protein: Catalytic Domain of Human c-H-*ras* p21. *Science* 239: 888-893.

Deng, H. and R. Callender. 1993. Enzymatic Catalysis and Molecular Recognition: the Energetics of Ligand binding to Proteins as Studies by Vibrational Spectroscopy. *Comments Mol. Cell. Biophys.* 8: 137-154.

Deng, H., D. Manor, G. Weng, C.-X. Chen, V. Balogh-Nair and R. Callender (1993a). Difference Raman spectroscopic studies of ligand-protein interactions. In Proccedings of International Society for Optical Engineering, 1890 (pp. 114-122). Los Angeles: International Society for Optical Engineering.

Deng, H., W. J. Ray, J. W. Burgner and R. Callender. 1993b. A Comparison of Vibrational Frequencies of Critical Bonds in Ground State Complexes and in a Vanadate-Based Transition

State Complex of Muscle Phosphoglucomutase. Mechanistic Implications. *Biochemistry* 32: 12984-12992.

Deng, H. (1987). Resonance Raman Studies of Visual Pigments and Bacteriorhodopsin. Ph.D diss. The City University of New York.

Downward, J., R. Riehl, L. Wu and R. A. Weinberg. 19--. Identification of a Nucleotide Exchange Promoting Activity for p21. *Proc. Natl. Acad. Sci (USA)* 87: 5998-6002.

Eckstein, F. 1983. Phosphorothioate Analogues of Nucleotides-Tools for the Investigation of Biochemical Processes. *Angew. Chem. Int. Ed. Engl.* 22:(6) 423-439.

Fasano, O., T. Aldrich, F. Tamanoi, E. Taparowsky, M. Furth and M. Wigler. 1984. Analysis of the transforming potential of the human H-ras gene by random mutagenesis. *Proc. Natl. Acad. Sci. U.S.A.*, 81: 4008.

Feder, J. 1976. The Chemistry of ATP. *Topics in Phosphorus Chemistry* 11: 1-18.

Feuerstein, J., R. S. Goody and M. R. Webb. 1986. The Mechanism of Guanosine Nucleotide Hydrolysis by p21 c-Ha-ras. *J. Biol. Chem.* 264:(11) 6188-6190.

Feuerstein, J., R. S. Goody and A. Wittinghofer. 1987. Preparation and Characterization of Nucleotide-free and Metal Ion-free p21 "Apoprotein". *J. Biol. Chem.* 262:(14) 6456-6458.

Franken, S. M., A. J. Scheidig, U. Krengel, H. Rensland, A. Lautwein, M. Geyer, K. Scheffzek, R. S. Goody, H. F. Kalbitzer, E. F. Pai and A. Wittinghofer. 1993. Three-Dimensional Structures and Properties of a Transforming and a Nontransforming Glycine-12 Mutant of p21 $^{H-ras}$. *Biochemistry* 32: 8411-8420.

Friess, S. L. 1953. Rates and Energetics of Activation of the Acid-Catalyzed Hydrolysis of Adenosine Triphosphate. *J. Am. Chem. Soc.* 75: 323-326.

Gilman, A. G. 1987. G Proteins: Transducers of Receptor-Generated Signals. *Ann. Rev. Biochem.* 56: 615-649.

Glasfeld, A., P. Zbinden, M. Dobler, S. A. Benner and J. D. Dunitz. 1988. Crystal Structure of Two Simple N-Substituted Dihydronicotinamides: Possible Implications for Stereoelectronic Arguments in Enzymology. *J. Am. Chem. Soc.* 110: 5152-5157.

Goody, R. S. 1994. How G Proteins Turn off. *Nature* 372: 220-221.

Guan, Y., C. J. Wurrey and J. Thomas G.J. 1994. Vibrational Analysis of Nucleic Acids. I. The Phosphodiester Group in Dimethyl Phosphate Model Compounds: $(Ch_3O)_2PO_2^-$, $(CD_3O)_2PO_2^-$, and $(^{13}CH_3O)_2PO_2^-$. *Biophys. J.* 66: 225-235.

Hall, A. 1990. The Cellular Functions of Small GTP Binding Proteins. *Science* 249: 635-640.

Hall, A. and A. J. Self. 1986. The Effect of Mg2+ on the Guanine Nucleotide Exchange Rate of p21 n-ras. *J. Biol. Chem.* 261:(24) 10963-10965.

Hall, A. D. and A. Williams. 1986. Leaving Group Dependence in the Phosphorylation of Escherichia coli Alkaline Phosphatase by Monophosphate Esters. *Biochemistry* 25: 4784-4790.

Heyde, M. E. and L. Rimai. 1971. A Raman Spectroscopic Study of the Interaction of Ca^{2+} and Mg^{2+} with the Triphosphate Moiety of Adenosine Triphosphate in Aqueous Solution. *Biochemistry* 10:(7) 1121-1128.

Jencks, W. P. 1969. Catalysis in Chemistry and Enzymology. New York: Mcgraw-Hill.

Joesten, M. and L. J. Schaad. 1974. Hydrogen Bonding. New York: Marcel Dekker, Inc.

John, J., I. Schlichting, E. Schiltz, P. Roesch and A. Wittinghofer. 1989. C-Terminal Truncation of $p21^H$ Preserves Crucial Kinetic and Structural Properties. *J. Biol. Chem.* 264:(22) 13086-13092.

John, J., R. Sohmen, J. Feurstein, R. Linke, A. Wittinghofer and R. S. Goody. 1990. Kinetics of Interaction of Nucleotides With Nucleotide- Free H-ras-p21. *Biochem.* 29: 6058-6065.

Krengel, U., I. Schlichtig, A. Schere, R. Schumann, M. Frech, J. John, M. Kabsch, E. F. Pai and A. Wittinghofer. 1990. Three Dimentional Structures of H-ras p21 Mutants: Molecular Basis for Their Inability to Function As Signal Switch Molecules. *Cell* 62: 539-548.

Lacal, J. C. and F. McCormick. 1993. The *ras* Superfamily of GTPases. CRC Press, Inc.

Lane, M. J. and J. Thomas G.J. 1979. Kinetics of Hydrogen-Deuterium Exchange in Guanosine 5' - Monophosphate and

Guanosine 3':5" - Monophosphate Determined by Laser-Raman Spectroscopy. *Biochemistry* 18:(18) 3839-3846.

Langen, R., T. Schweins and A. Warshel. 1992. On the Mechanism of Guanosine Triphosphate Hydrolysis in ras p21 Proteins. *Biochemistry* 31: 8691-8696.

Lanir, A. and N. T. Yu. 1979. A Raman Spectroscopic Study of the Interaction of Divalent Metal Ions with Adenine Moiety of Adenosine 5" - Triphqsphate. *J. Biol. Chem.* 254:(13) 5882-5887.

Lewis, A., N. Nelsoh and E. Racker. 1975. Laser Raman Spectroscopy as a Mechanistic Probe of the Phosphate Transfer from Adenosine Triphosphate in a Model System. *Biochemistry* 14:(7) 1532-1535.

Lowenstein, J. M. 1958. Traansphosphorylations Catalysed by Bivalent Metal Ions. *Biochem. J.* 70: 222-230.

Lowenstein, J. M. 1960. Synergism of Bivalent Metal Ions in Transphosphorylation. *Naturez* 187: 570-573.

Lowenstein, J. M. and M. N. Schatz. 1961. The Nonenzymatic Activation of Acetate by Adenosine Triphosphate-Bivalent Metal Chelates. *J. Biol. Chem.* 236:(2) 305-307.

Manor, D., G. Weng, H. Deng, S. Cosloy, C. X. Chen, V. Balogh-Nair, K. Delaria, F. Jurnak and R. H. Callender. 1991. An Isotope Edited Classical Raman Difference Spectroscopic Study of the Interactions of Guanine Nucleotides With Elongation Factor Tu and H-*ras* p 21. *Biochemistry* 30: 10914-10920.

Mathews, C. K. and K. E. van Holde. 1990. Biochemistry. The Benjamin/Cummings Publishing Company, Inc.

Milburn, M. V., L. Tong, A. M. DeVos, A. Brunger, Z. Yamaizumi, S. Nishimura and S. Kim. 1989. Molecular Switch for Signal Transduction: Structural Differences Between Active and Inactive Forms of Protooncogenic ras Proteins. *Science* 247: 939-945.

Miller, D. L. and H. Weissbach. 1970. Studies on the Purification and Properties of Factor Tu from *E. coli*. *Arch. Biochem. Biophys.* 141: 26-37.

Miller, D. L. and H. Weissbach. 1974. Elongation Factor Tu and the Aminoacyl-tRNA:EFTu:GTP Complex. *Adv. Enzymol.* 30: 219-232.

Mistou, M. Y., R. H. Cool and A. Parmeggiani. 1992. Effects of Icons on the Intrinsic Activities of c-H-ras Protein p21. *Eur. J. Biochem.* 204: 179-185.

Moore, K. J. M., M. R. Webb and J. F. Eccleston. 1993. Mechanism of GTP Hydrolysis by $p21^{N-ras}$ Catalyzed by GAP: Studies with a Fluorescent GTP Analogue. *Biochemistry* 32: 7451-7459.

Nishimura, Y., M. Tsuboi, T. Sato and K. Aoki. 1986. Conformation-Sensitive Raman Lines of Mononucleotides and Their Use in a Structure Analysis of Polynucleotides: Guanine and Cytosine Nucleotides. *J. Mol. Struct.* 146: 123-153.

Pai, E. F., W. Kabsch, U. Krengel, K. C. Holmes, J. John and A. Wittinghofer. 1989. Structure of the Guanine Nucleotide Binding Domain of the Ha-Ras Oncogene Product p21 in the Triphosphate Conformation. *Nature* 341: 209-214.

Pai, E. F., U. Krengel, G. A. Petsko, R. S. Goody, W. Kabsch and A. Wittinghofer. 1990. Refined Crystal Structure of the Triphosphate Conformation of H-ras p21 at 1.35 Å Resolution: Implication for the Mechanism of GTP Hydrolysis. *EMBO J.* 9: 2351-2359.

Prive, G. G., M. V. Milburn, L. Tong, A. M. de Bos, Z. Yamaizumi, S. Nishimura and S. H. Kim. 1992. X-ray Crystal Structures of Transforming p21 ras Mutants Suggest a Transition-State Stabilization Mechanism for GTP Hydrolysis. *Proc. Natl. Acad. Sci. USA* 89: 3649-3653.

Ramirez, F. and J. F. Marecek. 1981. Phosphoryl Transfer from Phosphomonoesters and Adenosine 5'-Triphosphate. *Organophophorus Chemistry (Royal Society of Chemistry, London)* 12: 142-163.

Ray, J., W.J. , J. W. Burgner, H. Deng and R. Callender. 1993a. Internal Chemical Bonding in Solutions of Simple Phosphates and Vanadates. *Biochemistry* 32:(48).

Ray, J. W. J., I. J. W. Burgner, H. Deng and R. Callender. 1993b. A Comparison of Internal Chemical Bonding in Solutions of Simple Phosphates and Vanadates. *Biochemistry* In press:.

Rensland, H., A. Lautwein, A. Wittinghofer and R. S. Goody. 1991. Is There a Rate-Limiting Step before GTP Cleavage by H-ras p21? *Biochemistry* 30: 11181-11185.

Rimai, L., T. Cole, J. L. Parsons, J. Hickmott J.T. and E. B. Carew. 1969. Studies of Raman Spectra of Water Solutions of Adenosine Tri-, Di-, and Monophosphate and Some Related Compounds. *Biophys. J.* 9: 320-329.

Rimai, L., D. Gill and J. L. Parsons. 1971. Raman Spectra of Dilute Solutions of Some Stereoisomers of Vitamin A Type Molecules. *J. Am. Chem. Soc.* 93:(6) 1353-1357.

Rosenfeld, T., B. Honig and M. Ottolenghi. 1977. *Cis-Trans Isomerization in the Photochemistry of Vision. Pure and Appl. Chem.* 49:(3) 341-351.

Schlichting, I., S. C. Almo, G. Rapp, K. Wilson, K. Petratos, A. Lentfer, A. Wittinghofer, W. Kabsch, E. F. Pai, G. A. Petsko and R. S. Goody. 1990. Time Resolved X ray Crystallographic Study of The Conformational Changes in Ha-Ras p21 Protein On GTP Hydrolysis. *Nature* 345: 309-315.

Schweins, T., R. Langen and A. Warshel. 1994. Why Have Mutagenesis Studies not Located the General Base in ras p21. *Nature Struct. Biol.* 1:(7) 476-484.

Snyder, R. G. and G. Zerbi. 1967. Vibrational Analysis of Ten Simple Aliphatic Ethers: Spectra, Assignments, Valence Force Field and Molecular Conformations. *Spectrochim. Acta* 23A: 391-437.

Sondek, J., D. G. Gambright, J. P. Noel, H. E. Hamm and P. B. Sigler. 1994. GTPase Mechanism of Gproteins from the 1.7-A Crystal Structure of Transducin α•GDP•AlF^-_4. *Nature* 372: 276-279.

Stryer, L. and H. R. Bourne. 1986. G Proteins: a Family of Signal Transducers. *Ann. Rev. Cell Biol.* 2: 391-419.

Taga, K., N. Hirabayashi and H. Okabayashi. 1988. Molecular Vibrations and Conformational Analysis of Methylphosphorodichloridate and Ethylphosphorodichloridate. *J. Mol. Struct.* 178: 89-99.

Taga, K., N. Hirabayashi, T. Yoshida and H. Okabayashi. 1989. Raman Spectra and Rotational Isomerism of Dimethylphosphorochloridate and Trimethyl Phosphate. *J. Mol. Struct.* 212: 157-168.

Taga, K., K. Miyagai, N. Hirabayashi, T. Yushida and H. Okabayashi. 1991. Vibrational Spectra and Normal Coordinate Analysis of Barium Dimethyl, Diethyl and Ethyl Methyl Phosphates. *J. Mol. Struct.* 245: 1-11.

Tajmir-Riahi, H. A., M. Langlais and R. Savoie. 1988. A Laser Raman Spectroscopic Study of the Interaction of the Methylmercury Cation with AMP, ADP and ATP. *Biochim. Biophys. Acta* 956: 211-216.

Tajmir-Riahi, H. A. and T. Theophanides. 1984. A Fourier Transform Infrared Study of the Electrophilic Attack at the N_7-site of Guanosine-5'-Monophosphate. *Can. J. Chem.* 62: 266-272.

Takeuchi, H., H. Murata and I. Harada. 1988. Interaction of Adenosine 5" - Triphosphate with Mg^{2+}: Vibrational Study of Coordination Sites by Use of ^{18}O-Labeled Triphosphates. *J. Am. chem. Soc.* 110: 392-397.

Thijs, R. and T. Zeegers-Huyskens. 1984. Infrared and Raman Studies of Hydrogen Bonded Complexes involving Acetone, Acetophenone, and Benzopenone-I. Thermodynamic Constants and Frequency Shifts of the νOH and νC=O stretching Vibrations. *Spectrochemica Acta.* 40A:(3) 307-313.

Tong, L., A. M. de Vos, M. V. Milburn, J. Jancarik, S. Noguchi, S. Nishimura, K. Miura, E. Ohtsuka and S. H. Kim. 1989. Structural Differences between a ras Oncogene Protein and the Normal Protein. *Nature* 337: 90-93.

Tu, A. T. 1982. Raman Spectroscopy in Biology, Princeples and Applications. John Wiley & Sons.

Tucker, J., G. Sczakiel, J. Feuerstein, J. John, R. S. Goody and A. Wittinghofer. 1986. Expression of p21 Proteins in Escherichia Coli and Stereochemistry of the Nucleotide-Binding Site. *EMBO J.* 5:(6) 1351-1358.

van der Veken, B. J., T. S. Little, Y. S. Li, M. E. Harris and J. R. Durig. 1986. Spectra and Structure of Organophosphorus Compounds - XXVIII. Bibrational and Conformational Analysis of Dimethylmethoxyphosphine and Some Isotopically Substituted Derivatives. *Spectrochim. Acta* 42A:(2/3) 123-140.

Webb, M. R. and J. F. Eccleston. 1981. The Stereochemical Course of the Ribosome-Dependent GTPase Reaction of Elongation Factor G from Escherichia Coli. *J. Biol. Chem.* 256:(15) 7734-7737.

Weng, G. (1993) The Interactions of G-Proteins with Nucleotides Probed by Classical Raman Difference Spectroscopy. The City University of New York.

Weng, G., C. X. Chen, Z. Chen, V. Balogh-Nair, R. Callender and D. Manor. 1993. The Hydrogen Bonding of G Proteins with the Guanine Ring Moiety of Guanine Nucleotides. *Protein Science* 3: 22-29.

Westheimer, F. H. 1987. Mechanism of Action of the Pyridine Nucleotides. In D. Dolphin,R. Poulson, & O. Avramovic (Eds.), Pyridine Nucleotide Coenzymes, Part A (pp. 253-322). New York: John Wiley & Sons.

White, J. C., R. W. Williams and M. I. Johnston. 1987. Raman Spectroscopy of Interferon-Induced 2", 5" - Linked Oligoadenylates. *Biochemistry* 26: 7737-7744.

Wilson, E. B. J., J. C. Decius and P. C. Cross. 1955. Molecular Vibrations. New York: Mcgraw-Hill.

Wittinghofer, A., U. Krengel, J. John, W. Kabsch and E. F. Pai. 1991. Three-Dimensional Structure of p21 in the Active Conformation and Analysis of an Oncogenic Mutant. *Envirom. Hlth. Perspec.* (93) 11-15.

Wittinghofer, A., W. F. Warren and R. Leberman. 1977. Structural Requirements of The GDP Binding Site of Elongation Factor Tu. *FEBS Lett.* 75:(1) 241-243.

Yue, K. T., J. P. Yang, C. L. Martin, S. K. Lee, D. Sloan and R. Callender. 1984. Raman Spectroscopy of Liver Alchohol Dehydrogenase. *Biochem. Biophys. Res. Comm.* 122: 225-229.

Zhelyaskov, V. and K. T. Yue. 1992. A Raman Study of the Binding of FeIII) to ATP and AMP. *Biochem. J.* 287: 561-566.